THESIS

EXPLORATION OF VOLATILE ORGANIC COMPOUNDS AND COMBUSTION GENERATED POLLUTANTS PRODUCED BY STRUCTURAL FUELS DURING WILDFIRES

Submitted by

Anna Helfrich

Department of Mechanical Engineering

In partial fulfillment of the requirements

For the Degree of Master of Science

Colorado State University

Fort Collins, Colorado

Summer 2025

Master's Committee:

Advisor: Christian L'Orange

Ellison Carter
Shantanu Jathar
Amy Sullivan

ABSTRACT

EXPLORATION OF VOLATILE ORGANIC COMPOUNDS AND COMBUSTION GENERATED POLLUTANTS PRODUCED BY STRUCTURAL FUELS DURING WILDFIRES

Emissions from structural fires in the Wildland-Urban-Interface (WUI) such as carbon dioxide, carbon monoxide, particulate matter, soot and volatile organic compounds (VOCs) remain poorly characterized despite growing concern about their contribution to air pollution. To address this gap emissions were quantified during structural fire experiments conducted as part of the Burning Homes and Structural MAterials (BHASMA) project. More than 70 small-scale experiments were carried out at Colorado State University (CSU) in the summer of 2023 across 19 structural fuels and fuel mixtures representing common building materials. In addition, over 20 large-scale burns were performed at the National Institute of Standards and Technology (NIST) in 2024 using standardized fuel cribs composed of wood, gypsum board, and plastic components. Emissions were analyzed across both pyrolysis and flaming phases, resulting in the identification of over 70 unique VOC species. Synthetic materials—including insulation, flooring, and sheathing—produced elevated levels of hazardous air pollutants such as benzene and styrene, which were largely absent in lumber-only combustion. Emission profiles varied with combustion phase and fuel composition but showed general consistency across fire scales. Increased emissions from crib experiments, with respect to pure wood experiments, were associated with the addition of synthetic materials in the crib's composition. These results indicate that structural materials contribute to a distinct and toxic suite of VOCs, with important

implications for human exposure, air quality modeling, and risk assessment in fire-prone WUI communities. Potential toxicological exposure and risk are evaluated using VOC emissions in a Gaussian plume model.

ACKNOWLEDGEMENTS

I would first like to thank my parents, Kurt and Sarah, for teaching me that education is one of our greatest gifts. My brother, Jack, for reminding me to have balance. My grandparents, who were the first ones to express their belief in my ability to achieve any and all goals. The rest of my family, friends and loved ones who unwaveringly support me.

I thank Jessica Noffsinger, who inspired me to explore engineering. Without her early mentorship, I would not have the same passion for math, science, and engineering.

I thank my advisor, Christian L'Orange, for his incredible wisdom and leadership. Christian and I first worked together in the summer of 2022, he exposed me to true critical thinking and research-based problem solving. I was intrigued by my summer internship experience and decided to pursue further endeavors in air quality research. This decision would not have been made if it weren't for Christian's dedication to first and foremost being a resource for his peers. I thank him endlessly for challenging me to become a better engineer and always taking the time to answer my laundry list of questions.

I thank my committee members, Shantanu Jathar, Ellison Carter, and Amy Sullivan, for their valuable feedback. I thank Shantanu for his curiosity and passion for science. Shantanu helped navigate the difficult and complicated analysis of our experimental results, always being prepared to sink a little bit further into the "why". I thank Ellison for providing a new perspective and asking questions that spurred powerful discussions. I thank Amy for her attention to detail and providing thoughtful advice regarding the analysis of my primary results.

I thank Kevin Ridgway, for being a reliable and inquisitive teammate. A successful study would not have been achievable without Kevin.

I thank the National Fire Research Laboratory team for hosting us for a portion of the study's experiments. We were warmly welcomed and enjoyed working together.

I thank the remaining members and collaborators of the Burning Homes and Structural Materials (BHASMA) study. I look forward to seeing the full breadth and impact of this work.

DEDICATION

Dedicated to Granddad, Nana, Bumpa, Bammi, Grandma, Grandpa, and Grandma Janice

TABLE OF CONTENTS

ABSTRACT ii
ACKNOWLEDGEMENTS iv
DEDICATION vi
CHAPTER 1: INTRODUCTION 1
CHAPTER 2: EMISSIONS FROM STRUCTURE FIRES: OVERVIEW OF BHASMA AND RESULTS FOR CO_2 AND SELECT POLLUTANTS BY FUEL, COMBUSTION MODE, AND SCALE 5
Chapter Overview 5
Introduction 6
Materials and Methods 8
Small-Scale Fires on Individual Fuels 9
Large-Scale Fires on Fuel Complexes 17
Data Analysis and Emission Factor Calculations 20
Results 23
Example Results from Small-Scale Fires for a Representative Lumber Fuel 23
Blank Correction and Experimental Variability 26
Relationships with Combustion Efficiency 28
Relationships with Fuel Categories 31
Discussion 34
Acknowledgements 37
Notes 37
CHAPTER 3: EXPLORATION OF VOLATILE ORGANIC COMPOUNDS PRODUCED BY STUCTURAL FUELS DURING COMBUSTION 38
Chapter Overview 38
Introduction 39
Methods and Materials 42
Small-scale fires (~1 kW): fuels and experiments 42
Large-scale fires (~500 kW): fuels and experiments 43
Gaseous (VOC) measurements and analysis 44

Plume Model 49
Results 53
Data cleaning 53
Species selection and experimental variability 53
Combustion Efficiency 57
Emissions by fuel group 60
Gaussian Plume Model at Varying Structural Emissions Contributions 64
Discussion 68
CHAPTER 4. COMPARISON BETWEEN VOC MEASUREMENT INSTRUMENTATION ACROSS BURN CAMPAIGNS 71
Chapter Overview 71
Introduction 71
Procedure 72
Results 72
CHAPTER 5: CONCLUSIONS 77
REFERENCES 83
APPENDIX A: CHAPTER 2 SUPPLEMENTAL FIGURES 92
APPENDIX B: CHAPTER 3 SUPPLEMENTAL FIGURES 101

CHAPTER 1: INTRODUCTION

As wildfires tear through the wildland-urban-interface (WUI), the intersection of wildland and populated areas, an increasing number of structures are being damaged or destroyed. In the southern Rocky Mountains, wildland fires in 2018 destroyed 24,448 homes—compared to just 245 in 2005, representing approximately 10% of all structures exposed to wildfire that year [1]. As wildfires increase in both frequency and severity, continued urban expansion into WUI regions places more structures at risk than ever before. This trend is expected to continue, as increasing fire frequency is strongly linked to climate change [2]. Spatial patterns suggest an inverse relationship between fire frequency and severity, indicating that previously unaffected WUI neighborhoods are likely to experience increasing fire impacts on vegetation and residential areas [3].

While there is an abundance of ambient air collected on 'smoky' days, there is a lack of data pertaining to structural fuel-specific emissions. Fires in WUI regions often damage or destroy structures, yet data on the emissions generated from burning structural materials remain limited [2]. Although the tangible effects and emissions of biomass burns are well understood, there is limited data available on the human health and environmental health impacts of fires [4]. Expected compounds include trace metals, semi-volatile organic compounds (SVOCS), greenhouse gases, and varying sizes of particulate matter [5]. Differences in the types and quantities of emissions from biomass versus synthetic or engineered structural fuels highlight a critical research gap.

Current datasets on WUI fire emissions are insufficient to support generalizable or predictive assessments of related health and human environmental impacts. Moreover, there is little data

available on emissions from specific structural fuel types [6]. Emissions factors (EF) are used to quantify the weight of species emitted per weight of fuel combusted. Emissions factors enable direct comparisons between fuel types by establishing quantitative relationships between emissions and fuel composition. These are valuable in understanding how emissions vary with fluctuating quantities of fuels (e.g. wood, plastics, synthetics, metals), as well as related signature emitted species to fuel types. Emissions plume data from U.S. fires involving structural combustion have shown elevated concentrations of nickel, copper, zinc, lead, and $PM_{2.5}$ [7]. Utilizing nationwide sensors provides valuable insight into regional variations in structural emissions. However, plume data does not allow for fuel-specific emission contributions to be identified without first testing and documenting structural fuels in isolation.

The onset threat of increased fire frequency demands new risk assessment and management methodologies [8]. Current fire mitigation strategies designed by the United States Department of Interior include a variety of land and response preparedness, fire suppression, fuel management, and burned area rehab [9]. One study found that through a mosaic of fuel treatments with varying spatial arrangements, focusing on treatment along roads helped contain fires in areas dominated by herbaceous fuels [10]. Established in August of 2000, the National Fire Plan (NFP) addresses five main concerns related to fire management: firefighting, rehabilitation, hazardous fuels reduction, community assistance, and accountability [11]. The NFP and the Hazardous Fires Initiative (HFI) have a common goal of reducing wildfire risks to human populations [11]. Research on structural fire emissions should inform fire and smoke policy by clarifying exposure risks and guiding the evolution of firefighting and mitigation strategies.

Recognizing the urgent need for a structural-fuel-based emissions database, the Burning Homes and Structural MAterials (BHASMA) study was launched through support from the National Oceanic and Atmospheric Agency. The primary objective was to investigate fire and smoke associated pollutants during WUI burn events. This study simulated structural fires and collected emissions under controlled laboratory conditions to assess their potential environmental and human health impacts. The first emissions campaign investigated individual structural fuels (e.g. carpet, plywood, wiring, insulation) under two bookending combustion modes, pyrolysis and flaming for smaller fire size (~1kW). The second campaign examined mixed-fuel burns under varying packing densities to simulate ventilation-limited conditions in large-scale fires (~500 kW). Particulate and gas phase compounds were both sampled during experiments.

An analysis of volatile organic compounds (VOC) emitted from these fires revealed compound-specific signatures that can serve as gas-phase fingerprints of individual fuel types. These gaseous compounds are estimated to represent around fifteen percent of all biomass emissions [12]. Compared to biomass, the VOC EF from urban fuels trends one to three orders of magnitude greater [13]. Although the mass contribution of VOCs to total structural emissions is uncertain, consistent inhalation of these compounds during wildfire events poses significant health risks [14]. There is a strong focus on the petroleum industry's associated VOC emissions of benzene, toluene, ethylbenzene and xylenes, known as BTEX compounds. The prominence of BTEX compounds in synthetic emissions may lead to underrepresentation of other potentially harmful VOCs in analytical efforts. This study chose to analyze over seventy unique VOCs to ensure no toxic emissions were missed. Analyzing commonly measured criteria pollutants (CO_2, CO, CH_4, $PM_{2.5}$, NOx, and soot) alongside VOCs may help reveal predictive relationships useful for understanding broader smoke composition.

This study seeks to identify the emissions of structural fuels in isolation as well as in complex combinations. We report emissions of both criteria pollutants and VOCs from small- and large-scale structural fuel burns conducted under controlled combustion and sampling conditions. We expect to see differences between biomass and man-made structural fuels, the quantity and rate at which these emissions differ is a primary source of interest. The BHASMA findings aim to inform risk assessment and planning for firefighters, WUI residents, downwind communities, and housing developers. In addition to generating emissions datasets, the results can support modeling efforts that estimate toxicological impacts of structural fire smoke.

CHAPTER 2: EMISSIONS FROM STRUCTURE FIRES: OVERVIEW OF BHASMA AND RESULTS FOR CO_2 AND SELECT POLLUTANTS BY FUEL, COMBUSTION MODE, AND SCALE[1]

Chapter Overview

With nearly 50 million houses in the United States located at the wildland-urban-interface (WUI) and wildfire frequency and activity on the rise, there is a growing concern that wildfire-related structure fires might be an important source of air pollutants in WUI regions, with implications for air quality and public health. However, pollutant emissions from structure fires are poorly understood and what we do understand remains fragmented and incomplete. In this work, we report on structure fire experiments performed as part of the Burning Homes and Structural MAterials (BHASMA) project. More than 70 small-scale experiments were performed at Colorado State University (CSU) in the summer of 2023 on 19 different fuels and fuel complexes, representing lumber (e.g., Douglas-fir), processed wood (e.g., oriented strand board), insulation (e.g., extruded polystyrene), carpet (e.g., polyester), roofing (e.g., asphalt shingles), electrical sheathing (e.g., polyvinyl chloride), and flooring (e.g., luxury vinyl plank), separately under pyrolysis and flaming conditions. More than 20 large-scale experiments were performed at the National Institute of Standards and Technology (NIST) in the summer of 2024 on different sizes and packing densities of a fuel test crib composed of lumber, processed wood, gypsum

[1] Reproduced with permission from "Emissions from Structure Fires: Overview of BHASMA and Results for CO_2 and Select Pollutants by Fuel, Combustion Mode, and Scale". Kevin Ridgway, Anna Helfrich, Lily Cast, Miranda Trujillo, Cristian Medina, Aika Y. Davis, Thomas G. Cleary, Ryan L. Falkenstein-Smith, Rodney A. Bryant, Matthew F. Bundy, John Flynn, Tami C. Bond, Thomas Borch, Christian L'Orange and Shantanu Jathar

board, and plastics. Emissions factors (EFs) for carbon dioxide (CO_2), carbon monoxide (CO), methane (CH_4), fine particulate matter ($PM_{2.5}$) and organic aerosol (OA) exhibited strong associations with combustion efficiency (CE). We observed that the EFs for these species at the same CE did not vary strongly with fuel category or the fire scale (~1 kW at CSU versus ~500 kW at NIST) and were generally consistent with emissions reported in the literature for biomass burning. However, EFs for soot (elemental carbon (EC) and black carbon (BC)) for non-wood-based fuels (e.g., insulation, carpet, electrical sheathing) under flaming conditions were an order of magnitude higher than those from wood-based fuels (e.g., lumber, processed wood). Our findings suggest that structure fires are likely to be similar to vegetation fires for some pollutants (e.g., CO) but not all (e.g., soot). As the first in a set of papers, this work contributes to the body of literature focused on understanding the emissions and consequent environmental impacts from WUI fires.

Introduction

The wildland-urban-interface (WUI), a region where urban development happens within or adjacent to forested areas, is rapidly growing in size across the planet [15, 16]. One in every three homes resides in the WUI and nearly 350,000 homes are being built in the WUI region each year in the United States (US) [2, 17]. With increased wildfire activity, especially in the western US [18, 19], WUI fires are on the rise and much of the WUI and wildland fire increase in recent decades has been attributed to human ignition [20]. Invariably, WUI fires are either a cause for or effect of structure fires, which have resulted in significant loss of property and human life over the past two decades in the US [21]. In a WUI fire, structure fires have the potential to contribute substantially to emissions of hazardous air pollutants, and consequently have impacts for first responders, emergency personnel, and downwind communities [22-24].

Yet, little is known about how structure fires may contribute to pollutant loadings in WUI smoke plumes and how they are likely to modulate impacts of WUI fires on human health and the environment.

While emissions from wildfires, and biomass burning more broadly (which includes prescribed burning, agricultural burning, and solid fuel combustion), are relatively well understood, air pollutant emissions from structure fires are highly uncertain [12, 25]. Specifically, several recent reviews and publications have highlighted the dearth of studies that characterize emissions from structure fires [5, 13]. Recently, Holder et al [13], compiled emissions data for structural fuel materials from 28 independent studies. They found that while primary emissions of criteria pollutants like carbon monoxide (CO) and fine particulate matter ($PM_{2.5}$) were similar to those from biomass burning, emissions for certain classes of pollutants were orders of magnitude higher per mass of fuel burned. For instance, when compared to biomass burning, they found that emissions of polycyclic aromatic hydrocarbons (PAHs), chlorinated compounds, dioxins, furans, and transition metals were all up to 3 orders of magnitude higher for structural fuels. While there is growing interest in this topic [26], the limited number of studies and large variability in emissions estimates point to an urgent need to quantify gas- and particle-phase emissions from structural fuel materials.

It is understandable that emissions from structure fires are not only heterogeneous but also higher than those from biomass burning. This is partly due to differences in the fuel composition, but also from differences in how structure fires may burn relative to biomass burning [5]. The combustible (or carbon-based) fraction of a residential structure is dominated by lumber (e.g., pine, fir, spruce), yet treated varieties (e.g., pressure-treated lumber) and processed wood (e.g., plywood, oriented strand board) are increasingly used in the construction of residential homes in

the US [27]. Treated lumber and processed wood, which contain chemicals used in their processing or production (e.g., pesticides, adhesives, solvents), could constitute up to half of the combustible fraction of a residential structure [5]. A residential structure also contains many other construction (e.g., flooring, roofing, insulation, siding, electrical) and household (e.g., furniture, appliances, textiles, consumer products, vehicles) fuels that are chemically distinct from wood. While each of these fuel types may not make up a substantial fraction, taken together, they could account for up to a quarter of the combustible fraction of a residential structure [5]. It is important then that we understand the fuel composition, combustion characteristics, and air pollutant emissions from these very different fuel types and chemistries.

In this work, we describe measurements of select gas- and particle-phase emissions from small (<1 kW) and large (<500 kW) fires from a survey of structural fuels. In this first publication, we focus on a description of the experimental (Sections 2.1 and 2.2) and analytical (Section 2.3) methods and showcase results for select gas and particle emissions (Section 3). We analyze the emissions data by combustion mode, fuel category and material, and scale, and compare against prior data. This work adds to the limited literature on structure fire emissions, noting that subsequent publications will focus on the detailed speciation of gas- and particle-phase compounds.

Materials and Methods

The structural fuel fire experiments were performed at two different scales: ‘small’ and ‘large’. The labels ‘small’ and ‘large’ are used in a relative sense and represent fires <1 kW and <500 kW, respectively, noting that an actual structure fire likely approaches 100 MW. In the sections below, we describe the experimental design, fuel choices, and measurements for the small- and large-scale fires separately.

Small-Scale Fires on Individual Fuels

Experimental Setup. The small-scale fire experiments were performed at the emissions testing facility at the Powerhouse Energy Institute at Colorado State University (CSU) in June to July of 2023; some visuals are shared in Figure 1. The emissions testing facility has been

Figure 1: Pictures show the (a) emissions hood in the testing facility, (b) furnace inside the emissions hood, (c) flaming experiment, (d) sample collection system, and (e) fuel samples for the small-scale fire tests performed at CSU.

described in detail in earlier work so we only describe it briefly for completeness[28-29]. A schematic of the testing facility and combustion setup is shown in Figure 2. The centerpiece of

the combustion setup was a furnace (outer diameter (OD) of 30.5 cm and inside diameter (ID) of 20.3 cm with a height of 15.2 cm), which consisted of a 2.6 kW resistance heater (Watlow VC408A06T-0001R), a H_2 burner installed on the floor of the furnace, and a coil of punched stainless steel tubing placed along the inside wall of the furnace to flush pure N_2 into the furnace

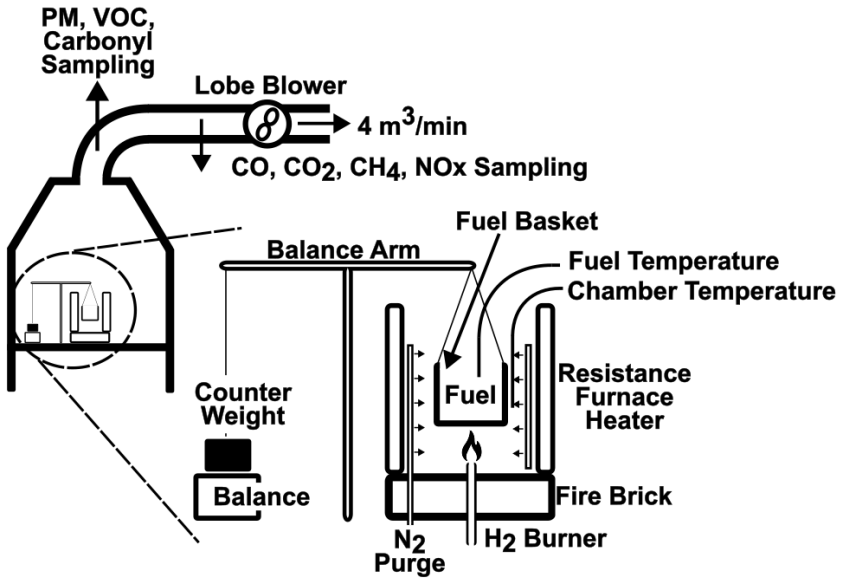

Figure 2: Schematic of the testing facility which shows the furnace, mass balance system, emissions hood, and sampling duct.

cavity. The furnace was placed on top of fire bricks and the entire assembly was centered inside an emissions hood (cross-section of 1.5 m × 1.5 m). A duct (ID of 10 cm) coupled to the emissions hood was connected to a lobe blower, set to produce a flow of ~4 m^3 min^{-1} through the duct. A probe ~2 m from the furnace was connected to a 0.95 cm (⅜ in) stainless steel line, which was used to isokinetically sample emissions onto several different media (discussed later). Another probe downstream of the sample probe was connected via a 0.95 cm (⅜ in) polyethylene to a suite of gas analyzers (discussed later).

Fuels. We chose nine broad categories of structural fuels to represent the diversity of carbon-based or combustible fuels found in residential homes in the WUI: lumber, processed wood,

roofing, insulation, siding, carpet, plumbing, electrical, and flooring [5]. For many of the fuel categories, we identified up to three fuel materials that best represented current-day choices for residential construction. In addition to performing a scoping review of the published literature on the fuel composition of a residential home [30-33], we had informal conversations with building contractors, interviewed a researcher in construction management at CSU, and considered availability of material at a local hardware store in deciding the number of fuel categories and choices for fuel materials. Table 1 lists the fuel categories, individual fuels, density, select elemental composition, and number of experiments performed by combustion mode. The number of experiments performed for fuel material under the specified combustion mode is also indicated.

Table 1: Fuel categories, individual fuels, select elemental composition, initial fuel mass, and number of experiments performed under pyrolysis and flaming conditions.

Fuel Category (#)	***Fuel Material***	***Density (kg m^{-3})***	***Elemental Composition@ (mass %)***			***Initial Fuel Mass (g)***	***Pyrolysis***	***Flaming***
			C	***O***	***Ash***			
Lumber (58%)	Douglas Fir (Untreated)	440	52	42	0.45	32-36 (P) 118-123 (F)	2	2
	Southern Yellow Pine (Treated)	375	52	41	1.23	34-126(P) 110-120 (F)	4	3
	Japanese Sugi	310	53	41	0.66	34 (P) 118 (F)	1	1
Processed Wood (23%)	Oriented Strand Board (OSB)	557	50	42	1.16	25-118 (P) 42-118 (F)	3	3
	Medium Density Fiberboard (MDF)	771	50	41	0.55	30-34 (P)	2	2

						120-123 (F)		
	Plywood	460	51	42	0.94	24-119 (P) 118-121 (F)	3	2
Roofing (14%)	Asphalt Shingles	1217	ND	ND	ND	29-99 (P) 100 (F)	2	1
Insulation (4%)	Polyurethane Foam (PUF)	ND	63	ND	ND	5-6 (P) 5-11 (F)	2	2
	Extruded Polystyrene (XPS)	28	95	0.01	0	5 (P) 8-10 (F)	2	2
	Cellulose	62	44	34	16	5 (P) 11 (F)	1	1
Siding (1%)	OSB Composite (OSBS)^	681	51	41	1.74	32 (P) 123 (F)	1	1
	Cement Fiber Siding	1291	4	7.19	87.5	40 (P) 120 (F)	1	1
Carpet (<1%)	Polyester	123	47	11	38.2	15-28 (P) 16-29 (F)	3	3
	Triexta	163	63	3	29.6	16-31 (P) 16-80 (F)	2	2
	Nylon	221	58	1.42	23	14 (P) 18 (F)	1	1
Plumbing (<1%)	Polyvinyl Chloride (PVC)	1463	38	50	6.63	13-14 (P) 13-15 (F)	2	2
	Chlorinated Polyvinyl Chloride (CPVC)	1560	35	57	3.7	16 (P) 14 (F)	1	1
Electrical	Wire (12 Gauge)*	4159	38	50	6.63	53 (P)	1	1

(<1%)						48 (F)		
	Wire (14 Gauge)*	4011	38	50	6.63	52 (P) 50 (F)	1	1
Flooring (<1%)	Luxury Vinyl Plank (LVP)	1828	20	12	67	19 (P) 18 (F)	1	1

*ND=no data; #=Reflects approximate percentage of the combustible fraction in a typical US residence[15]; ^Results for OSBS are combined with those for OSB; *Wire assumes the same composition as PVC, representing the combustible PVC jacketing; @Complete elemental composition available in Table 4.*

Experiments. Two types of experiments were conducted to study emissions under oxygen-poor, pyrolysis conditions or oxygen-rich, flaming conditions. These two types are expected to capture the extremes of oxygen availability in a structural fire. The furnace was pre-heated to ~500 °C and pure N_2 was introduced into the furnace for all pyrolysis experiments. Measurements suggested that the O_2 levels inside the furnace with N_2 flushing were low enough (<10%) to prevent fuel ignition (confirmed visually). The turbulent environment inside the furnace that promoted entrainment of O_2-rich air into the furnace prevented us from being more confident about the exact availability of O_2 during the experiment. The H_2 burner, which produced a diffusion flame, was run for the entire duration of the experiment for all flaming experiments and it provided most of the heat for fuel combustion. The radiant heater and N_2 flush were turned off during these experiments. Fuel was loaded into a wire-mesh fuel basket and lowered into the furnace. Once lowered, the fuel basket was connected to a cantilevered arm, which had a counterweight of 0.75 kg on a mass balance. Loss of fuel during the experiment was recorded as an increase in the counterweight, which was then used to compute a time-dependent loss of fuel mass. A thermocouple attached to the fuel basket recorded the temperature close to the fuel surface. Sampling was initiated once the fuel basket was lowered into the furnace. The average duration for an experiment was ~20 min, ranging from 15 min to 35 min for pyrolysis

experiments and ranging from 10 min to 30 min for flaming experiments. Several blank experiments were performed in the absence of any fuel, separately for pyrolysis (5) and flaming (4) conditions, to furnish data for blank corrections (10% of the data).

Measurements. A set of gas analyzers was used to measure real-time mixing ratios for CO_2 and O_2 (Siemens Ultramat/Oxymat 6), CO (Testo 350), CH_4 (Siemens Ultramat 23), and NO_X (Siemens NOxmat 6000) from the emissions duct. CO_2 (Licor LI-840A) was also monitored in the laboratory to determine background values. Gas analyzers were calibrated at the beginning of each test day and zeroed between experiments if there was a deviation from background. A combination of filter, sorbent tube, cartridge, and canister, time-integrated samples were collected over the course of each experiment. Sampling details and the analyses performed to estimate emissions are provided in Table 2 and the schematic in Figure 3 shows the arrangement

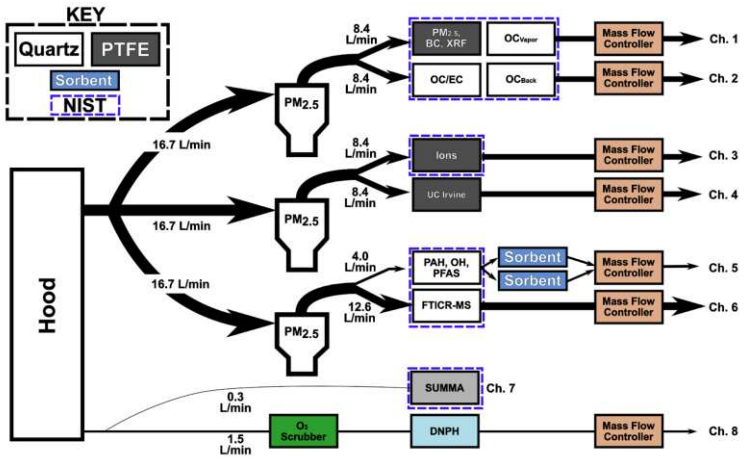

Figure 3: Sampling schematic for the small-scale CSU experiments that show the sample flow from the emissions hood to the mass flow controllers that were connected to a vacuum pump. All particle samples were collected on either a PTFE or quartz filter downstream of a $PM_{2.5}$ cyclone operating at 16.7 LPM. Arrow sizes correspond approximately to the magnitudes of the flow rate. Flow rates labeled in the schematic are nominal design flow rates and the actual flow rates deviated slightly from the design value. Legend identifies the sampling substrate. A similar but smaller setup was used for the large-scale NIST experiments; overlapping channels marked using a dashed blue box.

of the sample collection system. In this work, we analyzed the particles collected on the

polytetrafluoroethylene (PTFE) filter on channel #1 and the quartz filter on channel #2 to calculate emissions of fine particulate matter ($PM_{2.5}$), black carbon (BC), organic carbon (OC) or organic aerosol (OA), and elemental carbon (EC). Volatile organic compounds (VOCs), quantified from the SUMMA canisters and 2,4-dinitrophenylhydrazine (DNPH) cartridges, were summed to calculate total VOC emissions, which were then used to compute emission factors and combustion efficiencies; VOC speciation will be reported and discussed in detail in a subsequent publication. After collection, filters were stored at -20 °C, sorbent tubes and cartridges were stored at 4 °C, and canisters were stored at room temperature. Canisters were analyzed within a week while the filters and sorbent tubes were stored until they were pulled from storage for analysis.

Table 2: Sampling and analysis details for both the small- and large-scale experiments. Shaded rows indicate sampling and analysis common to the small- and large-scale experiments. Unshaded rows indicate sampling and analysis for only the small-scale experiments.

Channel Number	***Sampling Media***	***Phase Sampled***	***Flow Rate (LPM)^***	***Analysis Type***	***Data Product***
1	PTFE filter	Particles, <2.5 µm	8.4 (CSU) 4.4 (NIST)	Gravimetric	$PM_{2.5}$
				Attenuation of 880 nm light	BC
				X-Ray Fluorescence (XRF)	Elemental composition
2	Quartz filter	Particles and adsorbed vapors, <2.5 µm	8.4 (CSU) 4.4 (NIST)	OCEC thermo optical analyzer	OC, EC
1 and 2	Quartz behind PTFE/quartz filter	Adsorbed vapors, <2.5 µm			
3	PTFE filter			Ion chromatography (IC)	Inorganic ions

		Particles, <2.5 µm	8.4 (CSU) 4.4 (NIST)	Total organic carbon (TOC) analyzer	Water soluble organic carbon
				High performance anion-exchange chromatography coupled with pulsed amperometric detection	Anhydrosugars, sugars, sugar alcohols/polyols
4	PTFE or quartz filter	Particles, <2.5 µm	8.4 (CSU)	UV aging followed by high-resolution mass spectrometry and spectrophotometry	Chromophores, mass absorption coefficients, thermodynamic properties
5	Quartz filter	Particles and adsorbed vapors, <2.5 µm	4 (CSU) 4.4 (NIST)	Gas/liquid chromatography - mass spectrometry	Polycyclic aromatic hydrocarbons (PAH), organohalogens (OH), per- and polyfluoroalkyl substances (PFAS)
	XAD-2 sorbent tubes behind quartz filter[#]	Vapors	2 (CSU)		
6	Quartz filter	Particles and adsorbed vapors, <2.5 µm	12.6 (CSU)	Fourier-Transform Ion Cyclotron Resonance Mass Spectrometry (FTICR-MS)	Untargeted analysis
7	SUMMA canister	Gases	0.33 (CSU) 0.06 (NIST)	Gas chromatography with flame ionization detector (FID), electron capture detector (ECD) and mass spectrometry (MS)	C_2-C_{10} VOCs, C_1-C_2 halocarbons, C_1-C_5 alkyl nitrates, and reduced sulfur compounds
8	DNPH cartridges	Gases	1.5 (CSU)	High-performance liquid chromatography (HPLC) with UV detector	Carbonyls

[#]*Two XAD-2 sorbent tubes were placed in parallel downstream of the channel 5 quartz filter, each operating at 2 LPM; ^Reflects nominal flow rates, (CSU) refers to small-scale campaign, (NIST) refers to large-scale campaign*

Large-Scale Fires on Fuel Complexes

Experimental Setup. The large-scale fire experiments were performed at the National Fire Research Laboratory (NFRL) on the National Institute of Standards and Technology (NIST) campus in Gaithersburg, Maryland in June 2024; some visuals are shared in Figure 4. The testing facility is thoroughly documented in Bryant and Bundy [34], and the fuel and experiments have been described in detail in Davis et al [35]. A brief description follows. The fire experiments were conducted under the 500 kW emissions hood (cross-section of 3.1 m × 3.2 m). Emissions were ported to a large duct (ID of 0.48 m), which was operated between 150,000 L min^{-1} and 210,000 L min^{-1}. A 0.95 cm (⅜ in) stainless steel tube ~10 m in length was used to transfer emissions from the duct to our sampling system (details below). While sampling was designed to be isokinetic at 150,000 L min^{-1}, it was sub-isokinetic at higher duct flow rates.

Figure 4: Pictures show (a) flaming combustion of a fuel Crib under the 500kW emissions hood, (b) a large fuel crib being built, and (c) sample collection system for the large-scale fire tests performed at NIST.

Fuels. Fuels were built in the form of 'cribs' [36]. The crib was constructed as a cube using individual sticks glued to each other using a generic construction-grade glue (Figure 4b). Small

cribs, 0.3 m × 0.3 m × 0.29 m in size, were built using 1.91 cm square sticks while large cribs, 0.48 m × 0.48 m × 0.46 m in size, were built using 3.81 cm square sticks. All cribs had the same composition by mass percentage: 21% of spruce pine fir, 15% of oriented strand board (OSB), 46% of gypsum board, 7% of polyvinyl chloride (PVC), 6% of polyurethane (PU), and 5% of acrylonitrile butadiene styrene (ABS). The weight percentages were chosen to approximately represent combustible versus non-combustible fractions and a mix of structural and household materials found in a typical single family home [35]. In addition to crib size, the cribs were varied in packing density (low, medium and high) to produce differences in the 'ventilation factor', which facilitated varying burn behaviors exhibited by realistic structure fires [36]. The ventilation factor was varied between 0.014 cm (small crib with low packing density) and 0.187 cm (large crib with high packing density). Depending on the ventilation factor, the small cribs weighed between 7.8 and 14 kg and the large cribs weighed between 33 and 55 kg. Crib details along with the number of experiments performed are presented in Table 3.

Table 3: Crib sizes, packing density, initial crib mass, and number of experiments by size and packing density.

Crib Size	**Packing Density**	**Initial Crib Mass (kg)[&]**	**Number of Experiments**
Small 0.3 m × 0.3 m × 0.29 m	Low	7.8	4
	Medium	10	4
	High	14	4
Large 0.48 m × 0.48 m × 0.46 m	Low	33	3
	Medium	44	3
	High	55	3
Blank w/o fire starters	NA	0	6

[&]*Initial crib mass excludes mass of starters*

Experiments. Experiments were conducted to study the influence of crib size and packing density (or ventilation factor), however, we consider results from all crib tests together. Cribs were placed on a load cell to characterize loss of the fuel mass in real time. Two to ten fire starters, depending on the crib size (two for smaller cribs with a lower packing density and ten for larger cribs with higher packing density), were placed on the top of the crib and/or the contents squeezed into gaps between crib materials. The fire starters were composed of a mixture of high molecular weight hydrocarbons, and each fire starter weighed 51 g. Cribs were ignited by lighting the fire starters with a propane torch. The duration of the experiment varied significantly from about 30 min for a small crib with a lower packing density to 190 min for a large crib with a higher packing density. The crib was extinguished with water after slightly more than half of the crib mass was lost to combustion.

Measurements. Gas and Fourier Transform Infrared Spectroscopy (FTIR) analyzers were used to measure mixing ratios of CO_2, CO, select hydrocarbons, NO_X, and other small oxygenated organic and inorganic compounds (e.g., formaldehyde, SO_2). These species were measured for the entire duration of the experiment and until the heat release rate (HRR; HRR was computed and tracked in real time during the experiment) reached background levels. We initiated filter and canister sampling once the crib had started to burn, most of the fire starter was consumed, and the fire had reached its peak HRR. Emissions were sampled onto filters and canisters for approximately 10 min to 20 min. We opted not to sample onto filters and canisters over the entire duration of the experiment to avoid saturating the sample media. Biases introduced from sub-sampling are discussed in methods. Some of the same analyses as those described for the small-scale fires were performed to estimate emissions from the large-scale fires; the shaded rows in Table 2 represent the overlapping sampling and analysis. After

collection, filters were stored at -20 °C and canisters were stored at room temperature. Canisters were shipped from NIST to CSU at the end of each test week and analyzed within a week while the filters were stored until they were pulled from storage for analysis.

Data Analysis and Emission Factor Calculations

For the small-scale fires, time series data from the gas analyzers (CO_2, CO, CH_4, NO_X) were averaged over the duration of the experiment and corrected for background levels (from before and after the experiment) and drift (when evident) to calculate a time-integrated, background-corrected mixing ratio in ppmv. For the large-scale fires, time series data from the gas analyzers (CO_2, CO) and FTIR (CH_4, NO_X) were averaged over the sampling window (since filter and canister sampling was performed only when the fire had achieved peak HRR) and corrected for background levels (from before and after the experiment) to calculate a time-integrated, background-corrected mixing ratio in ppmv. The PTFE filter (channel #1) was weighed on a microbalance (Mettler Toledo XS3DU) before and after sample collection to determine the $PM_{2.5}$ mass in µg. Following the gravimetric measurement, the same filter was assessed for net attenuation of light at 880 nm to calculate BC mass in µg, assuming a mass absorption cross section (MAC) of 8.9 m^2 g^{-1} [37]. MAC values are known to be highly variable depending on factors such as fuel type and combustion mode, so a value was chosen in the middle of those reported in previous studies [37]. Both the $PM_{2.5}$ and BC measurements were performed in triplicate on the AIRLIFT facility, documented in Li et al [38]. A 1 cm^2 punch from the quartz filter (channel #2) was run on an OC/EC analyzer (Sunset OC/EC) following a method based on the NIOSH protocol [39] to determine OC and EC masses in µg C. An organic aerosol to organic carbon ratio of 1.6 was used to convert OC mass to OA mass [40]. The OA mass was not corrected for the artifact of adsorption of semi-volatile organic compounds onto the quartz filter

[41] and, hence, the OA mass represents emissions of organic species up to an effective saturation concentration of 10^4 µg m^{-3} at 298 K [42-43]. During the experiment, mass flow rates were recorded downstream of the sample collection using calibrated mass flow controllers. Ambient pressure and sample temperature were used alongside average mass flow rates to determine volumetric flow rates and subsequently mass concentrations for $PM_{2.5}$, BC, OA, and EC. All mixing ratios and mass concentrations were additionally blank-corrected by subtracting median values measured during the blank experiments. Mixing ratios for gases were converted to mass concentrations and then mass concentrations for gases and particles were converted to emission factors using Equation 2.1 and 2.2:

Equations 2.1 and 2.2: emission factor [g kg-$fuel^{-1}$] and cumulative carbon contribution, respectively

$$EF_i = \frac{M_i}{C_{eff}} x f_C x 10^3$$

$$C_{eff} = (\Delta CO_2 + \Delta CO + \Delta CH_4 + \Delta VOC) x \frac{P}{RT} x MW_C + \Delta EC + \Delta OC$$

Where EF_i is the emission factor in g kg-$fuel^{-1}$; Ai is the mass concentration of the pollutant in µg m^{-3}; C_{eff} is the cumulative carbon concentrations in µg m^{-3}; CO2, CO, and CH4 are the background-corrected CO_2, CO, and CH_4 mixing ratios in ppmv, respectively; VOC is the background-corrected mixing ratio for all VOCs in ppmC; P is the atmospheric pressure in Pa; R is the universal gas constant (8.314 J mol^{-1} K^{-1}); T is the sample temperature in K; AWC is the atomic weight of carbon in g mol^{-1}; OC and EC are the background-corrected OC and EC mass concentrations in µg m^{-3}; and f_c is the carbon fraction of the fuel. For some experiments, we could not compute C_{eff} reliably because the background-corrected concentrations of the carbon-containing emissions were close to the limit of quantification. In these instances, mainly limited

to pyrolysis experiments performed with non-wood-based fuels, we computed C_{eff} using the mass loss, f_c, and total duct flow. We also computed the combustion efficiency (CE) and modified combustion efficiency (MCE) for all experiments using equations (2.3) and (2.4), respectively:

Equation 2.3: Combustion Efficiency [units of %]

$$CE = \frac{\Delta CO_2}{\Delta CO_2 + \Delta CO + \Delta CH_4 + \Delta VOC + \frac{\Delta EC + \Delta OC}{\frac{P}{RT} x MW_C}}$$

Equation 2.4: Modified Combustion Efficiency [units of %]

$$CE = \frac{\Delta CO_2}{\Delta CO_2 + \Delta CO}$$

Samples of fuels from the small-scale experiments were sent to a local analytical laboratory to perform an ultimate analysis, which provides full elemental composition. The f_c values for all fuels studied during the small-scale fires are listed in Table 1 and the detailed elemental composition is presented in Table 4. An average f_c value for the NIST cribs (52.5%) was calculated from the mass percentages, as described in Davis et al [35], and f_c values for the individual fuel materials. Note that EFs described in Davis et al [35]. are measured and calculated using a different methodology.

Table 4: Detailed elemental composition for all fuel materials tested in the small-scale fires.

Fuel Material	**Fuel Category**	**Ash (%)**	**Sulfur (%)**	**Carbon (%)**	**Hydrogen (%)**	**Nitrogen (%)**	**Oxygen (%)**	**Total (%)**
Japanese sugi	Structural wood	0.66	0.036	53	5.9	0.11	41	100
Douglas fir	Structural wood	0.45	0.048	52	5.9	0.09	42	100

SYP	Structural wood	1.2	0.049	52	6.0	0.12	41	100
MDF	Manufactured wood	0.55	0.051	50	6.0	2.3	41	100
Plywood	Manufactured wood	0.94	0.039	51	6.0	0.1	42	100
OSB	Manufactured wood	1.2	0.04	50	6.0	0.4	42	100
Triexta	Carpet	30	0.065	63	4.7	0.06	3	100
Polyester	Carpet	38	0.084	47	4.0	0.06	11	100
Nylon	Carpet	23	0.14	58	8.6	8.8	1.42	100
CPVC	Siding/Electrical	3.7	0.38	35	3.9	0.05	57	100
PVC	Siding/Electrical	6.6	0.15	38	4.8	0.04	50	100
Cellulose	Sheathing/Insulation	16	0.58	44	5.3	0.13	34	100
XPS	Sheathing/Insulation	0	0.075	95	8.0	0.13	0.01	102
LVP	Siding/Electrical	67	0.054	20	1.4	0.05	12	100
Cement Fiber Siding	Siding/Electrical	87	0.36	32*	0.93	0.05	7.2	128
Composite	Siding/Electrical	1.7	0.039	51	5.7	0.82	41	100
Complex #1	Complex wood			47				47
PUF	Insulation			63				63
Asphalt shingle	Roofing			16				16
Wire	Electrical			38				38

**Carbon fraction adjusted to account for ash*

Results

Example Results from Small-Scale Fires for a Representative Lumber Fuel

Results from three sets of experiments from the small-scale fires performed with SYP (Southern Yellow Pine, pressure treated lumber) under pyrolysis and flaming conditions are shown in Figure 5. The results show time series data for background- and blank-corrected mixing ratios for CO_2, CO, and CH_4, MCE, fuel surface temperature, and fuel mass loss. In all

experiments, the fuel surface temperature increased rapidly from a laboratory temperature of 25 °C. This was because the fuel was stored at room temperature before being added to the cold fuel basket. As the pyrolysis experiments were performed with a furnace pre-heated to 500 °C, the fuel surface temperature profile did not vary much across the three repeats and leveled off at ~400 °C. However, we saw much larger variability in the fuel surface temperatures for the flaming experiments (low of 360 °C and high of 705 °C), where reaction rates are increased by radiative heat flux from the flame, which is variable, in addition to the imposed heat flux.

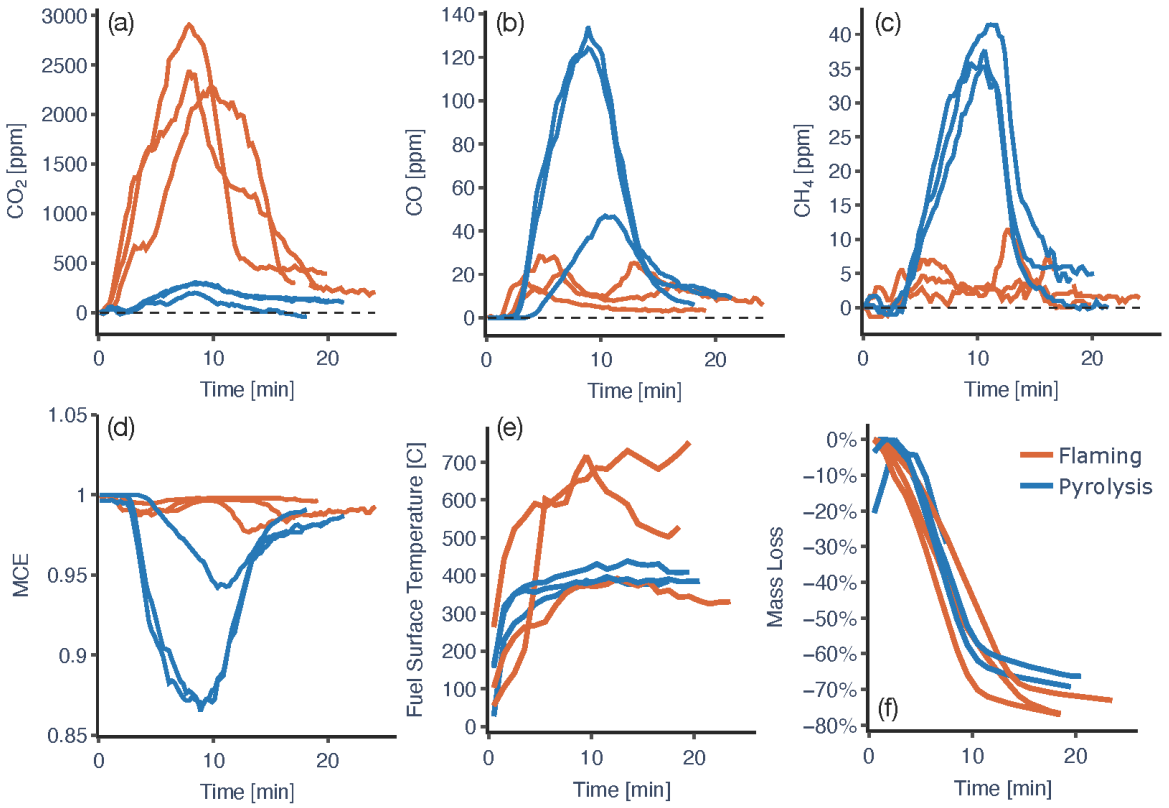

Figure 5: Background- and blank-corrected mixing ratios of (a) CO2, (b) CO, and (c) CH4, (d) modified combustion efficiency (MCE), (e) fuel surface temperature, and (f) fuel mass loss for small-scale experiments performed with southern yellow pine (SYP) under flaming (n=3) and pyrolysis (n=3) conditions.

The fuel surface temperature trends seemed to hold for all the other small-scale fire experiments; time series data for the fuel surface temperature for both pyrolysis and flaming conditions are

shown in Appendix A, Figure A1, a-b. While we acknowledge that differences in the fuel surface temperature may drive differences in emissions, the small number of samples for the same fuel and combustion mode prevented us from exploring this further.

Pyrolysis conditions tended to produce higher pollutant emissions (described and shown later) and, hence, a smaller starting fuel mass was used in these experiments to prevent overloading onto our sampling media. Across the three repeats, both combustion modes produced a consistent loss in fuel mass, with ~70% of the fuel mass lost in ≈15 min. The slight increase in fuel mass lost for one of the pyrolysis experiments at the beginning of the experiment was likely an artifact of the mass balance adjusting to thermal expansion of the cantilever that hosted the fuel basket. Time series data for loss of fuel mass for all experiments are shown in Appendix A, Figure A1, c-d.

Pyrolysis and flaming conditions produced significant differences in both the magnitude and temporal profiles for CO_2, CO, CH_4, and MCE. CO and CH_4, generated from pyrolysis, originate in the solid-fuel matrix and are emitted regardless of gas phase reactions. In the presence of a flame, these species are converted to CO_2. Hence, flaming conditions resulted in high CO_2 mixing ratios (peaking between 2300 ppbv and 2900 ppbv) and MCEs (>0.97), indicating complete combustion, while pyrolysis conditions produced much higher CO (peaking between 45 ppbv and 130 ppbv) and CH_4 (peaking between 35 ppbv and 42 ppbv) mixing ratios and lower MCEs (as low as 0.86), indicating incomplete combustion. Regardless of the combustion conditions, all three pollutants (CO_2, CO, CH_4) showed uniformity in their time profiles where mixing ratios increased initially due to greater release rates as the fuel heated and then pyrolyzed or combusted and later decreased as the fuel was spent. Temporal profiles for NO_X during the pyrolysis experiments were similar to CO and CH_4 (Appendix A, Figure A2); we did not plot

NO_X mixing ratios for the flaming experiments as most of the NO_X in these experiments was attributed to H_2 combustion. In the following sections, the pollutant and MCE data were integrated over the duration of the experiment and used alongside the other measurements to present time-integrated and experiment-specific emission factors.

Time series profiles for many of the combustion variables (e.g., HRR) and gas-phase mixing ratios (e.g., CO_2) for the large-scale fires were similar to those for small-scale fires. We do not discuss those here since they have been described previously in Davis et al [35]. Since we only sampled over a short window during the large-scale fire tests, we used the real-time data for CO_2, CO, CH_4, and NO_X to test differences in the emissions between the sampling window and the entire experiment. Results shown in Appendix A, Figure A3 indicate that sub-sampling resulted in little to no bias in the emissions estimates and that the EFs from this work should be applicable to the entire fire experiment.

Blank Correction and Experimental Variability

On account of a high experimental load (several experiments per day for several weeks) in a combustion and emissions laboratory setting, we observed higher-than-expected blank concentrations when small-scale fire experiments were performed without any structural fuels. Figures A4-A5 in Appendix A compare mixing ratios and concentrations from blank experiments against those measured during the structural fuel experiments from the small-scale fires. Even with higher-than-expected blank concentrations, for most of the pollutants (i.e., CO_2, CO, $PM_{2.5}$, OA, EC), most of the sample values were much higher than the blank values and blank corrections resulted in robust, above detection-limit estimates; blank corrections were performed using the median estimates from the blank experiments. However, in a few instances, median blank values were comparable to sample values from some of the experiments, which resulted in

loss of data (i.e., values below 0) after blank correction. This was most pronounced for CH_4 (Appendix A, Figure A4) and NO_X (Appendix A, Figure, A4) under pyrolysis conditions and CH_4 (Appendix A, Figure A5) and BC (Appendix A, Figure A5) under flaming conditions. More than 25% of the data were above detection limits, even after considering the higher-than-expected blank concentrations. Most of the data loss was limited to CH_4 and NO_X under flaming conditions. We speculate that experiments performed with the non-wood-based fuels (i.e, carpet, insulation, electrical sheathing) during the middle of the experimental campaign resulted in higher pollutant loadings that influenced the blank experiments interspersed with those structural fuels. The sample concentrations were much higher than the blank concentrations during the large-scale fires and did not present problems with blank correcting the data (Appendix A, Figure A6).

It is well documented that small differences in experiments, from differences in fuel composition, moisture content, combustion characteristics, environmental conditions, and operator practices, can result in large differences in emission factors [25, 44]. These variations result in large uncertainties in emissions estimates for open burning, which includes wildfires, prescribed fires, and solid biofuel combustion. For the small-scale fires, we studied experiment-to-experiment variability by comparing EFs from three repeat experiments performed on SYP, OSB, and polyester carpet against the average from those three experiments, separately for pyrolysis and flaming conditions (Appendix A, Figure A7). We do the same for the low and high packing density large-scale fires (Appendix A, Figure A8). While some pollutants showed little to no variability across experiments (e.g., CO_2), most (e.g., CO, $PM_{2.5}$) varied by less than a factor of 3. The experiment-to-experiment variability was generally lower in the large-scale fires than the small-scale fires. Across all fires (small- and large-scale), ~85% of the data for each

species lay within a factor of 2 of the mean, and ~95% of the data for each species lay within a factor of 3 of the mean. This variability was qualitatively considered when identifying significant trends in the EFs with combustion mode and fuel category in the results section.

Relationships with Combustion Efficiency

Emission factors (EFs) for CO_2, CO, CH_4, NO_X, $PM_{2.5}$, OA, EC, and BC are plotted as a function of CE for all experiments in Figure 6; EFs from experiments when the CE could not be calculated are not plotted in Figure 6. On the same figure, we also plot EFs against MCE, derived from the Smoke Emissions Reference Application (SERA) dataset [45]; as most of the SERA data have an MCE above 0.85, these efficient combustion conditions should result in the MCE values being very close to the CE values. SERA is an online, searchable database of biomass burning EFs based on nearly 50 unique laboratory and field studies with information for 250+ species and it was specifically created to support development of emissions inventories. A version similar to Figure 6 but with data plotted against MCE is included in the supplementary material (Appendix A, Figure A9).

For CO_2, CO, CH_4, $PM_{2.5}$, and OA, the EFs from both the small- and large-scale fires exhibited a strong relationship with CE, over the entire CE range. CO_2 emissions increased with CE while CO, CH_4, $PM_{2.5}$, and OA emissions decreased with CE, reflecting the transition from pyrolysis to flaming conditions as the CE increased. Barring a few exceptions (e.g., most notably for CO_2 and CO for other fuels), the EFs for these species, at the same CE, were only weakly influenced by fuel category or fire scale. For CE values above 0.8, the EFs were generally consistent with EFs for biomass burning reported in the SERA database; EFs for CO were slightly lower than those from SERA. These comparisons suggest that emissions for CO_2, CO, CH_4, $PM_{2.5}$, and OA are unlikely to be very different between biomass burning and structural

fuels, especially when viewed in light of the experiment-to-experiment variability and measurement uncertainties. This finding is reasonable as biomass burning fuels share the same

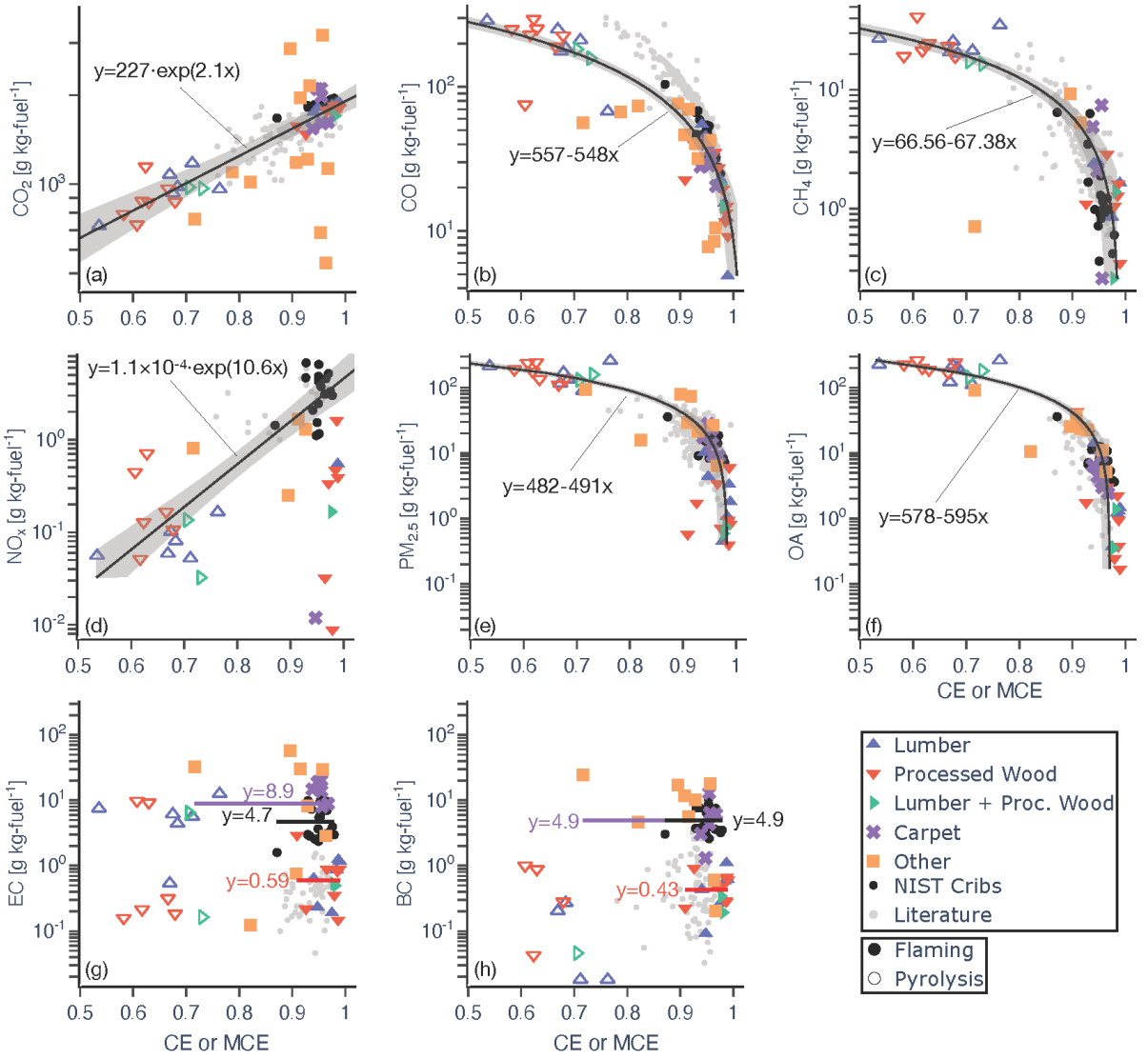

Figure 6: Emission factors for (a) CO_2, (b) CO, (c) CH_4, (d) NO_X, (e) $PM_{2.5}$, (f) OA, (g) EC, and (h) BC from all small- and large-scale fires analyzed in this work plotted against the modified combustion efficiency (MCE) or combustion efficiency (CE). Symbols are used to represent different fuel materials with open and solid symbols representing pyrolysis and flaming conditions, respectively. Literature data for biomass burning from the SERA database are plotted as light gray dots, noting that those emission factors are plotted against MCE (not CE). Solid lines with bands for uncertainty represent the best fits to the small- and large-scale data from this work and do not include SERA data. Flaming data for 'Other' fuels are ignored in determining the fit for CO, flaming data for all fuels are ignored in determining the fit for NO_X, and pyrolysis data for all fuels are ignored in determining the fits for EC and BC.

composition as structural fuels made from wood (e.g., lumber, processed wood). Yet, this same finding is surprising as biomass burning fuels are very different in composition relative to the non-wood-based fuels (i.e., roofing, insulation, siding, carpet, plumbing, electrical, and flooring), many of which contain substantial proportions of different kinds of plastic.

EFs for NO_X, EC, and BC exhibited different features than the species reported above. NO_X emissions from the small-scale fires were more than an order of magnitude lower than those from the large-scale fires and they did not show strong associations with CE. Even though they are visualized in Figure 6d, our estimates for NO_X emissions from the small-scale fires for the flaming experiments were quite uncertain (and therefore quite variable) as most of the NO_X in those experiments was produced via thermal pathways from H_2 combustion. In contrast, we are more confident of the NO_X emissions from the large-scale fires, which were quite consistent with those in the SERA database. Under pyrolysis conditions, NO_X emissions are likely to be produced from the nitrogen in the fuel (i.e., fuel NO_X) and low-temperature reactions of the pyrolyzed gases with N_2 in the air (i.e., prompt NO_X), which are less important pathways for NO_X production under flaming conditions [46].

We observed distinct differences in the EFs for soot (EC, BC) with fuel type. Under flaming conditions, EFs for soot from the small-scale fires were more than an order of magnitude higher for non-wood-based fuels (i.e., carpet, 'Other') than wood-based fuels (i.e., lumber, processed wood, lumber + processed wood). Soot EFs were similarly higher for the large-scale fires, where a third of the combustible fuel mass was composed of plastic or non-wood-based fuels (i.e., PVC, PU, and ABS). Unlike the other species, the observed differences in the soot emissions were not associated with differences in CE but likely due to differences in the sooting tendency and fuel composition [47]. Differences in EC and BC were similar to those observed for other

combustion sources[48] but these differences will be explored in more detail in subsequent work. For wood-based fuels under flaming conditions, EC and BC EFs increased slightly with CE, as has been seen with biomass burning [49-50]; these trends were unobservable for non-wood-based fuels. EFs for soot were highly variable under pyrolysis conditions and were mostly limited to data for wood-based fuels since the soot concentrations produced during the non-wood-based fuel experiments were indistinguishable from blank concentrations. Soot formation under pyrolysis conditions might be an indicator for intermittent, yet unobservable, flaming conditions.

To aid comparisons with other studies and eventually the development of emission inventories for structure fires, lines or curves were fit to all data from this work, which included both small- and large-scale fires and flaming and pyrolysis conditions. An exponential relationship was used for CO_2 and NO_X and a linear relationship was used for CO, CH_4, $PM_{2.5}$, OA, EC, and BC. Flaming data were ignored for NO_X, pyrolysis data were ignored for soot (EC, BC), and constant fit lines were developed for EC under flaming conditions but separately for wood-based and non-wood fuels, for reasons listed earlier. Similar fits were developed with MCE for flaming conditions to aid comparison of the data from this work with historical and future data where only MCE values were and may be calculated (Appendix A, Figure A9).

Relationships with Fuel Categories

EFs presented in Figure 6 are visualized again in Figure 7 while resolving the data by fuel material, combustion mode and fuel category. Figure 7 also includes EF data that were not presented in Figure 6 because of missing CE values. SERA data are presented as gray bands, representing one standard deviation around the mean, on the same plot. In addition to the insight developed from Figure 6, there are several features that are discernible from these plots.

First, EFs under pyrolysis conditions for CO, CH_4, $PM_{2.5}$, and OA were one to two orders of magnitude higher than those under flaming conditions. As mentioned earlier, these species originate in the solid-fuel matrix from pyrolysis processes but are combusted to CO_2 in the presence of a flame. EFs for CO_2, NO_X, and soot (EC, BC), in contrast, were lower or similar under pyrolysis conditions, relative to flaming conditions. This EF dataset, alongside the parameterizations listed in Figure 6, can be used to construct emissions estimates from structure fires, with information or assumptions made about fuel composition and combustion conditions.

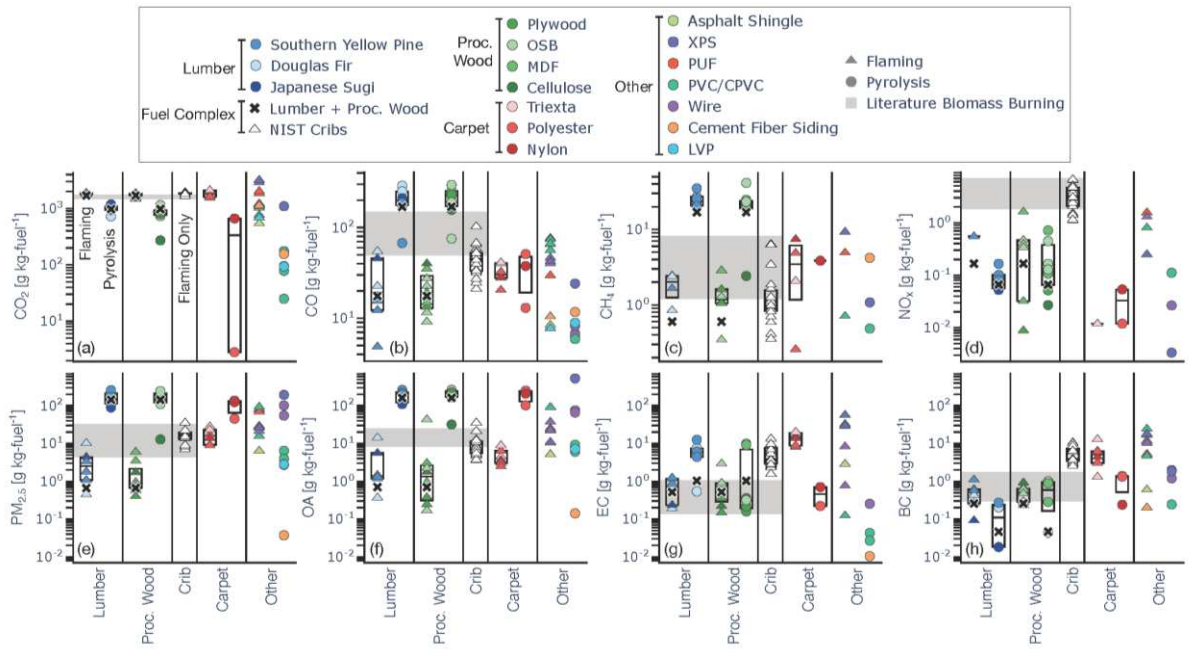

Figure 7: Emission factors for (a) CO_2, (b) CO, (c) CH_4, (d) NO_X, (e) $PM_{2.5}$, (f) OA, (g) EC, and (h) BC from all small- and large-scale fires analyzed in this work resolved by fuel category (Lumber, Processed Wood, NIST cribs, Carpet, and Other) and combustion mode (flaming and pyrolysis). Triangles represent flaming conditions while circles represent pyrolysis conditions. Data for NIST cribs from the large-scale fires are shown in open triangles. Box plots show the median and interquartile range for all fuel categories except for 'Other' fuels. Literature data for biomass burning from the SERA database are plotted as light gray bands, representing the ±1 standard deviation range.

Second, all lumber and processed wood fuels and mixtures of those fuels, seemed to produce a nearly identical range of EFs for all species under both pyrolysis and flaming conditions during

the small-scale fires. After accounting for differences in CE, the flaming emissions for these fuel types were in agreement with historical biomass burning data and, for all species except NO_X and soot, they were also consistent with flaming emissions from the large-scale fires involving NIST cribs. Benedict et al [26], who recently quantified emissions from different wood-based construction materials, came to the same conclusion. Taken together, we can conclude that there are few if any differences in the combustion emissions from different types of woods found in structures and that these are also indistinguishable from biomass burning emissions.

Third, as described in fuel group results, soot (EC, BC) emissions for many of the fuel materials in the carpet and 'Other' categories under flaming conditions and those from the NIST cribs were an order of magnitude higher than the fuel materials in the lumber and processed wood categories. This was understandable since a third of the combustible fuel mass by weight in the NIST cribs was composed of plastics. These findings suggest that the presence of household materials will result in much higher soot emissions from structure fires relative to vegetation fires.

Fourth, because many different types of fuel materials were considered under the 'Other' fuel category, EFs for nearly all species within this fuel category were found to be much more variable, relative to EFs from other fuel categories; this was also the reason why an interquartile box range was not plotted for this fuel category in Figure 7. However, we did observe similarities in the distribution of emissions between the carpet and 'Other' fuel categories. With little data on EFs from non-wood-based fuels, a statistical average from data from these two fuel categories may serve as a starting point to estimate emissions and their uncertainties from combustion of household materials.

Fifth, the small number of replicates for each fuel material prevented us from studying emissions differences within the carpet and 'Other' fuel categories. There is some indication that plastics with aromatics rings (e.g., Triexta, XPS, PUF) produced higher soot (i.e., EC) emissions relative to plastics with no aromatic rings (e.g., PVC, CPVC, nylon, polyester), although this might need to be explored systematically in future studies. Finally, knowing the uncertainties inherent in the EF calculation, we could not perceive large differences in species emissions between different fuels within a fuel category, nor did we see differences in emissions variability across combustion modes.

Discussion

In this work, we have reported EFs for CO_2 and selected pollutants from combustion of a diverse set of structural fuels. We performed more than 90 laboratory experiments on 20 different fuels and fuel complexes across 9 fuel categories, under two different combustion conditions (pyrolysis and flaming) and at two different scales (~1 kW and ~500 kW). We found that while many of the emitted species exhibited strong associations with CE, they did not vary strongly with fuel category or the fire scale and were generally consistent with emissions reported in the literature for biomass burning. We did find that emission factors for soot for non-wood-based fuels (e.g., insulation, carpet, electrical sheathing) and NIST cribs (33% of the mass was plastic) under flaming conditions were an order of magnitude higher than those from wood-based fuels (e.g., lumber, processed wood). We saw similar enhancements for $PM_{2.5}$ and OA for non-wood-based fuels but they were weaker than those observed for soot. Although we only highlighted emissions for a few species in this work, this effort represents one of a handful of studies that have attempted to systematically study structure fire emissions from individual fuels as well as fuel complexes at varying scales.

To summarize the primary outcomes from this work, we plot EFs for three different model structures under flaming-like conditions in Figure 8. EFs for model structure 1 were determined from fitting the lumber and processed wood data under flaming conditions in conjunction with the SERA data; see Appendix A, Figure A9 for fits with MCE. EFs for model structure 2 were calculated using weighted averages of the median EFs representing two fuel categories (lumber + processed wood + SERA and 'exotics' representing insulation, carpet, roofing, electrical sheathing, and flooring) while EFs for model structure 3 reflected median EFs for the NIST cribs from the large-scale fires. The EFs for model structure 1 were adjusted to compare EFs across all model structures at approximately the same MCE (~97%). EFs for CO_2, CO, and CH_4 were generally similar between the three model structures. In contrast, when adjusted to the same MCE, EFs for $PM_{2.5}$, OA, and soot (EC, BC) were higher for model structures 2 and 3, relative to model structure 1; $PM_{2.5}$ was a factor of 4 to 7 higher, OA was a factor of 2 to 3 higher, and soot was a factor of 4 to 10 higher. Overall, the trends in Figure 8 make it clear that structures containing a modest fraction of non-wood fuels will produce similar emissions for gas-phase species but elevated emissions for particle-phase species.

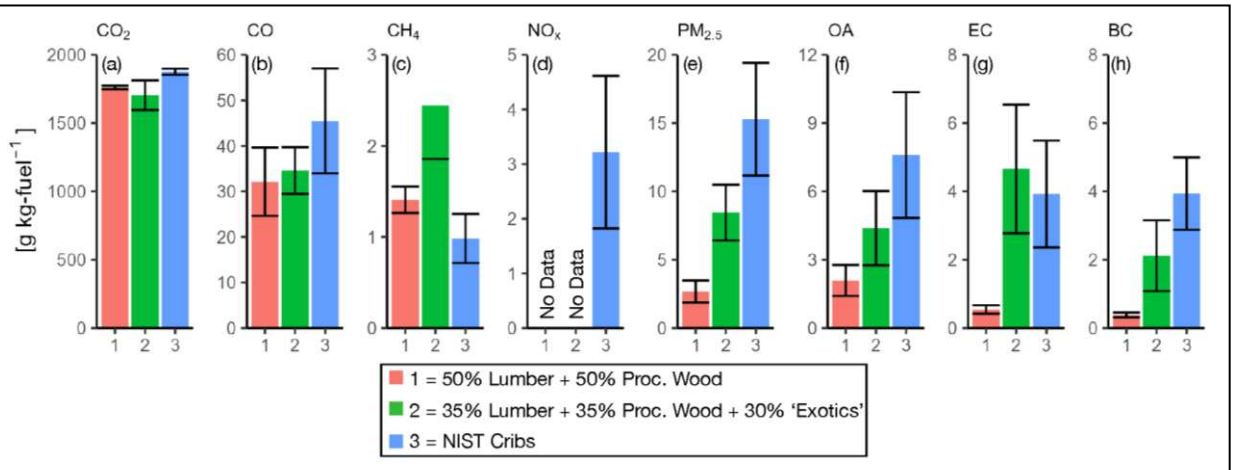

Figure 8: Median emission factors for three different model structures: (1) 50% lumber and 50% processed wood, (2) 35% lumber, 35% processed wood, and 30% exotics (modeled as carpet and 'Other' fuels), and (3) NIST cribs. Error bars represent data variability

While there are many reasons that make our work novel, there are admittedly several limitations. First, by studying structural material choices available today, our work is limited to explaining fire emissions from structures that will be built in the future. Residential homes in the US have an average age of ~40 years and nearly three-quarters of the US housing stock is more than 25 years old [27]. Accordingly, our results may not be directly applicable to many of the structure fires in WUI regions over the next several decades if emissions are expected to be a strong function of structural fuels used in different time periods. On the other hand, one of the advantages of studying the current generation of structural fuels is that insight from this work could be used to inform material choices for new construction in WUI regions. Second, even though we have studied structure fires at two different scales (~1 kW and ~500 kW), these are 2 to 5 orders of magnitude smaller than the scale for a fully developed house fire (~100 MW) [51]. There are numerous challenges in measuring emissions from a real structure fire, simulated or otherwise, that will likely require the development of aerial platforms and rapidly deployable technologies. Third, we observed modest experiment-to-experiment variability in our tests and an even larger variability in the EFs within each fuel category. Yet, this level of variability in the emissions data is not surprising as it mirrors the variability reported in the literature for open biomass burning. In fact, structure fire emissions in the real world are likely to be even more variable than presented here if we are to look at the literature for a similar source (e.g., cookstoves [52-53]).

Our work aligns with one of the outstanding objectives discussed in the Consensus Study Report published on the chemistry of wildfires at the WUI [5]. The data presented here should enable applications ranging from the development of emissions inventories for WUI fires to studying the toxicity of structural fuel emissions.

Acknowledgements

This work was primarily supported by the Atmospheric Chemistry, Carbon Cycle and Climate (AC4) program at the National Oceanic and Atmospheric Administration (NA22OAR4310537) and partly supported by the Atmosphere Cluster program at the National Science Foundation (AGS-2519789). We also acknowledge support from a National Science Foundation Research Experience for Undergraduates grant (2150387), which provided funding for a student researcher who contributed to this project. We thank Prof. Sergey Nizkorodov, Prof. Alexander Laskin, Prof. Allen Goldstein, and Prof. Joost de Gouw and two internal reviewers at NIST for reviewing the manuscript.

Notes

Certain commercial equipment, instruments, or materials are identified in this paper in order to specify the experimental procedure adequately. Such identification is not intended to imply recommendation or endorsement by the National Institute of Standards and Technology, nor is it intended to imply that the materials or equipment identified are necessarily the best available for the purpose.

Please refer to Appendix A for the mentioned supplemental information figures mentioned throughout Chapter 2.

CHAPTER 3: EXPLORATION OF VOLATILE ORGANIC COMPOUNDS PRODUCED BY STUCTURAL FUELS DURING COMBUSTION[2]

Chapter Overview

Volatile organic compound (VOC) emissions from structure fires remain poorly characterized despite growing concern about their contribution to air pollution in wildland-urban-interface (WUI) regions. To address this gap, VOC emissions were quantified during structure fire experiments conducted as part of the Burning Homes and Structural MAterials (BHASMA) project. More than 70 small-scale experiments were carried out at Colorado State University (CSU) in the summer of 2023 across 19 structural fuels and fuel mixtures representing common building materials. In addition, over 20 large-scale burns were performed at the National Institute of Standards and Technology (NIST) in 2024 using standardized fuel cribs composed of wood, gypsum board, and plastic components. Emissions were analyzed across both pyrolysis and flaming phases, resulting in the identification of over 70 unique VOC species. Synthetic materials—including insulation, flooring, and sheathing—produced elevated levels of hazardous air pollutants such as benzene, toluene, and styrene, which were largely absent in lumber-only combustion. Emission profiles varied with combustion phase and fuel composition but showed general consistency across fire scales. These results indicate that structural materials contribute to a distinct and toxic suite of VOCs, with important implications for human exposure, air quality modeling, and risk assessment in fire-prone WUI communities. Toxicological exposure

[2] 'In preparation' with permission from "Exploration of Volatile Organic Compounds Produced by Structural Fuels During Combustion (with respect to fire scales, combustion mode, packing density and fuel type)". Anna Helfrich, Kevin Ridgway, Amy Sullivan, Christian L'Orange, Shantanu Jathar

and risk are evaluated using VOC emissions in a Gaussian plume model. To assess emission evolution for varying wildland fire composition (wildland fire versus complete structural fire), the model varied ratios of biomass to structure combustible mass.

Introduction

Fires in the wildland-urban-interface (WUI)—zones where human development borders vegetated lands—are becoming more frequent and severe due to climate change and expanding human development into fire-prone areas [2]. While these WUI fires often damage or destroy residential structures, most emission research has still historically focused only on biomass fuels. Emissions from biomass combustion—such as carbon dioxide, methane, and particulate matter—are relatively well characterized [13], but much less is known about the emissions from combustion of structural materials. Data on gas-phase compounds like volatile organic compounds (VOCs) from structural fires is limited, despite the well-established human health and atmospheric impacts.

Volatile organic compounds are known to pose acute and chronic health risks through inhalation exposure [14]. There is also evidence of VOC contribution to the formation of tropospheric ozone and secondary organic aerosol production, affecting regional air quality [54]. Even at low concentrations, many VOCs can have health implications when inhaled. VOCs are estimated to account for approximately 15% by mass of total emissions from biomass combustion [12]; however, VOC emissions released from structural fires remain largely unquantified.

Most wildfire emissions studies have focused on a limited subset of VOCs, often benzene, toluene, ethylbenzene, and xylenes (BTEX compounds), due to their prevalence in petroleum products and emissions in urban air [55]. Benzene has a well-documented toxicity [56].

However, a wide array of other VOC species—many of which are combustion-phase dependent and fuel-specific—remain underreported. For example, biomass combustion has been shown to emit compounds such as α-pinene, isoprene, pentanes, and hexanes [14], indicating that relatively minimal changes in fuel composition (biomass to man-made) or combustion conditions can produce significant shifts in the VOC emission profile. This suggests that additional, potentially hazardous compounds may be present but undetected in standard monitoring frameworks.

Air quality measurements from over 700 sites across the United States indicate that combustion-related pollutants—including VOCs, particulate matter, and trace metals—consistently increased substantially over background levels during forest fires [7]. Although VOCs contribute a relatively small fraction of total emission by mass, their high toxicity and atmospheric reactivity make them an important element of exposure and environmental health assessments.

Pollutants are emitted in non-negligible quantities for both oxygen-rich and oxygen-deprived flaming wildfires, diversity in emission products correlates to combustion mode [25]. We can compare combustion modes by converting experimental information into (modified) combustion efficiency which gives insight into approximate percents of flaming or pyrolyzing (smoldering) [57]. If sufficient oxygen is supplied during combustion, the carbon available in the fuel ideally produces only carbon dioxide during the combustion reaction. In complete flaming combustion we expect to see elevated levels of carbon dioxide. Smoldering combustion leads to incomplete carbon oxidation, resulting in higher emissions of carbon monoxide (CO), particulate carbon species (organic, elemental and black carbon), and varying levels of VOCs.

Measurements from three wildfires and one prescribed fire in the northern Rocky Mountains revealed higher emissions for CO and methane (CH_4) alongside a decrease in carbon dioxide (CO_2) emission at lower combustion efficiencies, in comparison to previous studies [58]. Fire's combustion efficiency is expected to vary throughout the burn, being highly influenced by moisture, fuel content, and weather conditions [58]. Fluctuation of combustion conditions throughout a fire's lifetime indicates a need for characterization of emissions at extreme ends of the oxygen availability scale (i.e. fully flaming versus smoldering).

Insights from research on waste incineration may provide a useful parallel, as the combustion of household waste—often rich in plastics and synthetic materials—has been shown to produce a complex mixture of toxic emissions. Given that WUI fires frequently involve the burning of household contents and manufactured materials, findings from waste combustion studies can help predict the emissions behavior of man-made structural fuels during WUI fire events.

Waste to energy research has identified plastic as a primary source of pollution concern, this offers insight and interest into the plastics that combust during structural burns [59]. Plastic combustion emits mono and polycyclic aromatic hydrocarbons and chlorinated compounds [60]. Municipal solid waste incineration emits a broad range of toxic pollutants and has been linked to adverse health outcomes, regardless of the combustion technology employed [61]. Plastics are of high concern within structural wildfires, as more synthetic materials are being used in the construction of homes and home goods. Twelve to twenty six percent of a home's contents are plastic [5]. Based on waste incineration outcomes, it is expected that the burning of structural fuels alongside biomass during wildfires will introduce a new array of pollutants.

This study characterizes VOC emission profiles from a range of structural building materials combusted under controlled conditions designed to span the range of combustion environments

typical of forest and wildland-urban-interface (or wildland) fires. The experimental fuel matrix consisted of a mix of biomass (lumber and treated stock) and "exotics" (synthetic, man-made materials that are expected to be present in a home). Emissions were collected at oxygen-rich and oxygen-deprived combustion conditions across a range of fire magnitudes (1–500 kW) and fuel packing densities (simulation of varying ventilation conditions). The work was conducted as part of the *Burning Homes and Structural MAterials* (BHASMA) campaign—an experimental emissions study examining gas- and particle-phase pollutants from structural materials. This paper will present gas-phase VOCs and aims to address critical gaps in our understanding of structural fire emissions and supports ongoing efforts to assess the toxicological impacts of VOCs released during wildland fires.

Methods and Materials

A combination of small- and large-scale experiments were conducted to characterize VOC emissions from structural materials under a range of combustion and density conditions. The dual-scale approach allowed for controlled testing of combustion extremes—oxygen-rich and oxygen-poor scenarios—while also capturing the complex, fluctuating behavior typical of large-scale fires. Small-scale experiments allow easier control of the oxygen available to the system, while large-scale tests better approximate the variable dynamics and energy output of real-world fire events.

Small-scale fires (~1 kW): fuels and experiments

Small-scale experiments were conducted during summer 2023 at the Colorado State University (CSU) Powerhouse Energy Institute. A total of 80 experiments were performed using 20 individual fuels grouped into nine structural categories. Categories included carpet, electrical wiring, plumbing, laminate flooring, insulation, processed wood, siding and structural wood.

Most experiments involved burning individual fuels, while several “complex wood” trials involved mixed wood and composite materials to simulate more realistic structural fuel scenarios.

Testing was conducted under a total capture emissions hood with sampling duct. A sampling system drew from the duct. Combustion of materials below the hood was carried out in an electrical resistance furnace (Watlow VC408A06T-0001R). Two combustion conditions were tested:

Oxygen-rich (flaming) achieved using a hydrogen-fueled diffusion burner to initiate burning.

Oxygen-deprived (pyrolysis/smoldering) simulated by introducing nitrogen as a purge gas to reduce oxygen availability with thermal decomposition driven using the furnace.

Fuel samples were placed in mesh baskets suspended from a precision scale and lowered into the furnace. Emissions were drawn into an exhaust duct with samples then collected using a sampling train designed to collect both gas-phase and particle-phase pollutants. Combustion energy for these tests was limited to approximately 1 kW. Ten background air samples were collected throughout the sampling campaign to establish baseline laboratory conditions. Further details are available in ‘Emissions from Structure Fires: Overview of BHASMA and Results for Select Pollutants by Fuel, Combustion Mode, and Scale’ [62, Chapter 2].

Large-scale fires (~500 kW): fuels and experiments

Large-scale fire experiments were performed in the summer of 2024 at the National Fire Research Laboratory (NFRL) on the National Institute of Standards and Technology (NIST) campus in Gaithersburg, Maryland. The investigation of complex (mixed) fuel experiments was represented by a stacked cubic fuel matrix, known as cribs. Six crib configurations were used for

500 kW burn experiments. The crib configuration was determined by size (large or small, 47.5x47.5x45.7cm or 30x30x28.6cm, respectively) and packing density of stacked fuels (low, medium, high). By weight, cribs were 21% spruce pine fir, 15% oriented strand board (OSB), 46% gypsum board, 7% polyvinyl chloride (PVC), 6% polyurethane (PU) and 5% acrylonitrile butadiene styrene (ABS). The mass percentage for all crib variations was consistent. The crib composition was designed to be representative of a single-family home's composition of wood, drywall, and plastics. Burns were conducted under a 500 kW capture hood, and cribs were placed on a scale to record real-time mass loss over experiment duration. A more detailed investigation of crib material and construction can be found in 'Burning Characteristic and Smoke Emission from Mixed Fuel Cribs' [35]. Like the small-scale fire experiments, a gaseous- and particle-phase sampling system took isokinetic samples of emissions off the duct. Cribs were ignited using EZFire fire starters, lit with a propane torch, that were spread and emptied across the top layer of material, the number of fire starters varied with crib size. In total, 25 experiments were conducted, and 6 background samples were taken.

Gaseous (VOC) measurements and analysis

Volatile organic compounds (VOCs) were quantified using two complementary approaches: (1) SUMMA canisters for whole-air sampling and (2) 2,4-dinitrophenylhydrazine (DNPH)-coated sorbent cartridges (SKC 226-30-06) for carbonyl compound characterization.

DNPH Cartridge Sampling and Analysis: DNPH cartridges were extracted with 3 mL of acetonitrile using a vacuum manifold, followed by the addition of 2 mL of acetonitrile to reach a final extract volume of 5 mL. The extracts were analyzed by high-performance liquid chromatography (HPLC) equipped with a UV detector (Agilent 1260 Infinity), monitoring absorbance at 360 nm—corresponding to DNPH-derivatized carbonyls. Chromatographic

separation was performed using a Waters Nova-Pak C18 4 μm column. The mobile phase consisted of two eluents: (A) 60% deionized water / 30% acetonitrile / 10% tetrahydrofuran, and (B) 40% water / 60% acetonitrile. This method follows protocols similar to those described in Bilsback et al. (2019), Fedak et al. (2018), and Van Zyl et al. (2019) [28, 29, 63]. Limit of detection (LOD) for the carbonyls is approximately 0.1 $\mu g/m^3$.

Canister Sampling and Analysis: Canister samples were analyzed using a five-channel Shimadzu GC-17A gas chromatograph with multiple detector-column pairings. Three channels were configured with flame ionization detectors (FIDs) paired with CP-AL_2O_3/Na_2SO_4 PLOT, VF-1ms, and CP-PoraBond Q columns. One channel was coupled with an electron capture detector (ECD; results not used), and one with a mass spectrometer (MS) via an OV-624 column. Prior to injection, sample air was pre-concentrated in a glass bead trap submerged in liquid nitrogen. After thermal desorption, helium served as the carrier gas to transfer analytes through the chromatographic columns. In the MS channel, compounds were separated based on their retention times and identified by their mass-to-charge (m/z) ratios. In the FID channels, analytes were combusted to form ions, and their concentrations were determined based on the ion-generated current. These methods align with previous analyses described in Sive (1998), Russo et al. (2010), and Zhou et al. (2010) [64, 65, 66]. LOD corresponded to an individual VOC, ranging anywhere from 0.02 pptv to 0.006 ppbv. The measurement precision (relative standard deviation of peak areas) for each compound in the whole air standards were 3-15% for halocarbons, 1-8% for the non-methane hydrocarbons, 3-8% for the alkyl nitrates, 3-5% for the sulfur compounds and 8-10% for the oxygenated VOCs.

Calibration and Limitations: For both the canisters and cartridges the instrumentation is calibrated using sample solutions of known analytes and their corresponding known

concentrations. The standard analyte is processed by instrumentation, agreement between results and documented concentrations produce the calibration curve. The developed curve is used to identify analytes while processing experimental samples. Instrumentation is limited to previously performed calibrations of specific analytes. This means the instrumentation is restricted to quantifying VOCs that have established calibration curves. Unknown compounds detected by the diode would not be able to be accurately determined.

VOC samples during the large-scale experiments were collected using only the SUMMA canisters, while the small-scale experiments used both SUMMA canisters and the DNPH cartridges. Detected VOCs were grouped into seven chemical families based on molecular structure: carbonyls, alcohols, alkanes, alkenes, aromatics, biogenics, and chlorinated compounds. Approximately 70 unique species were identified across these categories. Carbonyl compounds (~15 species) were primarily measured using sorbent cartridges, while SUMMA canisters were used to quantify the remaining compound classes (~55 species). Background "blank" experiments—where no fuels were combusted, but air was pulled through the sampling system—were conducted to support background correction and ensure data quality.

Trends in criteria pollutant concentrations serve as valuable indicators for predicting emissions and can inform analyses of VOC emissions. Because these species are often co-emitted during combustion, their concentration patterns can reflect shifts in combustion efficiency or source strength, providing indirect insight into VOC emission behavior. In BHASMA, CO_2, CO, and CH_4 mixing ratios were measured in real-time using gas analyzers. Concurrently, particulate matter ($PM_{2.5}$) was collected on polytetrafluoroethylene (PTFE) filters and quartz for subsequent analysis. The filter samples were analyzed to quantify $PM_{2.5}$ mass and chemical composition, including inorganics, black carbon (BC), elemental carbon (EC), and

organic carbon (OC; which can be converted to organic aerosol, OA, by accounting for carbon and hydrogen with a conversion factor). The characterization of primary criteria pollutants of structural WUI materials was outlined previously in 'Emissions from Structure Fires: Overview of BHASMA and Results for Select Pollutants by Fuel, Combustion Mode, and Scale' [62, Chapter 2]. Outcomes from the previous study suggested a focus on criteria pollutant trends may be useful in drawing conclusions about VOC emissions.

This work extends prior analyses by focusing on VOCs, using emission factors to quantify their contribution to structural fire emissions. Emission factors represent the mass of compound (pollutant) per mass of burned fuel, Equations 3.1 and 3.2, which provides a convenient way to quantify the composition and quantity of released pollutants. Another metric which provides valuable insight into combustion characteristics is combustion efficiency (CE), Equation 3.3, and variant of it, modified combustion efficiency (MCE), Equation 3.4. Combustion efficiency and modified combustion efficiency are expressed as the fraction of carbon emitted as CO_2 relative to total carbon emissions. MCE includes only CO and CO_2, while CE, in this publication, also accounts for carbon contributions from VOCs, CH_4, EC, and OC. During flaming combustion, relatively high complete combustion would be expected, meaning most carbon would emit in the form of CO_2. When combustion is incomplete or smoldering occurs, remaining carbon does not fully oxidize or combust, generating non-CO_2 carbon-containing pollutants.

Equations 3.1 and 3.2: Emission factor [g kg-fuel^{-1}] and cumulative carbon contribution

$$EF_i = \frac{M_i}{C_{eff}} x f_C x 10^3$$

$$C_{eff} = (\Delta CO_2 + \Delta CO + \Delta CH_4 + \Delta VOC) x \frac{P}{RT} x MW_C + \Delta EC + \Delta OC$$

Where M_i is the mass concentration of the species, f_c is the carbon fraction of the fuel and C_{eff} is the cumulative carbon contribution. Carbon fractions were obtained through literature review or ultimate analysis of fuel. The cumulative carbon contribution is a mass concentration ($\mu g/m^3$), where CO_2, CO and CH_4 are the background corrected mixing ratios (ppm), VOC is the corrected mixing ratio for all VOCs measured (ppm). Ppm concentrations are converted to μg/m3 using atmospheric pressure P (Pa), sample temperature T (K), the gas constant R (8.314 J/mol-K) and the molecular weight of carbon, MW_c. EC and OC are quantified in $\mu g_{carbon}/m^2$, then converted to concentration using filter diameter (final units of $\mu g_{carbon}/m^3$).

Equation 3.3: Combustion efficiency [units of %]

$$CE = \frac{\Delta CO_2}{\Delta CO_2 + \Delta CO + \Delta CH_4 + \Delta VOC + \frac{\Delta EC + \Delta OC}{\frac{P}{RT} x MW_C}}$$

Equation 3.4: Modified combustion efficiency [units of %]

$$CE = \frac{\Delta CO_2}{\Delta CO_2 + \Delta CO}$$

Equations 3.3 and 3.4 calculate combustion efficiency based on the cumulative carbon contributions from CO_2, CO, VOCs, CH_4, and particulate carbon (soot). In principle, complete combustion would convert all fuel carbon to CO_2, making combustion efficiency a key indicator of combustion completeness.

Results from the BHASMA study were compared to the Smoke Emissions Reference Application (SERA) [45], a database for wildfire emissions compiled from a variety of sources (i.e. experimental, prescribed burn, wildfire, laboratory). Comparison to SERA results provides an opportunity to understand where BHASMA results agree or differ from historical data.

Calculations from the SERA database have varying methods for EF and MCE, as SERA is a collection of multiple experimental campaigns, laboratory work and ambient measuring. Around forty of the seventy VOC species collected during the BHASMA study have corresponding results from the SERA data set.

To help identify emissions patterns, fuels were grouped into five generalized categories—lumber (untreated wood), processed wood (treated or engineered wood), carpets, other synthetic materials, and cribs (from the large-scale campaign). These categories are referred to as “fuel groups” in the remainder of the document.

Plume Model

The potential for residents to be in close proximity to active fires in the WUI means that emission factors alone are insufficient; potential human exposure depends on resulting ambient concentrations. Exposure to emissions containing high VOC concentration presents the possibility of negative toxicological health effects. A Gaussian plume model was used to estimate how emissions will disperse and diffuse downstream of a WUI fire. An emission source rate (in grams of pollutant per second) was established by combining experimentally determined EFs with literature-based estimates of fuel-loading and fire activity rates. Forest fuel density values (tons per hectare of forest) were obtained from Woodall, Perry and Miles (“The Relative Density of Forests in the United States”, 2006) which provides estimates of forested areas across the US [67]. These values were used to estimate the amount of combustible material per acre for wildfire scenarios. For Northern Colorado the respective forest density was ~125 tons per hectare.

Fire behavior data was taken from the National Interagency Fire Center's Fire Perimeter database, which includes fire area (in acres) and ignition/extinguishment times for fires across the United States [68]. To focus on wildland conditions, the dataset was filtered to exclude

prescribed burns and fires dominated by non-timber fuels (e.g., grass, shrubs). After removing outliers, fire duration and area data were used to calculate the average rate of fuel consumption (in acres burned per hour). The resulting average fuel consumption rate was 1.12 acres consumed per hour.

An emission source rate was obtained by multiplying EF, relative density, and acres consumed per hour (grams of fuel per hour), assuming steady state conditions. This variable was then fed into a Gaussian plume function in RStudio [69]. Additional model parameters include wind speed and effective emission height. To characterize atmospheric conditions, a Pasquill-Gifford constant is selected (A-G), which represents the stability of different wind speeds, solar radiation, cloud cover, convection and mixing [70]. The Pasquill-Gifford stability was set to 'D' representing neutral atmospheric and mixing conditions (modeling across multiple days, conditions are constantly stochastic).

The model was intended to evaluate how downwind VOC concentrations vary with changing fire composition, specifically as structural material contributions increase. To establish a baseline emission rate representing a real wildland fire, model parameters were calibrated using $PM_{2.5}$ measurements from the 2012 High Park Fire. The High Park Fire had minimal structural involvement, despite high acreage affected (~260 structures destroyed and 87,284 acres burned) [71]. This tuning allowed the model to reflect realistic fire behavior and emission dispersion under known conditions. Model inputs were tuned using historical wind speed (at 50 meters) data from coordinates close to the High Park Fire (June 9^{th} – 30^{th} of 2012, Fort Collins, Colorado). An average wind speed from the 21 days of the fire was used, 5.23 m/s [72]. Relative emission source height was set to 50m to be in line with wind data. Recorded particulate matter data from the local EPA Fort Collins's monitor was averaged across the fire's 21-day period, 13.8

$\mu g/m^3$ [73]. Modeled $PM_{2.5}$ (median of lumber results from small-scale campaign used to represent wildland emissions) was observed at the approximate monitor location with respect to the fire's coordinates. The burn rate (acres per hour) was adjusted until plume results were within 1% of recorded results. The adjusted burn rate was used for further analysis of VOCs in the plume model. The burn rate was adjusted from the calculated 1.12 acres per hour to 3 acres per hour, with recorded and modeled $PM_{2.5}$ at the location of the measurement reading ~13 $\mu g/m^3$. Before tuning the burn rate, the resulting $PM_{2.5}$ reading was ~5 $\mu g/m^3$, which was already within a factor of 5%. The remaining variables (forest density and Pasquill-Gifford rating) remained unchanged. The plume model assumes steady state conditions. Concentration results from the plume model were measured across a grid that simulated 1500 meter in both vertical directions (y-axis) and 30000 meters horizontally (x-axis) away from the point source. All concentrations were measured at a height in the z-plane of 1.8 meters, about the height of an average American male [74].

Subsequent simulations systematically altered the emission profile by varying the proportion of structural material burned. Five fire composition scenarios were modeled, ranging from 100% biomass (all wildland) to 100% structure fire. These scenarios capture the transition of purely vegetative to structure-dominated fires. Allowing baseline assessments of how structural contributions could influence VOC concentrations downwind of a fire source. This model is not intended to simulate a specific fire event, but rather to examine how changes in the fraction of structural materials influence VOC emissions and resulting downwind concentrations. The goal is to illustrate potential exposure differences associated with varying combustion mixtures, providing insight into the range of conditions that might be encountered during WUI fires.

A standardized “house EF” was developed using individual fuel results from the small-scale campaign to represent a typical home’s combustible mass composition. Individual fuel EFs were scaled by percentages representing the relative contribution of each material to the total combustible mass of a structure. The mass contributions were allocated as follows: 92% for structural and home content wood (lumber and processed wood), 2% for asphalt shingles, 4% for home content plastics (carpets, PVC, vinyl flooring, etc.), and 2% for structural insulation (PUF and XPS) [5].The median emission factors from flaming-phase experiments for each respective fuel were weighted by their estimated structural mass contributions and summed to produce the composite “house EF.” The small-scale campaign’s lumber results were used to represent emissions of a wildfire containing only vegetation (wildland). The “house EF” serves as the 100% structure fire scenario and the lumber emissions serve at the 100% wildland fire scenario. Plume modeling gives insight into the spread of smoke outside of fire perimeters which has the potential to cause toxicological harm and should be considered during firefighting, evacuation and safety procedures.

The Photochemical Assessment Monitoring Stations (PAMS) reports average concentrations of VOCs. We use points from the 2024 average data from a monitoring location near Boulder, Colorado are used to provide context for typical ambient VOC concentrations for available species [75]. Permissible exposure limits (PELs) are the established exposure standards for workplaces [76], all PELs will typically exceed ambient VOC concentrations by a couple orders of magnitude. Species used for comparison are benzene, styrene, toluene, propane, ethane, acetylene and acetaldehyde.

Results

Data cleaning

Experimental results were background-corrected by subtracting the median of blank samples collected during the same campaign and under matching experimental control conditions. In some cases, background corrections were greater than the results from an experiment; in these cases, experiments were excluded from analysis. There was suspected contamination due to use of cleaning products and/or experimental mishandling during the small-scale campaign. Experiment hardware was cleaned between campaign days with a mixture of acetone, dichloromethane and hexane followed by a rinse of deionized water. Other pieces of equipment (i.e. tweezers, surfaces, small instruments) were wiped with isopropanol alcohol wipes. Within background samples high concentration of isopropanol, n-h exane, chlorinated compounds, and acetonitrile were identified. As a result, there is suspected contamination due to cleaning products that resulted in the removal of species from further analyses. Figure 9 and related figures Appendix B, Figure B1-B2, are the blank mixing ratios next to experimental mixing ratio results prior to performing background corrections for flaming combustion.

Acetone and acetaldehyde were measured using both canister and cartridge methods. For consistency, the canister-based results were used in further analysis, as this method was employed for the majority of VOC quantifications. It is acknowledged that differences between analytical methods may lead to variability in reported concentrations.

Species selection and experimental variability

Nine VOC compounds were selected for the primary analysis: benzene, toluene, styrene, ethane, ethene, acetylene, acetaldehyde, propene and propane. The full data set for all

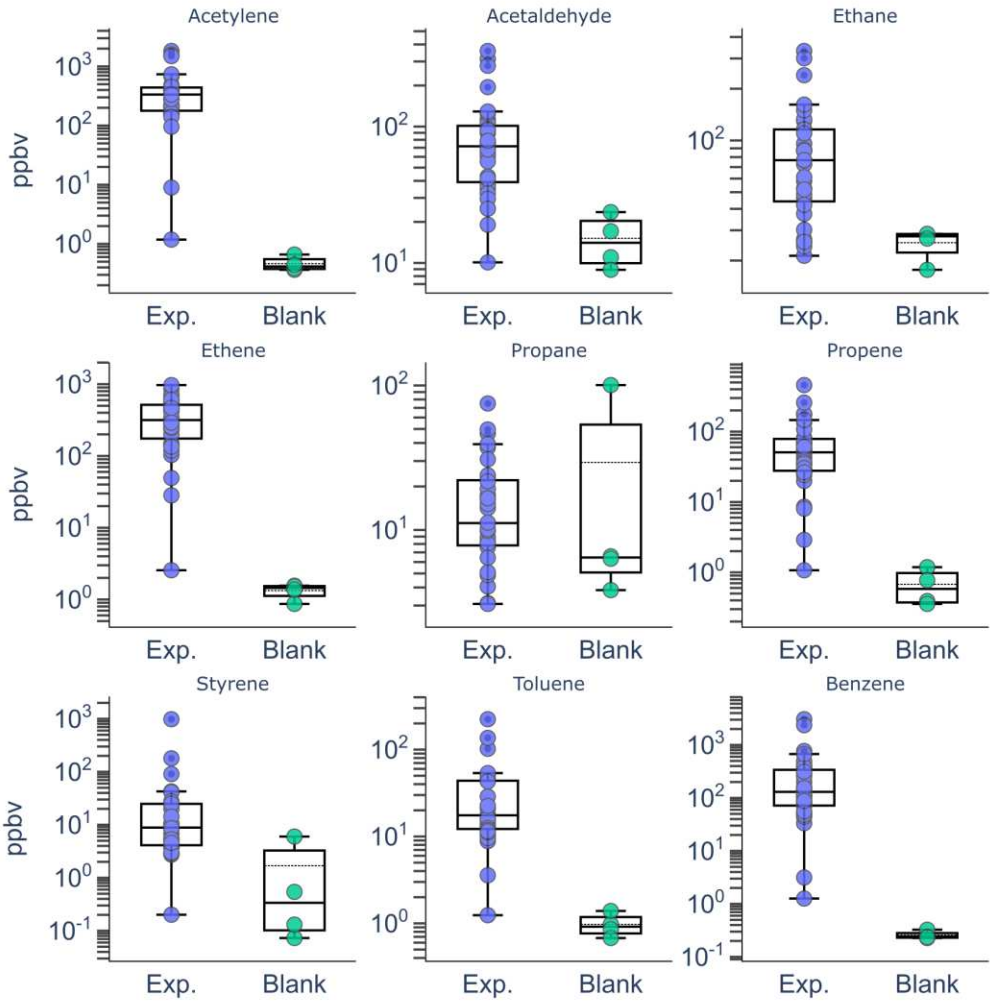

Figure 9: Blank versus experimental mixing ratios for select VOC species under flaming combustion conditions for the small-scale campaign. Raw experimental results in left column and colored blue, note that concentration values are plotted prior to background correction. Blank experiment in right column and colored green. Over both columns are statistical boxplots where solid black line within boxplot is the median and dashed line is the mean.

compounds is available in supplemental information. VOC selection was based on each species' contribution to cumulative emissions. Median EFs from the small-scale campaign were calculated by combustion mode, then ranked from highest to lowest. A cumulative contribution was computed in rank order to identify the most prevalent species. This approach prioritizes compounds emitted in large quantities, under the assumption that they have a greater impact on

overall emissions. The top ten contributors from pyrolysis and flaming represented 79% and 86% of the total concentration of measured VOCs emitted (with overlap between top species for both combustion modes).

Due to shifting instrumentation used between both the large- and small-scale campaigns, the carbonyl VOCs (primarily quantified using sorbent tubes from small-scale campaign) did not have measurements for the large-scale campaign. For both combustion modes one to three carbonyls were ranked highly in cumulative contribution but were removed from the detailed analysis, as a priority of analysis was comparison across fire scales. More detailed analysis was then performed for the top ten to eleven cumulative contributors. The final selection of nine primary VOCs was narrowed down to most unique and notable emission trends, resulting in the removal of acetone and trans-2-butene from the primary figures. Figure 10 and corresponding appendix figure, Appendix B Figure B3, are the cumulative distributions with top ranking carbonyls removed for both combustion modes. The detailed analysis began to outline signature VOC species for exotic fuel materials, providing true insight into how structural fuels impact overall emissions. Using data from the small-scale campaign allowed unique identification of species on a fuel basis to then be confirmed with the large-scale campaign's combined fuel experiments.

For the small-scale campaign, experimental variability was assessed using fuel materials (Southern Yellow Pine (SYP), Oriented Strand Board (OSB), and Polyester) that had been tested in triplicate under both flaming and smoldering combustion conditions.

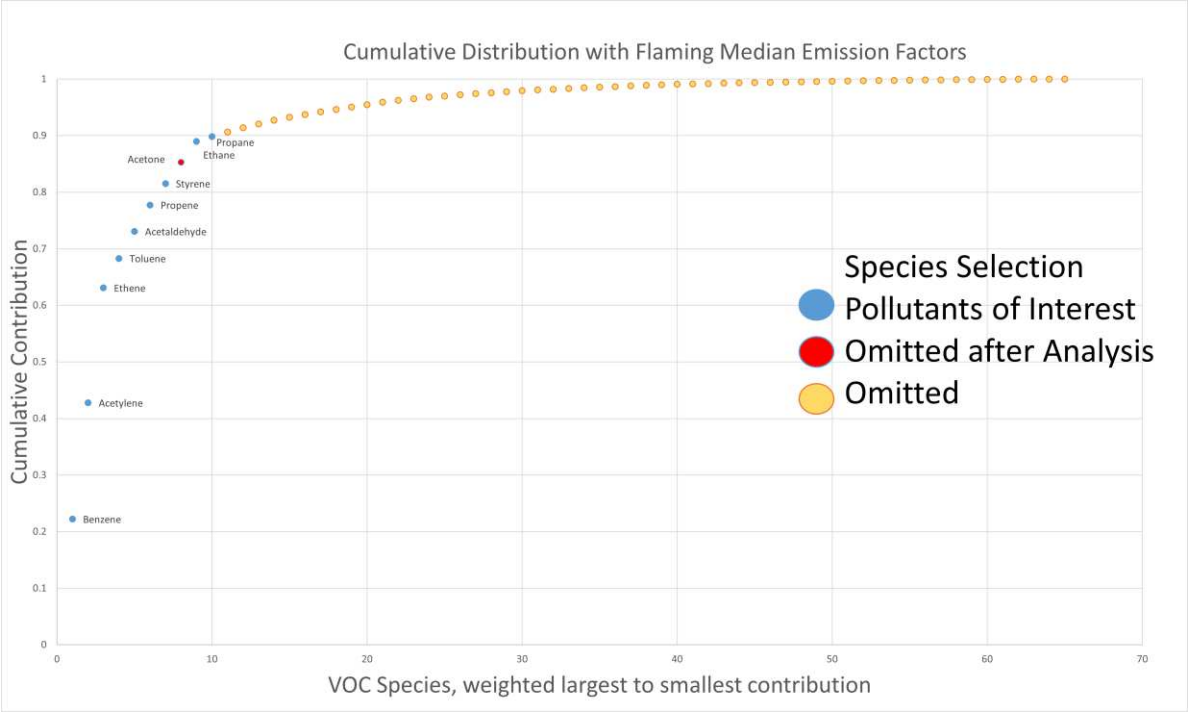

Figure 10: Cumulative distribution for flaming combustion mode. Species selected for primary analysis colored in blue, with post-analysis removal done for species in red. All species in yellow have considerably lower cumulative contribution and were removed from the detailed primary analysis.

Figure 11 illustrates this variability on a species-specific basis, where the average EF for each VOC is plotted on the x-axis and individual EF results on the y-axis. This visualization allows for evaluation of the spread in measured emissions relative to the mean. Across all small-scale measurements, 89% of individual VOC emission factors fell within a factor of two of the average, and 95% fell within a factor of three. On the OSB variability plot, there are four considerably low magnitude EFs from benzene, acetaldehyde, propene and ethene. All points belong to the same experiment, and it has been determined that this outlier is a resultant of experimental error. However, the exact error source is not determined and therefore the point remains in the dataset for transparency. The same outlier is plotted in the following figures. The

VOCs containing the outlier point are all greater than a factor of 25 away from the average EF.

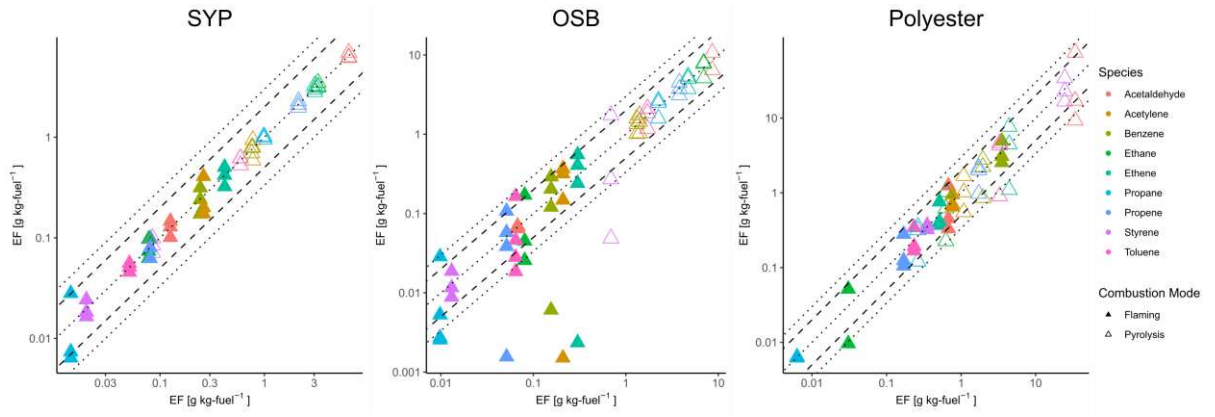

Figure 11: Variability across SYP, OSB, and Polyester small-scale campaign experiments. Figure highlights bias between results resolved by VOC and combustion mode basis, where x-axis is average EF and y-axis is individual result. VOC species is dictated by color and fill of triangle determines the combustion mode.

Combustion Efficiency

Figure 12 displays a subset of the VOC dataset, graphing EF versus CE. For comparison, gray dots present data from the SERA database. Although MCE and CE differ slightly, values are generally comparable, particularly for the high combustion efficiencies seen during flaming experiments. Most SERA points fall above an MCE of 0.8, typically considered the lower bound for active wildfire biomass combustion [77], making the comparison appropriate. Emissions from the large-scale crib experiments are also overlaid as black points and are categorized as flaming burns, with all CE values exceeding 0.87.

An inverse relationship is typically seen between EF and CE as combustion efficiency decreases, VOC emissions typically increase (omitting CO_2 and NO_X trends, [62, Chapter 2]). Under pyrolysis conditions, distinct trends between emissions and fuel group are difficult to discern. In contrast, flaming conditions show more distinct separation between biomass-based fuels and synthetic materials, with aromatic compounds such as benzene, toluene, and styrene

displaying emission factors up to two to three orders of magnitude higher for synthetics.

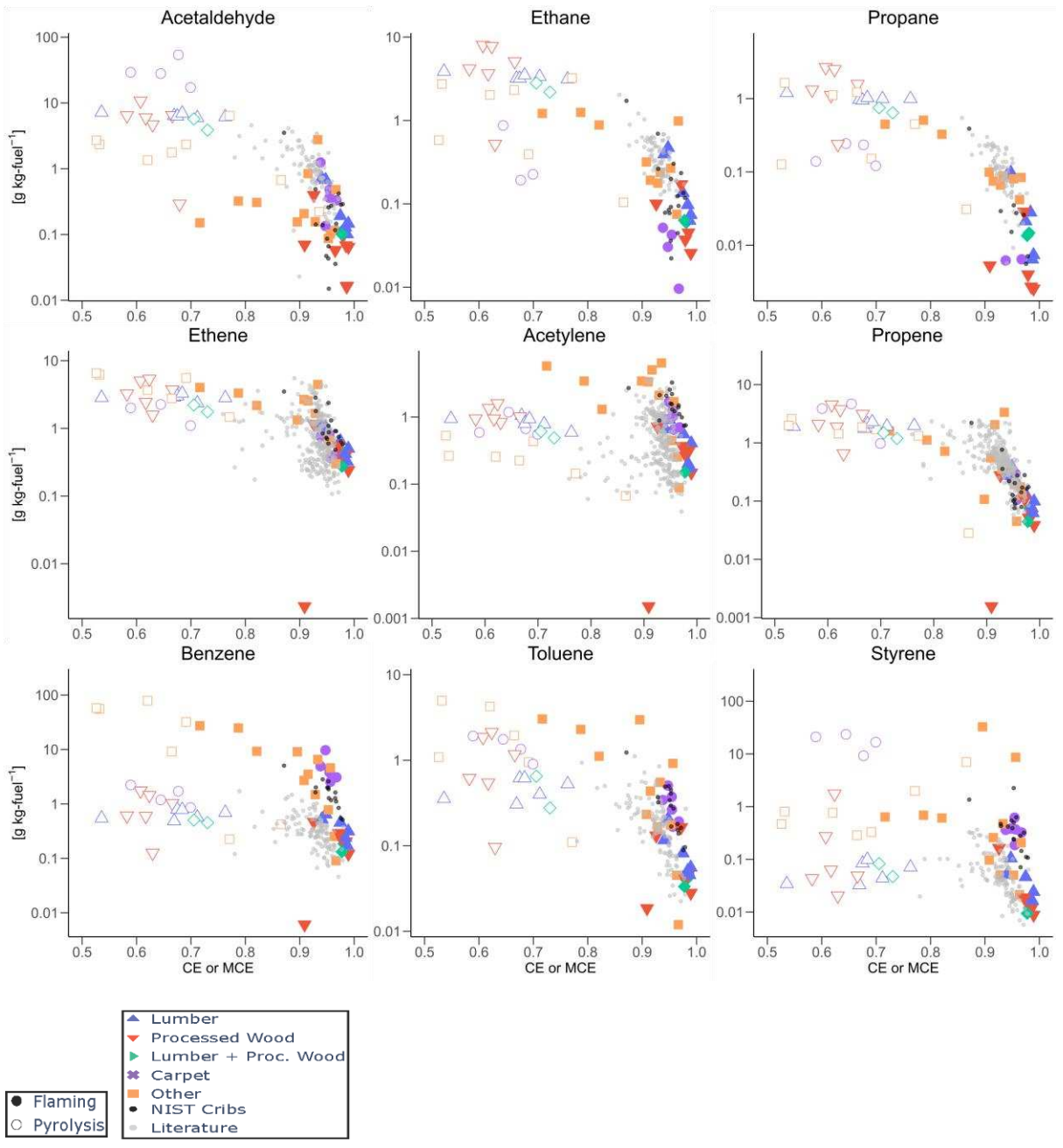

Figure 12: Emission factors versus combustion efficiency (SERA results versus modified combustion efficiency) for primary VOCs of interest. Results from large-scale tests (~500 kW) presented as black dots. Shapes and colors (separated by fuel group) used for small-scale (~1 kW) tests. Filled shapes for flaming combustion. Outlined shaped for pyrolysis combustion. SERA emissions inventory presented as grey dots.

Within the wood fuel categories, flaming combustion produces similar EFs for both lumber and processed wood across most VOCs. Under pyrolysis, there is more variability in CE across these groups, but EF magnitudes remain relatively consistent. Among synthetic materials, the carpet group exhibits less variability in both EF and CE compared to the 'Other' synthetic category, which includes a broader range of materials such as PVC, wiring, insulation, and shingles. This variability is likely attributable to compositional heterogeneity within the 'Other' category.

At high CE, some unintuitive trends are seen. Due to the synthetic composition of fuels from the “Carpet” and “Other” groups, it is expected that VOC EFs will be greater than biomass emissions. Yet, in ethane and propane the EFs for carpets and a few exotic fuels were within the same magnitude or of lower value than the lumber and processed wood results. In these cases, the small magnitude of emissions from exotics is not the key finding but rather points to an emission that is more signature of woods.

The cribs are considered as flaming results as the minimum CE measured was 0.87, well within flaming region. VOC emission factors for the crib burns often fell between those seen for wood and exotic fuels from the CSU burns – this makes sense as the cribs were comprised of a mix of wood and plastic fuels. Data from SERA provides the ability to see how emissions trend with historical data. Most data points from SERA were collected at slightly lower MCE than the flaming experiments, but SERA data trends with the flaming fuel groups. The variance between EFs from SERA and BHASMA experiments for certain species like benzene and styrene help predict that structural material emissions will not mirror emissions from biomass-based fire events. In general, within the flaming regime there is an ability to delineate between emission

factors from various structural fuels. A complete predictability of EF using CE is not viable due to the uniqueness of fuel composition across fire events.

Emissions by fuel group

Figure 13 presents EFs by fuel and combustion mode for select pollutants. Statistical boxplots were not used for the 'Other' fuel group due to large data spread and the relatively small sample sizes for the individual fuels. The large-scale crib burns are included as a separate fuel group and plotted alongside the small-scale results. Additionally, the "complex wood" trials from the small-scale campaign are overlaid across both the lumber and processed wood categories to illustrate their compositional relevance to both groups.

SERA data is shown as a gray bar, representing the mean plus or minus one standard deviation for each compound. For highly variable species such as styrene, where the standard deviation exceeded the mean, the lower bound of the SERA colored bar is extended to zero, with negative values removed for clarity. While the SERA data exhibits a wide range of values across species, most fall between the flaming and pyrolysis results from this study, supporting the interpretation that the experimental conditions effectively bracket the range of combustion behavior observed in real-world fires.

Figure 13 supports the conclusion that pyrolysis conditions generally produce higher VOC EFs than flaming combustion. In one specific case, the flaming carpet EFs from benzene are higher than pyrolysis. We hypothesize this is because the burning of plastics often can leave behind a residual material that does not fully combust. Meaning the heating and smoldering from pyrolysis does not provide enough heat to release a full benzene ring.

Emission factors from the crib burns typically fall between those of biomass and synthetic fuels, reflecting their mixed material composition. The emissions being book-ended by those

seen for the individual fuels support the interpretation that crib burns represent a realistic composite of residential structural fuel emissions.

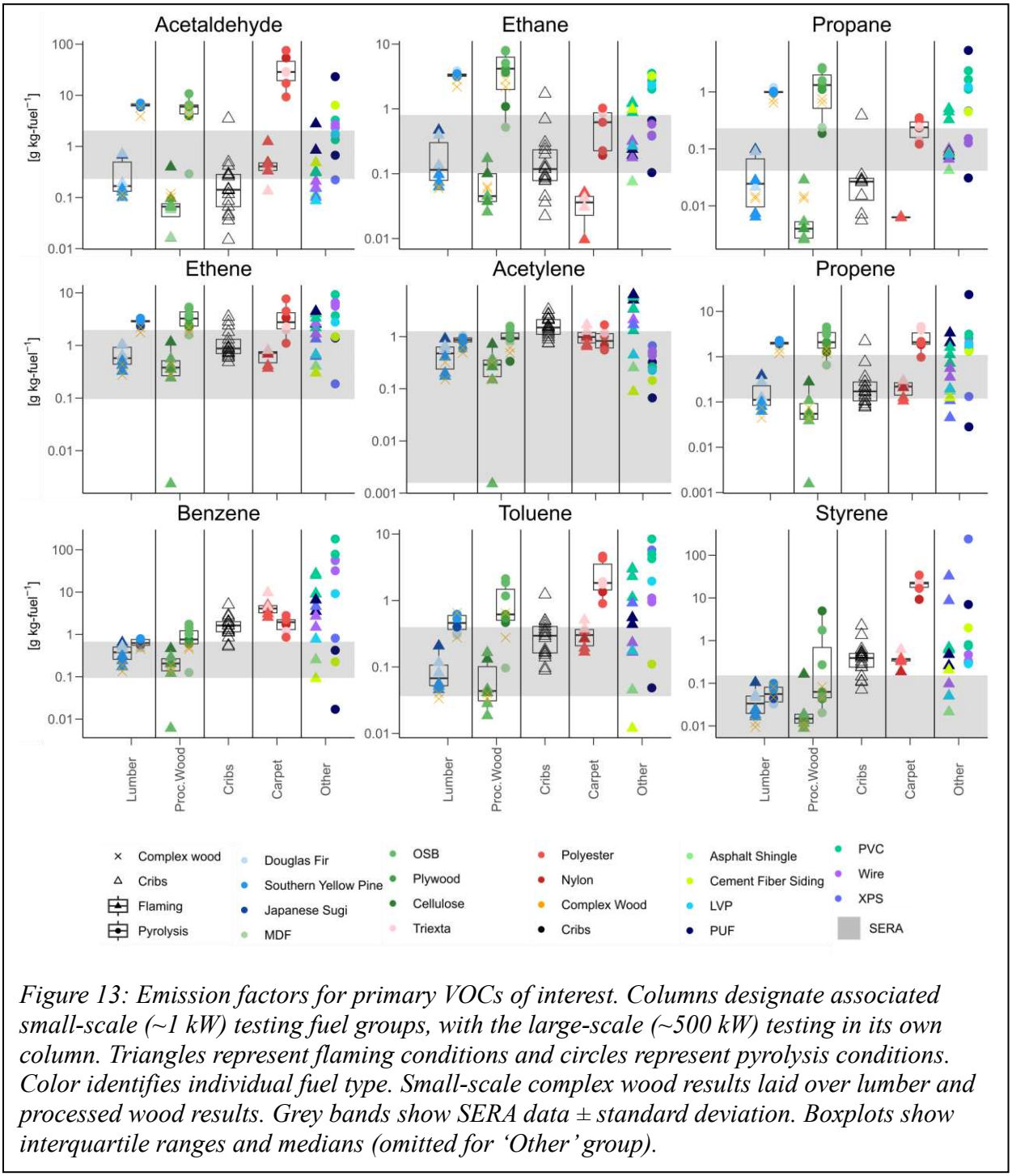

Figure 13: Emission factors for primary VOCs of interest. Columns designate associated small-scale (~1 kW) testing fuel groups, with the large-scale (~500 kW) testing in its own column. Triangles represent flaming conditions and circles represent pyrolysis conditions. Color identifies individual fuel type. Small-scale complex wood results laid over lumber and processed wood results. Grey bands show SERA data ± standard deviation. Boxplots show interquartile ranges and medians (omitted for 'Other' group).

Across fuel groups, signature VOC emissions are more apparent. In species like ethene, acetaldehyde, propane, and propene, the EFs between fuel groups (biomass and synthetic) for each combustion modes were close to identical, with minimal statistical spread or high exotic fuel outliers. In species where EFs from multiple fuel groups do not exhibit spread, structural materials will not create a significant or recognizable difference in measured emissions from biomass fires.

There are distinct differences across woods and exotic fuels in species like benzene, ethane and styrene. The aromatic species' emissions for synthetic fuels, specifically insulation, wiring, polymer-based fuels and carpets, produced EFs up to three magnitudes greater than woods. This indicates that certain exotic materials produce unique and notable VOC emissions. In the 'Other' group some cases had even greater EFs than carpets (often observed from PUF, PVC, wire, and XPS). It is expected that due to similar material origin (plastics and polymers), carpets, wiring, insulation and piping will produce similar signature emission fingerprints. A collection of primary observations is stated next. Benzene and toluene (both in the BTEX family) show higher emissions primarily from PVC and wire (PVC jacketing), as well as PUF and XPS. Within the styrene emissions, the results from carpet and XPS are two to three orders of magnitude higher than woods (very pronounced with pyrolysis but less so for flaming). Ethane is unique in the fact that it is the one of the only species with high magnitude wood EFs, though the cement fiber siding board, luxury vinyl plank (LVP) and PVC flaming results are more striking in their magnitude compared to other synthetics. Like benzene, flaming acetylene results for PUF, PVC and wire EFs were higher than their pyrolysis counterpart, but there is consistent clumping with little difference between combustion modes for the other fuel groups. While the ultimate magnitude of VOC species can be almost 1000 times less than that of carbon dioxide or

particulate matter, the introduction of toxic species from structural emissions in comparison to biomass emissions can be claimed. Small concentrations of VOC exposure should not be overlooked.

Figure 14 shows a broken-down contribution of the exotic fuels from the "Other" fuel group with processed wood, lumber, and carpet as reference. The values on the radar plot depict the median EF in g_species/kg_fuel for the exotic species across the nine primary VOCs. The left plot is flaming combustion experimental results, and the right plot is pyrolysis combustion experimental results. This plot provides slightly more resolution to the 'Other' fuel group column from Figure 13. Giving an idea of how individual synthetic materials compare against

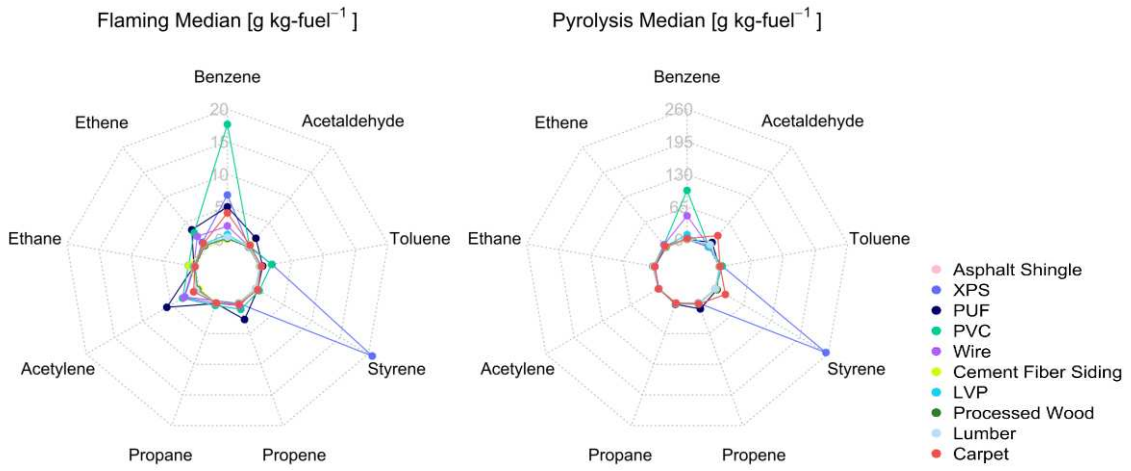

Figure 14: Relative contribution of emission factors from individual fuels falling within the 'Other' fuel group. Each value depicts the median emission factor for flaming and pyrolysis combustion conditions from the small-scale campaign. Color denotes fuel material.

one another and their emission magnitudes. For both combustion modes the notable results for both benzene and styrene are now resolved on an individual fuel scale basis. XPS, PVC, and PUF appear to be dominant in the contribution of median flaming emissions. Refer to Appendix B, Figure B4 for log-scaled radar plot axes.

Gaussian Plume Model at Varying Structural Emissions Contributions

The Gaussian plume results provide a general baseline for VOC concentrations as they travel downwind of a fire source. While the cloud that travels away from a fire is typically visible, the depth and reach of the smoke is not clear to the visible eye. The plume model depicts a generalized prediction of gaseous concentrations at human height.

Presented in Figure 15, concentrations were taken on the centerline of the plume from zero to 30 kilometers downwind of the fire, for each of the wildland to structural emission ratio scenarios. The maximum VOC concentrations in the plume do not occur directly at the fire source (0 km) because concentrations are modeled at a height of 1.8 meters, representing human breathing level, while emissions are released at an elevation of approximately 50 meters. As a result, the plume must disperse vertically before reaching this lower height, causing the peak ground-level concentration to occur downwind. In this model, peak concentrations were observed approximately 1,000 meters from the source. Beyond this point, concentrations decrease with increasing distance from the fire.

Even at distances of 10 to 20 kilometers downwind of the fire, modeled VOC concentrations remain elevated, suggesting a persistent exposure risk. The shape and magnitude of each plume varied by compound, reflecting species-specific dispersion behavior. While the general expectation was that VOC concentrations would rise with increasing structural fuel content, the degree of increase differed by species, highlighting the complex relationship between fire composition and downwind pollutant exposure.

Benzene plume concentration results peaked at between ~130 $\mu g/m^3$-180 $\mu g/m^3$ (100% biomass and 100% structure emissions, respectively). Measurements at the peak concentration downwind of the source are almost 30% greater for the 100% structure emission than 100%

biomass emission model. Trends in changing VOC emissions with increasing fraction of exotic

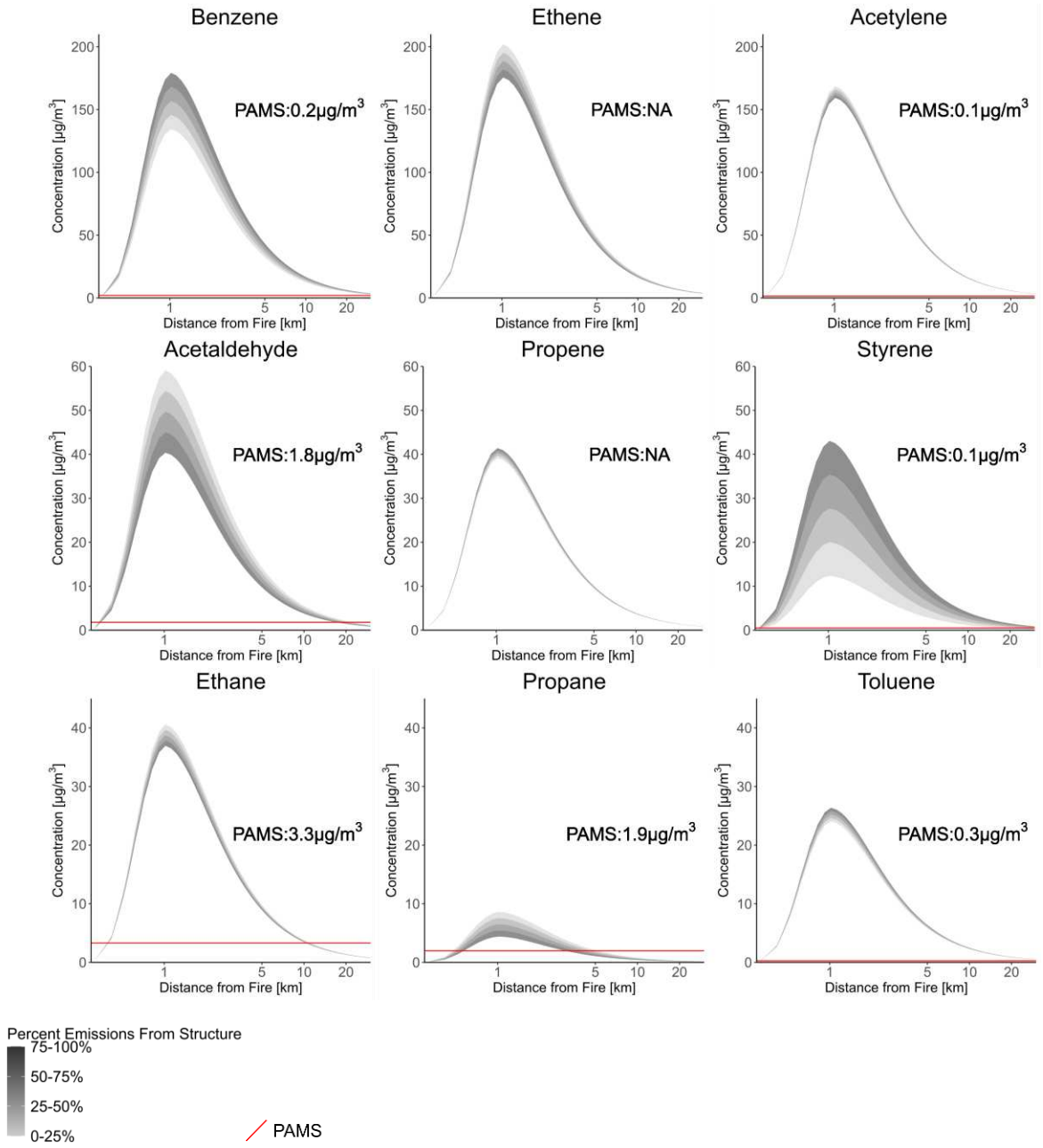

Figure 15: VOC emissions results of Gaussian plume models for five fire scenarios of varying ratios of forest to structure combustible material. Structure combustible material emission calculated from individual fuel emission factors combined to respectively represent relative contribution of combustible mass in a home. Each contour presents results of different fire scenarios ranging from 0% (lightest) to 100% (darkest) structure combustible mass. 2024 average ambient concentration from Colorado's Photochemical Assessment Monitoring Stations (PAMS) for seven of nine VOCs marked with red line. If species not documented by PAMS value is marked as "NA". Concentrations modeled at 1.8m (average human height).

fuels for emissions are not always intuitive, such as those seen for ethane, ethene, acetylene, acetaldehyde, and propane. For these compounds, the highest concentrations occur for 100% biomass fires. The most striking case is the peak at 0% combustible structure mass for ethene at ~200 $\mu g/m^3$. Variability and spread between the different species were significant. For some, across the different scenarios the spread between the peak concentrations was less than 5 $\mu g/m^3$ (ethane, toluene, propane, and propene). Styrene's difference in peak concentrations is greater than 30 $\mu g/m^3$ and a significant gap between scenarios remains until around twenty kilometers downwind. Despite various scales and spread between cases, as concentrations decay, most other VOC scenarios typically begin to converge within a few thousand meters. In all results, the 100% structural emissions represent the tail end of emissions (smallest or greatest magnitude) based on behavior of the species' emissions.

Where PAMS data is available, the expected ambient VOC concentration marks where the plume begins to produce higher concentrations. For another baseline comparison across species, Figure 16 outlines expected plume values under the five wildfire scenarios for commonly measured pollutants, CO and $PM_{2.5}$. The concentration of VOC results remain factors lower than CO and $PM_{2.5}$. Refer to Appendix B Figure B5 for concentration and ppb axes versions of the plume figures.

A representation of plume effects at 1.8m above ground level depicted in Figure 17 combines a map of Fort Collins with the corresponding plume concentration for the 50% structure combustible mass scenario for benzene. Even 30km away from the source (in this case simulated version of the High Park Fire), there is benzene from the fire source. Beyond the visible red concentration on the figure, any concentrations less than 1 $\mu g/m^3$ were grayed to clearly indicate

the general plume shape, but dispersion continues to occur outward in all directions.

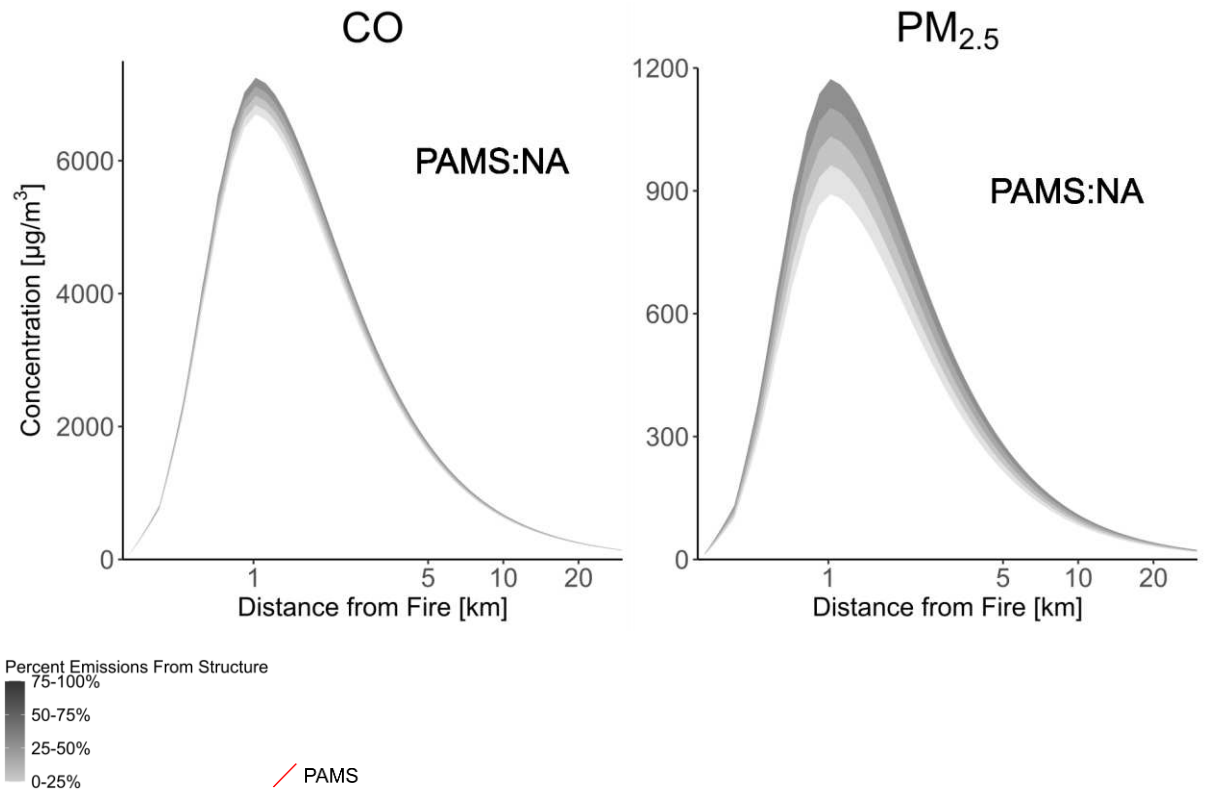

Figure 16: VOC emissions results of Gaussian plume models for five fire scenarios of varying ratios of forest to structure combustible material for criteria pollutants, carbon monoxide and particulate matter 2.5.

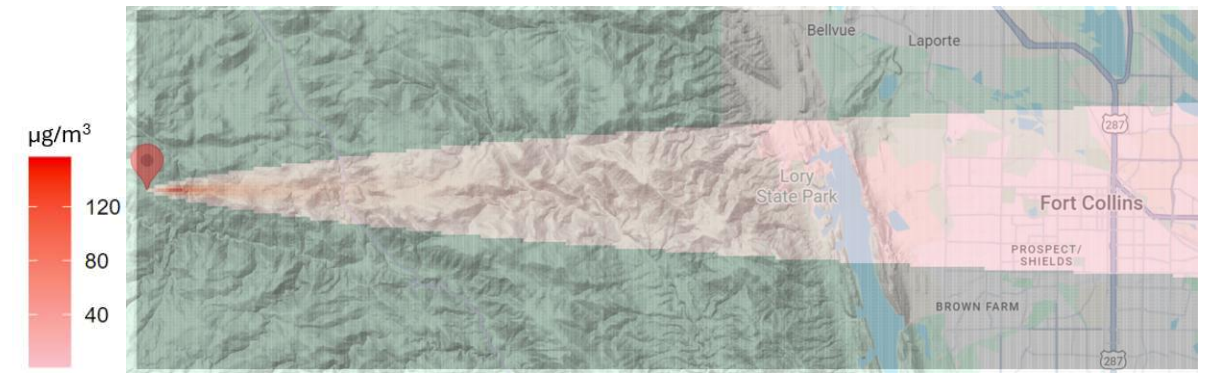

Figure 17: Approximate location of High Park Fire and associated Gaussian plume model results with benzene for a 50% structure combustible mass in combination with 50% combustible biomass mass. Plume modelled horizontally for 30km and vertically for 5km

Discussion

This study focused on characterizing VOC emissions for common structural materials. Emissions factors were determined for various fuel categories, combustions modes, and fuel mixtures. A few distinct VOC signatures are one of the primary outcomes of the fuel burning campaigns.

Fuel groups showed a general inverse relationship between EF and CE, with clearer trends under flaming conditions (CE > 0.8). In this regime, fuels tended to cluster by type, and emission magnitudes varied by orders of magnitude depending on the compound. Under pyrolysis conditions, EF values were more variable and less consistently grouped, reflecting the less predictable nature of oxygen-limited combustion. As expected, pyrolysis yielded higher EFs, consistent with lower CE values, indicating greater conversion of fuel into partially oxidized gaseous species.

The plastic-based carpets were found to consistently produce higher emissions than wood for several VOCs under flaming and pyrolysis conditions, making them strong candidates for source attribution. Other synthetic materials (e.g., PVC, insulation) also showed elevated emissions, though with more variability. In contrast, cement fiber siding, which includes some biomass content tended to have higher EFs than fully synthetic materials for VOCs with high EFs from lumber and processed wood.

Among the VOC compounds considered, benzene and styrene emerged as the most reliable indicators of structural (non-wood) fuel combustion. Ethene was more strongly associated with biomass, with the most distinct delineation between lumber/processed wood to carpet and synthetics. These trends were seen for both small- and large-scale experiments.

Biogenic VOC emissions factors were not found to be above background for many experiments despite compounds such as alpha-pinene and beta-pinene being commonly associated to biomass materials [78]. This is suspected to be partially due to the high background levels found in the laboratory air, which resulted in many of these results not being statistically different from background and therefore were omitted from analysis. While this paper focuses on nine primary VOCs, emissions data were also collected for over fifty additional compounds. Although many of these species had relatively low emission factors, their inclusion adds valuable depth to the dataset by capturing fuel-specific emission profiles that are often overlooked. This level of compound-level resolution offers novel insights into the chemical complexity of structural fire emissions.

The Gaussian plume model helps to place VOCs from structural emissions in the context of potential toxicological implications for individuals downwind of wildland fires. This analysis highlights key VOC emissions from structural fuels in the context of potential human exposure. The generalized plume model—representing smoke dispersion in areas where direct fire impact is not imminent and evacuations do not occur—provides valuable context for informing fire safety and public health policy. The PAMS data serves as a baseline comparison for expected ambient concentrations of seven of the nine species (two species not available). The plume model allows the reader to understand just how significantly concentrations of VOCs can increase due to a fire event. Model results for the signature species, benzene and styrene, fluctuated significantly between the 100% wildland fire scenario and 100% structural fire scenario. For some species the slight variation in total emissions, by introducing the “house EF”, does not make a notable difference in overall emissions (ex. propene and acetylene), or in some cases causes a decrease in yielded VOC concentration. Yet for benzene and styrene varying the

ratio of “house EF”, which collectively contains 7% mass contribution from synthetic fuels, to biomass EF from 0% to 100% causes a concentration increase of over 20%.

Structural emissions can alter a fire’s overall chemical signature. Although homes are typically dominated by wood-based materials, even modest contributions from plastics can significantly influence VOC emission factors. Although concentration results are a few orders of magnitude below permissible exposure limits [76], the acute effects of inhaling smoke containing VOCs are predicted to still present health risks. The substantial rise of VOC concentration in comparison to ambient levels during fire events leads to an exponentiated risk of toxic exposure. Using the developed emissions factor references for further detailed plume analysis and smoke dispersion studies can formally resolve any discourse on exposure firefighters and those living in the WUI receive during burn events.

CHAPTER 4. COMPARISON BETWEEN VOC MEASUREMENT INSTRUMENTATION ACROSS BURN CAMPAIGNS

Chapter Overview

For two emissions collection campaigns, multiple instruments quantified and interpreted gas-phase samples. The comparable outcome between instruments focuses on volatile organic compound (VOC) results. Quantification of VOCs across methods looked primarily for disagreement and fluctuation across methods. It was found that regardless of one-to-one agreement or R^2 value, a general positive linear association occurs for most of the species for all instruments. The best agreement was between the small-scale campaign's VOCUS (mass spectrometry) and SUMMA canisters. The large-scale campaign's experiment count was fewer than the small-scale campaigns, resulting in less comparable points between instrumentation and increased bias. Note that all figures are placed at the end of the chapter's text content.

Introduction

The interpretation of volatile organic compound (VOC) emissions can be compared against emission results from alternative instrumentation. For both small-scale and large-scale emission campaigns, at least two instruments were able to quantify VOC results. Here we examine the agreement across instrumentation, specifically SUMMA gas canisters (gas chromatography with flame ionization and gas chromatography with mass spectroscopy), VOCUS (proton-transfer-reaction mass spectrometry) and FTIR-MS (Fourier-Transform Ion Cyclotron Resonance Mass Spectrometry, also referred to as FTIR). Here SUMMA canisters are treated as the baseline "gold standard" instrumentation and compared to VOCUS and FTIR results. Numerical comparisons occurred after data had been converted to emission factors (g_species/kg_fuel). Refer to Table 5

for instrumentation information as well as VOCs dually quantified between instrument of interest and the SUMMA canisters. Analysis of emissions directly was not the primary goal of the comparison, but rather to identify how instrumentation will impact emission quantification and magnitude of result. There is an expected slight disagreement based on associated uncertainty, calibration, and nature of collection between instruments.

Table 5: Instrumentation and associate structural emissions campaign. Final column provides species that were dually quantified between instrument of focus and SUMMA canister.

Instrumentation	**Campaign**	**Overlapping VOC species with SUMMA canister (baseline instrument)**
SUMMA canister	Small-scale	--
University of Colorado VOCUS	Small-scale	Acetaldehyde, Acetone, Acrolein, Benzaldehyde, Benzene, Isoprene, Styrene, Toluene
SUMMA canister	Large-scale	--
NIST VOCUS	Large-scale	Acetaldehyde, Acetone, Benzene, Ethane, Ethene, Isoprene, Propene, Styrene, Toluene
NIST FTIR	Large-scale	Ethane, Ethene, Ethyne, Propane, Propene

Procedure

A linear regression was performed between the three variations of comparable instrumentation to the baseline SUMMA canister method. For each campaign, instrumentation that had emission factors for corresponding experiments were plotted against one another for the regression analysis.

Results

Figures 18, 19, and 20 graph the associated regressions for each respective VOC on a one-to-one, log-log axis with the associated linear regression line, regression equation, and R^2 value (all figures shown at end of chapter). Log scales are selected as some emission results span multiple

magnitudes. Multiple bias presents themselves across comparisons. The conclusion is that there are not enough data points to accurately assess instrument agreement for the large-scale tests. However, there is enough data from the small-scale tests to establish a working positive linear relationship between the VOCUS and SUMMA canister. Between EFs, on the log-log scale it outlines a positive linear agreement between most species. However, with fewer comparison points for some VOCs the agreement between instrumentation is blurred.

Figure 18 shows a relatively positive agreement for all eight comparable species. Omitting acrolein, isoprene, benzaldehyde and benzene the regression slopes are near or within reasonable bounds of one. The small-scale campaign had almost four times the experimental points to compare against as opposed to the large-scale campaign. The abundance of comparable points creates an agreeable relationship between the VOCUS and SUMMA canisters. For all species but benzene, the VOCUS emission result is of greater magnitude than the canister.

Figure 19 has a high R^2 value for two (ethane and propene) of the five species compared. In terms of one-to-one agreement, the species seems to be of higher magnitude (slope greater than one) from the FTIR for ethane and propane. Acetylene and ethene have an opposing trend where the SUMMA canister results have higher emissions. Propene has the best agreement, with tight R^2 correlation and a slope approaching a one-to-one relationship.

Figure 20 is incredibly variable in terms of R^2 correlation. In all cases the SUMMA canister emissions are greater than the VOCUS. Yet, among species it is difficult to identify any existing trends. The potential for better agreement is possible with an increased sample size available for comparison.

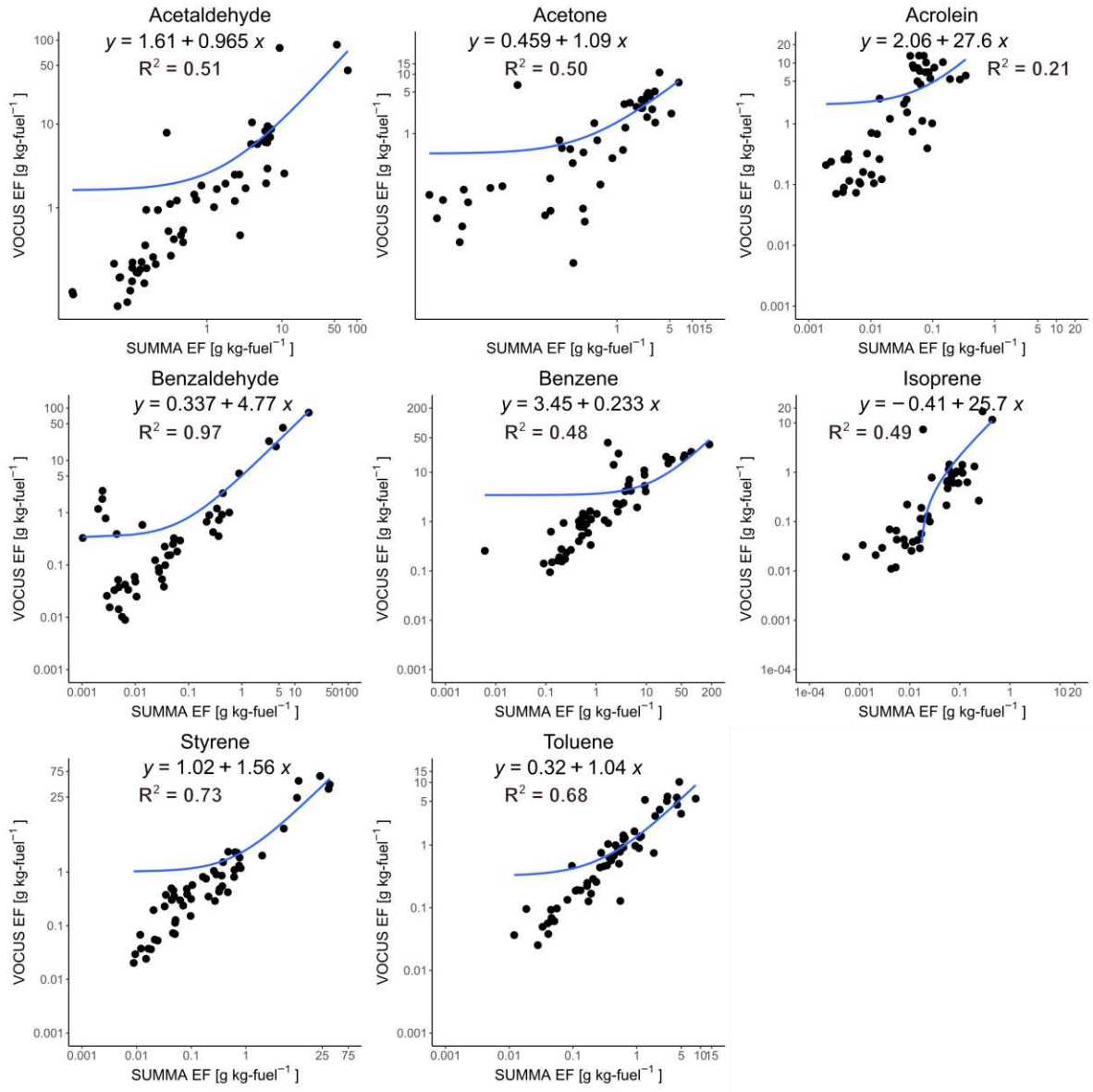

Figure 18: Instrument comparison between small-scale campaign VOCUS (PTR-MS) and SUMMA canister measurements. Between the two instruments, 8 species were dually quantified. Each species shown on an individual plot with experimental results plotted against one another, the linear regression line, equation and R^2 also shown.

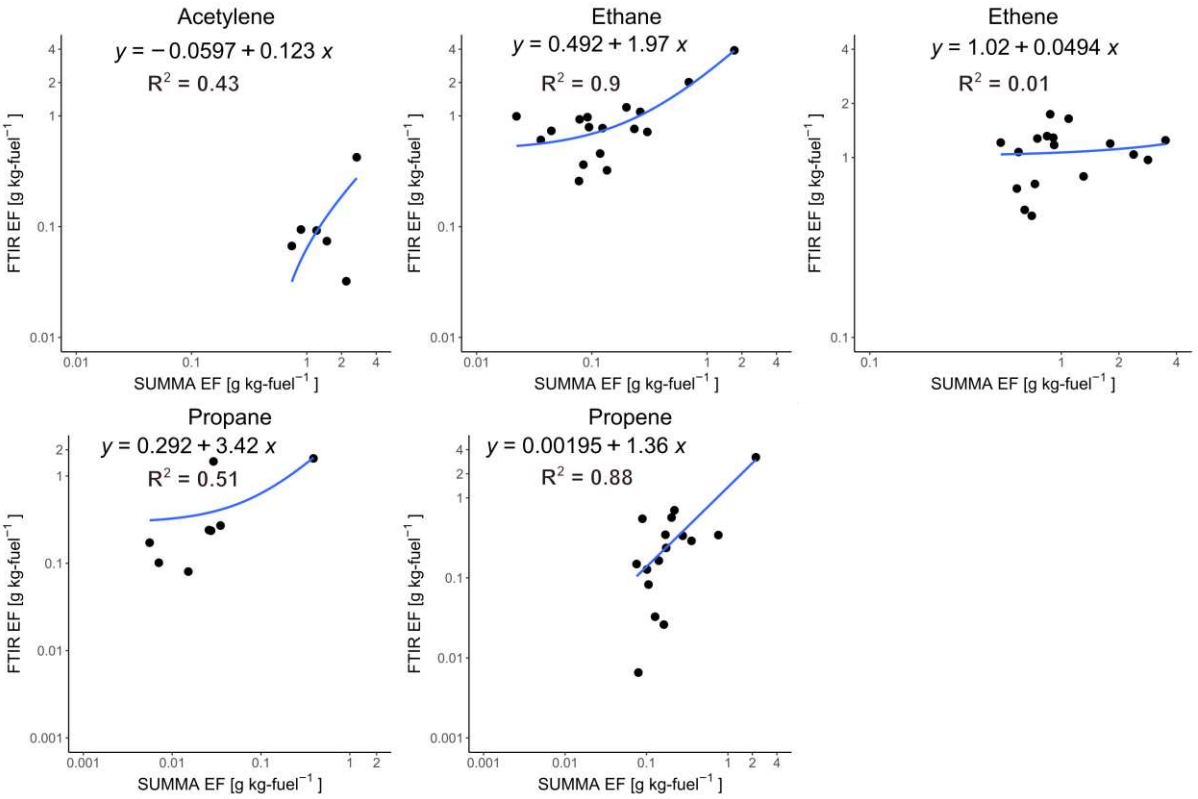

Figure 19: Instrument comparison between large-scale campaign FTIR and SUMMA canister measurements. Between the two instruments, 5 species were dually quantified. Each species shown on an individual plot with experimental results plotted against one another, the linear regression line, equation and R^2 also shown

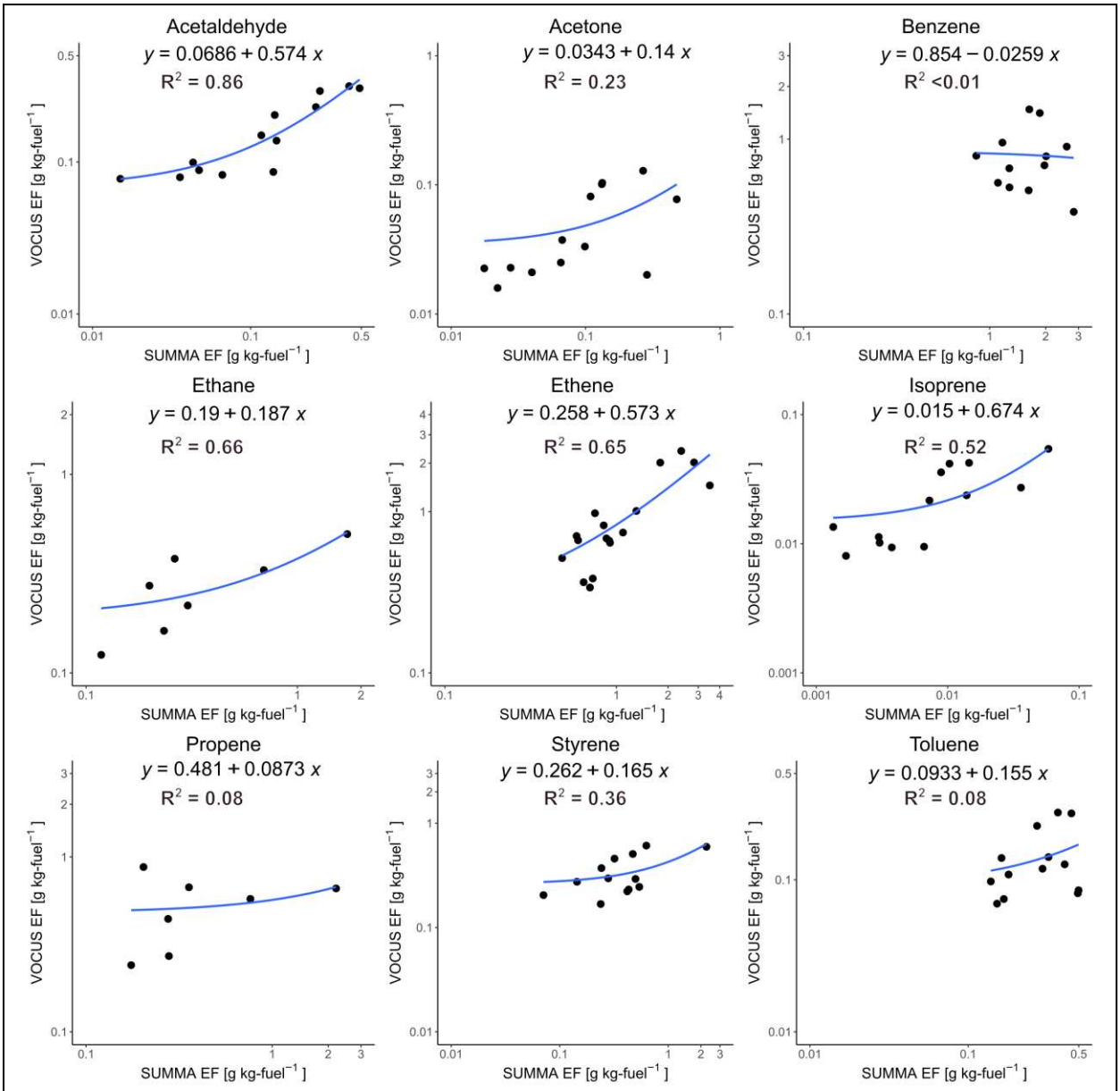

Figure 20: Instrument comparison between large-scale campaign VOCUS (PTR-MS) SUMMA canister measurements. Between the two instruments, 9 species were dually quantified. Each species shown on an individual plot with experimental results plotted against one another, the linear regression line, equation and R^2 also shown

CHAPTER 5: CONCLUSIONS

Assessment of structural fuel combustion impacts during wildfire events remains in its early stages. This study identified combustion trends, signature species, and characteristic conditions associated with synthetic structural materials, both individually and in mixed-fuel configurations. By assessing criteria pollutants (CO_2, CO, CH_4, $PM_{2.5}$, NO_X, soot, OA) and key VOCs (e.g., acetylene, acetaldehyde, benzene, ethane, ethene, propane, propene, toluene, and styrene), this work helps address critical data gaps regarding emissions from structural and vehicular materials during wildfires. Information regarding biomass-based emissions from wildfires is well documented and agrees with the BHASMA study's lumber experiments. By developing a structural-material-specific emissions inventory, this study supports the development of improved fire safety regulations, firefighting strategies, and building material guidance for WUI communities.

The analysis began with criteria pollutants, confirming expected combustion efficiency trends and offering insights into soot formation. Then, a detailed analysis of nine top contributing VOCs was performed. The VOC analysis revealed that emissions from exotic structural materials were characterized by distinct chemical signatures. A distinct relationship was found between pyrolysis and flaming conditions with reference to combustion efficiency. For most species—excluding CO_2 and NO_x—emissions were higher under smoldering (pyrolysis) conditions and lower during flaming combustion. Under pyrolysis conditions, emissions were highly variable and lacked consistent trends across fuel types. In contrast, emissions under flaming conditions were more consistent and fuel specific. Black carbon, elemental carbon, and benzene were notable exceptions, with higher emission factors observed under flaming rather than pyrolysis

conditions. This may be due to the elevated temperatures required to release soot and benzene, given their specific molecular formation pathways. While criteria pollutants such as CO_2, CO, and NO_x lack distinct emission signatures by fuel type—often trending with combustion efficiency rather than fuel composition—certain VOCs seem to have more fuel-specific diagnostic value. VOCs such as styrene and benzene were consistently associated with elevated emissions from exotic structural materials like synthetic carpets, insulation foams, and plastics. These compounds are not only chemically linked to the breakdown of polymer-based materials under high-temperature conditions, but may also serve as reliable indicators of synthetic fuel involvement in mixed-combustion scenarios. Their presence in elevated concentrations can then potentially be used as chemical fingerprints of potentially burning of non-biomass materials during a wildfire or structural fire. This has important implications for both ambient source apportionment and real-time fire monitoring: the detection of these species downwind of a fire could be used to estimate the proportion of synthetic vs. natural fuels involved. Because many of these compounds are classified as hazardous air pollutants with known health risks, their fuel-specificity provides a valuable link between combustion composition and potential toxicological outcomes for affected populations.

Controlled combustion conditions allowed the experimental campaign to effectively bracket the emissions ranges seen from uncontrolled combustion of the same fuels. Comparison with the SERA database, comprised of emissions data from experimental burns, prescribed fires, and field studies—confirmed that the controlled flaming and pyrolysis experiments captured the full range of realistic emission behaviors. The strong agreement between the BHASMA biomass experiments and the SERA biomass results support the validity of the combustion setup and sampling methodology.

The strong agreement between the two datasets underscores the value of controlled burns for isolating key variables such as fuel composition, combustion phase, and ventilation, which are often difficult to isolate in real-world fire scenarios. By maintaining consistent burn conditions while systematically varying fuel types, the BHASMA study was able to generate emission factors with high specificity, making the data ideally suited for integration into emissions inventories, air quality models, and health risk assessments.

Emission factors were used to model pollutant dispersion and evaluate potential toxicological implications and exposure to surrounding environments. Modeling scenarios of varying WUI house compositions (e.g., all-wood cabins vs. modern homes with synthetic materials) showed that adding plastics and carpets increased particulate-phase pollutant emissions. In contrast, gas-phase pollutants (CO_2, CO, CH_4) exhibited minimal variation with changing fuel ratios. A Gaussian plume model identified concentrations of VOCs downwind of a fire source at varying emission rates (ratios of biomass combustible mass to structure combustible mass). In the plume model, VOCs with signature flaming emissions for carpets and plastics exhibited a rise in emitted concentrations as the contribution from structure mass increased. Where emissions for VOCs with little variation between biomass and exotics (or cases where the exotics emissions are less than biomass emissions) the 100% biomass fire scenario had the highest VOC concentration.

The plume model can be taken a step further by integrating spatial population data, such as U.S. Census data, to estimate not only pollutant concentrations but also the proportion of the surrounding population potentially affected at varying distances from the fire source. By overlaying modeled concentration fields with high-resolution demographic information, the model enables population-weighted exposure assessments that account for spatial heterogeneity

in both emissions and human presence. This provides a more meaningful and actionable interpretation of fire emissions, particularly for public health and emergency planning.

Compared to computationally intensive 3D dispersion models (e.g., CFD-based or coupled meteorology-chemistry systems), this Gaussian plume approach offers advantages in speed, scalability, and interpretability. It can be run in near real-time with minimal computational resources, making it suitable for integration into rapid decision-support tools during active fire events. Additionally, the model's relative simplicity allows for sensitivity testing across a wide range of fire compositions and environmental conditions, enabling exploratory analysis where data or computing power may be limited. While it lacks the fine-scale resolution and vertical dispersion fidelity of advanced models, the Gaussian approach is ideal for screening-level assessments and scenario comparisons.

Comparing plume predictions to observed fire event data for criteria pollutants like CO and $PM_{2.5}$ can be used to assess model agreement and tune assumptions. Once validated, the same framework can be applied to VOCs to estimate downwind exposure concentrations under different fire compositions. This can help develop baseline expectations for different community scenarios (e.g., biomass-only vs. modern synthetic-rich structures). Refining these models with real-time emissions data such as that collected from field-deployed sensors during active wildfires could substantially improve predictive accuracy and help bridge the gap between controlled laboratory burns and uncontrolled wildfire events. Although the 1 kW and 500 kW experimental campaigns showed consistent trends, validation against full-scale structural fire data remains a critical next step.

BHAMSA's robust data set provides multiple pathways for future research. An area of focus should be the continued expansion of structural fuel-related emissions with new experimental

matrices. Test matrices could encompass more fuels associated with structural emissions like batteries, electronics and vehicles. Further testing on geographically unique biomass will also be beneficial to adjust expected emissions based on specific environments (forest, grassland, wetland, etc.) and those region's commonly used construction materials (wood, stucco, brick etc.). If further testing is conducted, strict experimental instrument configuration, post-experiment cleaning, and sample treatment standards should be developed and adhered to. These practices can prevent sample loss, contamination, and handling errors.

While the expansion of the structural emissions database remains a key near-term priority, an equally important step is the development of decision-oriented models that translate emissions data into actionable decisions. These models needed to help move from emission factors to usable data products such as estimated exposure, hazard quotients, atmospheric concentrations, and health risks; these are the metrics that ultimately can help decision-making and long-term planning. With the development of emission factors for both criteria pollutants and VOCs, emissions data can be used to predict, confirm, and compare data collected ambiently. Ratios between criteria pollutants and VOCs can be useful for emissions predictions. Pollutants commonly measured with real-time instrumentation can be quickly analyzed, then emissions predictions, based on developed relationships between compounds, can be formed. These conclusions provide insight into what matrix of fuels are actively burning during a combustion event.

The BHASMA study successfully identified a robust, fuel-specific emissions dataset and established clear relationships between structural materials and associated pollutant profiles—addressing a critical and previously underexplored gap in wildfire emissions research. By linking laboratory-controlled combustion conditions to representative real-world scenarios, the study

provides a foundation for both scientific advancement and practical application. These findings support the development of exposure assessment tools, health risk models, and fire response strategies tailored to mixed-fuel environments at the wildland–urban-interface. Ongoing analysis and future validation with full-scale and real-time data will further strengthen the relevance of this work, paving the way for improved public health protections, more accurate climate models more informed building practices, and enhanced fire mitigation policies.

REFERENCES

[1]

"Changes in wildfire occurrence and risk to homes from 1990 through 2019 in the Southern Rocky Mountains, USA - Hawbaker - 2023 - Ecosphere - Wiley Online Library." Accessed: Sep. 25, 2023. [Online]. Available: https://esajournals.onlinelibrary.wiley.com/doi/full/10.1002/ecs2.4403

[2]

V. C. Radeloff *et al.*, "Rapid growth of the US wildland-urban interface raises wildfire risk," *Proceedings of the National Academy of Sciences*, vol. 115, no. 13, pp. 3314–3319, Mar. 2018, doi: 10.1073/pnas.1718850115.

[3]

Z. L. Steel, H. D. Safford, and J. H. Viers, "The fire frequency-severity relationship and the legacy of fire suppression in California forests," *Ecosphere*, vol. 6, no. 1, p. art8, 2015, doi: 10.1890/ES14-00224.1.

[4]

K. Boaggio *et al.*, "Beyond Particulate Matter Mass: Heightened Levels of Lead and Other Pollutants Associated with Destructive Fire Events in California," *Environ. Sci. Technol.*, vol. 56, no. 20, pp. 14272–14283, Oct. 2022, doi: 10.1021/acs.est.2c02099.

[5]

The Chemistry of Fires at the Wildland-Urban Interface. Washington, D.C.: National Academies Press, 2022. doi: 10.17226/26460.

[6]

W. Tang *et al.*, "Disproportionately large impacts of wildland-urban interface fire emissions on global air quality and human health," *Science Advances*, vol. 11, no. 11, p. eadr2616, Mar. 2025, doi: 10.1126/sciadv.adr2616.

[7]

E. K. Southworth *et al.*, "The influence of wildfire smoke on ambient chemical species concentrations in the contiguous US," Aug. 2024, Accessed: Oct. 25, 2024. [Online]. Available: https://eartharxiv.org/repository/view/7545/

[8]

N. Khakzad, "Modeling wildfire spread in wildland-industrial interfaces using dynamic Bayesian network," *Reliability Engineering & System Safety*, vol. 189, pp. 165–176, Sep. 2019, doi: 10.1016/j.ress.2019.04.006.

[9]

"Programs | U.S. Department of the Interior." Accessed: Jun. 02, 2025. [Online]. Available: https://www.doi.gov/wildlandfire/program72

[10]

M. Salis *et al.*, "Modeling the effects of different fuel treatment mosaics on wildfire spread and behavior in a Mediterranean agro-pastoral area," *Journal of Environmental Management*, vol. 212, pp. 490–505, Apr. 2018, doi: 10.1016/j.**jenvman**.2018.02.020.

[11]

"Previous Wildland Fire Management Initiatives." Accessed: May 31, 2025. [Online]. Available: https://www.forestsandrangelands.gov/resources/overview/

[12]

D. A. Jaffe *et al.*, "Wildfire and prescribed burning impacts on air quality in the United States," *Journal of the Air & Waste Management Association*, vol. 70, no. 6, pp. 583–615, Jun. 2020, doi: 10.1080/10962247.2020.1749731.

[13]

A. L. Holder, A. Ahmed, J. M. Vukovich, and V. Rao, "Hazardous air pollutant emissions estimates from wildfires in the wildland urban interface," *PNAS Nexus*, vol. 2, no. 6, p. pgad186, Jun. 2023, doi: 10.1093/pnasnexus/pgad186.

[14]

G. N. Dickinson *et al.*, "Health Risk Implications of Volatile Organic Compounds in Wildfire Smoke During the 2019 FIREX-AQ Campaign and Beyond," *GeoHealth*, vol. 6, no. 8, p. e2021GH000546, 2022, doi: 10.1029/2021GH000546.

[15]

B. Chen *et al.*, "Wildfire risk for global wildland–urban interface areas," *Nat Sustain*, vol. 7, no. 4, pp. 474–484, Apr. 2024, doi: 10.1038/s41893-024-01291-0.

[16]

W. Tang, C. He, L. Emmons, and J. Zhang, "Global expansion of wildland-urban interface (WUI) and WUI fires: insights from a multiyear worldwide unified database (WUWUI)," *Environ. Res. Lett.*, vol. 19, no. 4, p. 044028, Mar. 2024, doi: 10.1088/1748-9326/ad31da.

[17]

M. Burke, A. Driscoll, S. Heft-Neal, J. Xue, J. Burney, and M. Wara, "The changing risk and burden of wildfire in the United States," *Proceedings of the National Academy of Sciences*, vol. 118, no. 2, p. e2011048118, Jan. 2021, doi: 10.1073/pnas.2011048118.

[18]

Z. A. Holden *et al.*, "Decreasing fire season precipitation increased recent western US forest wildfire activity," *Proceedings of the National Academy of Sciences*, vol. 115, no. 36, pp. E8349–E8357, Sep. 2018, doi: 10.1073/pnas.1802316115.

[19]

A. L. Westerling, “Increasing western US forest wildfire activity: sensitivity to changes in the timing of spring,” *Philosophical Transactions of the Royal Society B: Biological Sciences*, vol. 371, no. 1696, p. 20150178, Jun. 2016, doi: 10.1098/rstb.2015.0178.

[20]

P. E. Higuera, M. C. Cook, J. K. Balch, E. N. Stavros, A. L. Mahood, and L. A. St. Denis, “Shifting social-ecological fire regimes explain increasing structure loss from Western wildfires,” *PNAS Nexus*, vol. 2, no. 3, p. pgad005, Mar. 2023, doi: 10.1093/pnasnexus/pgad005.

[21]

U. S. J. E. Committee, “Climate-exacerbated wildfires cost the U.S. between $394 to $893 billion each year in economic costs and damages - Climate-exacerbated wildfires cost the U.S. between $394 to $893 billion each year in economic costs and damages - United States Joint Economic Committee.” Accessed: Jun. 01, 2025. [Online]. Available: https://www.jec.senate.gov/public/index.cfm/democrats/2023/10/climate-exacerbated-wildfires-cost-the-u-s-between-394-to-893-billion-each-year-in-economic-costs-and-damages

[22]

N. Averett, “After the Smoke Clears: Wildland–Urban Interface Fires and Residues in Nearby Homes,” *Environmental Health Perspectives*, vol. 132, no. 7, p. 072001, Jul. 2024, doi: 10.1289/EHP14770.

[23]

B. Rooney, Y. Wang, J. H. Jiang, B. Zhao, Z.-C. Zeng, and J. H. Seinfeld, “Air quality impact of the Northern California Camp Fire of November 2018,” *Atmospheric Chemistry and Physics*, vol. 20, no. 23, pp. 14597–14616, Dec. 2020, doi: 10.5194/acp-20-14597-2020.

[24]

J. M. Silberstein *et al.*, “Residual impacts of a wildland urban interface fire on urban particulate matter and dust: a study from the Marshall Fire,” *Air Qual Atmos Health*, vol. 16, no. 9, pp. 1839–1850, Sep. 2023, doi: 10.1007/s11869-023-01376-3.

[25]

M. O. Andreae and P. Merlet, “Emission of trace gases and aerosols from biomass burning,” *Global Biogeochemical Cycles*, vol. 15, no. 4, pp. 955–966, 2001, doi: 10.1029/2000GB001382.

[26]

Katherine. B. Benedict *et al.*, “Wildland Urban Interface (WUI) Emissions: Laboratory Measurement of Aerosol and Trace Gas from Combustion of Manufactured Building Materials,” *ACS EST Air*, vol. 1, no. 12, pp. 1673–1686, Dec. 2024, doi: 10.1021/acsestair.4c00217.

[27]

R. A. Sianchuk, E. K. Ackom, and P. N. McFarlane, “Determining Stocks and Flows of Structural Wood Products in Single Family Homes in the United States between 1950 and 2010,” Mar. 2012, doi: 10.13073/0015-7473-62.2.90.

[28]

K. R. Bilsback *et al.*, “A Laboratory Assessment of 120 Air Pollutant Emissions from Biomass and Fossil Fuel Cookstoves,” *Environ. Sci. Technol.*, vol. 53, no. 12, pp. 7114–7125, Jun. 2019, doi: 10.1021/acs.est.8b07019.

[29]

K. M. Fedak *et al.*, “Chemical Composition and Emissions Factors for Cookstove Startup (Ignition) Materials,” *Environ. Sci. Technol.*, vol. 52, no. 16, pp. 9505–9513, Aug. 2018, doi: 10.1021/acs.est.8b02218.

[30]

P. Blomqvist, L. Rosell, and M. Simonson, “Emissions from Fires Part II: Simulated Room Fires,” *Fire Technology*, vol. 40, no. 1, pp. 59–73, Jan. 2004, doi: 10.1023/B:FIRE.0000003316.63475.16.

[31]

B. Persson and M. Simonson, “Fire Emissions into the Atmosphere,” *Fire Technology*, vol. 34, no. 3, pp. 266–279, Sep. 1998, doi: 10.1023/A:1015350024118.

[32]

“Fuel loads and their composition, and compartment characteristics in educational, office and library buildings - Nayak - 2024 - Fire and Materials - Wiley Online Library.” Accessed: Jun. 01, 2025. [Online]. Available: https://onlinelibrary.wiley.com/doi/10.1002/fam.3178

[33]

“Estimation of CO2-Emissions from Fires in Dwellings Schools and Cars in the Nordic Countries,” *SP Technical Research Institute of Sweden,* 2009

[34]

R. A. Bryant and M. F. Bundy, “The NIST 20 MW calorimetry measurement system for large-fire research,” National Institute of Standards and Technology, Gaithersburg, MD, NIST TN 2077, Dec. 2019. doi: 10.6028/NIST.TN.2077.

[35]

A. Y. Davis, T. G. Cleary, R. L. Falkenstein-Smith, and R. A. Bryant, “Burning Characteristics and Smoke Emission from Mixed Fuel Cribs,” *ACS EST Air*, vol. 2, no. 4, pp. 540–547, Apr. 2025, doi: 10.1021/acsestair.4c00275.

[36]

N. P. Bryner and G. W. Mulholland, “Smoke emission and burning rates for urban structures,” *Atmospheric Environment. Part A. General Topics*, vol. 25, no. 11, pp. 2553–2562, Jan. 1991, doi: 10.1016/0960-1686(91)90172-4.

[37]

P. Presler-Jur, P. Doraiswamy, O. Hammond, and J. Rice, “An evaluation of mass absorption cross-section for optical carbon analysis on Teflon filter media,” *Journal of the Air & Waste Management Association*, vol. 67, no. 11, pp. 1213–1228, Nov. 2017, doi: 10.1080/10962247.2017.1310148.

[38]

X. Li *et al.*, “Socioeconomic and Demographic Associations with Wintertime Air Pollution Exposures at Household, Community, and District Scales in Rural Beijing, China,” *Environ. Sci. Technol.*, vol. 56, no. 12, pp. 8308–8318, Jun. 2022, doi: 10.1021/acs.est.1c07402.

[39]

S. Brown *et al.*, “Review of Sunset OC/EC Instrument Measurements During the EPA’s Sunset Carbon Evaluation Project,” *Atmosphere*, vol. 10, no. 5, Art. no. 5, May 2019, doi: 10.3390/atmos10050287.

[40]

A. C. Aiken *et al.*, “O/C and OM/OC Ratios of Primary, Secondary, and Ambient Organic Aerosols with High-Resolution Time-of-Flight Aerosol Mass Spectrometry,” *Environ. Sci. Technol.*, vol. 42, no. 12, pp. 4478–4485, Jun. 2008, doi: 10.1021/es703009q.

[41]

R. Subramanian, A. Y. Khlystov, J. C. Cabada, and A. L. Robinson, “Positive and Negative Artifacts in Particulate Organic Carbon Measurements with Denuded and Undenuded Sampler Configurations Special Issue of Aerosol Science and Technology on Findings from the Fine Particulate Matter Supersites Program,” *Aerosol Science and Technology*, vol. 38, no. sup1, pp. 27–48, Dec. 2004, doi: 10.1080/02786820390229354.

[42]

A. A. May *et al.*, “Gas-particle partitioning of primary organic aerosol emissions: 3. Biomass burning,” *Journal of Geophysical Research: Atmospheres*, vol. 118, no. 19, p. 11,327-11,338, 2013, doi: 10.1002/jgrd.50828.

[43]

B. N. Murphy *et al.*, “Reactive organic carbon air emissions from mobile sources in the United States,” *Atmospheric Chemistry and Physics*, vol. 23, no. 20, pp. 13469–13483, Oct. 2023, doi: 10.5194/acp-23-13469-2023.

[44]

S. K. Akagi *et al.*, “Emission factors for open and domestic biomass burning for use in atmospheric models,” *Atmospheric Chemistry and Physics*, vol. 11, no. 9, pp. 4039–4072, May 2011, doi: 10.5194/acp-11-4039-2011.

[45]

S. J. Prichard *et al.*, “Wildland fire emission factors in North America: synthesis of existing data, measurement needs and management applications,” *Int. J. Wildland Fire*, vol. 29, no. 2, pp. 132–147, Jan. 2020, doi: 10.1071/WF19066.

[46]

S. R. Turns, “An Introduction to Combustion Concepts and Applications – McGraw-Hill Internat”, 2018

[47]

Y. Yang, A. L. Boehman, and R. J. Santoro, “A study of jet fuel sooting tendency using the threshold sooting index (TSI) model,” *Combustion and Flame*, vol. 149, no. 1, pp. 191–205, Apr. 2007, doi: 10.1016/j.combustflame.2006.11.007.

[48]

S. H. Jathar *et al.*, “Measuring and modeling the primary organic aerosol volatility from a modern non-road diesel engine,” *Atmospheric Environment*, vol. 223, p. 117221, Feb. 2020, doi: 10.1016/j.atmosenv.2019.117221.

[49]

C. N. Jen *et al.*, “Speciated and total emission factors of particulate organics from burning western US wildland fuels and their dependence on combustion efficiency,” *Atmospheric Chemistry and Physics*, vol. 19, no. 2, pp. 1013–1026, Jan. 2019, doi: 10.5194/acp-19-1013-2019.

[50]

“Emissions of trace gases and aerosols during the open combustion of biomass in the laboratory - McMeeking - 2009 - Journal of Geophysical Research: Atmospheres - Wiley Online Library.” Accessed: Jun. 01, 2025. [Online]. Available: https://agupubs.onlinelibrary.wiley.com/doi/10.1029/2009JD011836

[51]

C. Hopkin, M. Spearpoint, and D. Hopkin, “A Review of Design Values Adopted for Heat Release Rate Per Unit Area,” *Fire Technol*, vol. 55, no. 5, pp. 1599–1618, Sep. 2019, doi: 10.1007/s10694-019-00834-8.

[52]

C. L’Orange, D. Leith, J. Volckens, and M. DeFoort, “A quantitative model of cookstove variability and field performance: Implications for sample size,” *Biomass and Bioenergy*, vol. 72, pp. 233–241, Jan. 2015, doi: 10.1016/j.biombioe.2014.10.031.

[53]

C. A. Roden, T. C. Bond, S. Conway, A. B. Osorto Pinel, N. MacCarty, and D. Still, “Laboratory and field investigations of particulate and carbon monoxide emissions from traditional and improved cookstoves,” *Atmospheric Environment*, vol. 43, no. 6, pp. 1170–1181, Feb. 2009, doi: 10.1016/j.atmosenv.2008.05.041.

[54]

A. Sinha, I. George, A. Holder, W. Preston, M. Hays, and A. P. Grieshop, “Development of volatility distributions for organic matter in biomass burning emissions,” *Environmental Science: Atmospheres*, vol. 3, no. 1, pp. 11–23, 2023, doi: 10.1039/D2EA00080F.

[55]

H. B. Singh, L. Salas, W. Viezee, B. Sitton, and R. Ferek, “Measurement of volatile organic chemicals at selected sites in California,” *Atmospheric Environment. Part A. General Topics*, vol. 26, no. 16, pp. 2929–2946, Nov. 1992, doi: 10.1016/0960-1686(92)90285-S.

[56]

D. Loomis *et al.*, “Carcinogenicity of benzene,” *The Lancet Oncology*, vol. 18, no. 12, pp. 1574–1575, Dec. 2017, doi: 10.1016/S1470-2045(17)30832-X.

[57]

I. R. Burling *et al.*, “Laboratory measurements of trace gas emissions from biomass burning of fuel types from the southeastern and southwestern United States,” *Atmospheric Chemistry and Physics*, vol. 10, no. 22, pp. 11115–11130, Nov. 2010, doi: 10.5194/acp-10-11115-2010.

[58]

S. P. Urbanski, “Combustion efficiency and emission factors for wildfire-season fires in mixed conifer forests of the northern Rocky Mountains, US,” *Atmospheric Chemistry and Physics*, vol. 13, no. 14, pp. 7241–7262, Jul. 2013, doi: 10.5194/acp-13-7241-2013.

[59]

T. Cole-Hunter *et al.*, “The health impacts of waste-to-energy emissions: a systematic review of the literature,” *Environ. Res. Lett.*, vol. 15, no. 12, p. 123006, Dec. 2020, doi: 10.1088/1748-9326/abae9f.

[60]

A. A. K. Karunathilake *et al.*, “Hexaphenylbenzene and hexabenzocoronene-based porous polymers for the adsorption of volatile organic compounds,” *RSC Advances*, vol. 6, no. 70, pp. 65763–65769, 2016, doi: 10.1039/C6RA14263J.

[61]

P. W. Tait *et al.*, “The health impacts of waste incineration: a systematic review,” *Australian and New Zealand Journal of Public Health*, vol. 44, no. 1, pp. 40–48, Feb. 2020, doi: 10.1111/1753-6405.12939.

[62]

K. Ridgway & A. Helfrich, “Emissions from Structure Fires: Overview of BHASMA and Results for CO2 and Select Pollutants by Fuel, Combustion Mode, and Scale,” *Environmental Science and Technology*, 2025, [under review]

[63]

L. van Zyl *et al.*, “Effects of Fuel Moisture Content on Emissions from a Rocket-Elbow Cookstove,” *Environ. Sci. Technol.*, vol. 53, no. 8, pp. 4648–4656, Apr. 2019, doi: 10.1021/acs.est.9b00235.

[64]

Y. Zhou *et al.*, “Air Toxic Emissions from Snowmobiles in Yellowstone National Park,” *Environ. Sci. Technol.*, vol. 44, no. 1, pp. 222–228, Jan. 2010, doi: 10.1021/es9018578.

[65]

R. S. Russo, Y. Zhou, M. L. White, H. Mao, R. Talbot, and B. C. Sive, “Multi-year (2004–2008) record of nonmethane hydrocarbons and halocarbons in New England: seasonal variations and regional sources,” *Atmospheric Chemistry and Physics*, vol. 10, no. 10, pp. 4909–4929, May 2010, doi: 10.5194/acp-10-4909-2010.

[66]

B.C. Sive, “Atmospheric nonmethane hydrocarbons: Analytical methods and estimated hydroxyl radical concentrations - ProQuest.” Accessed: Jun. 17, 2025. [Online]. Available: https://www.proquest.com/openview/f9a8e162afe9b62e796c2a78640305c2/1?pq-origsite=gscholar&cbl=18750&diss=y

[67]

C. W. Woodall, C. H. Perry, and P. D. Miles, “The relative density of forests in the United States,” *Forest Ecology and Management*, vol. 226, no. 1–3, pp. 368–372, May 2006, doi: 10.1016/j.foreco.2006.01.032.

[68]

“WFIGS Interagency Fire Perimeters.” Accessed: May 30, 2025. [Online]. Available: https://data-nifc.opendata.arcgis.com/datasets/5e72b1699bf74eefb3f3aff6f4ba5511_0/explore

[69]

D. Holstius, “An Introduction to Steady-State Gaussian Dispersion Modeling in R”.

[70]

R. R. Draxler, “Estimating vertical diffusion from routine meteorological tower measurements,” *Atmospheric Environment (1967)*, vol. 13, no. 11, pp. 1559–1564, Jan. 1979, doi: 10.1016/0004-6981(79)90065-9.

[71]

Colorado Department of Fire Prevention and Control, “Historical Wildfire Information | Fire Prevention and Control.” Accessed: Jun. 17, 2025. [Online]. Available: https://dfpc.colorado.gov/sections/wildfire-information-center/historical-wildfire-information

[72]

“NASA POWER | API Pages.” Accessed: May 30, 2025. [Online]. Available: https://power.larc.nasa.gov/api/pages/?urls.primaryName=Daily#/

[73]

“AirData website File Download page.” Accessed: May 30, 2025. [Online]. Available: https://aqs.epa.gov/aqsweb/airdata/download_files.html

[74]

U.S. NCHS, “Vital and Health Statistics, Series 3, Number 46”.

[75]

O. US EPA, “Photochemical Assessment Monitoring Stations (PAMS).” Accessed: May 30, 2025. [Online]. Available: https://www.epa.gov/amtic/photochemical-assessment-monitoring-stations-pams

[76]

“Permissible Exposure Limits - Annotated Tables | Occupational Safety and Health Administration.” Accessed: May 30, 2025. [Online]. Available: https://www.osha.gov/annotated-pels

[77]

N. L. Briggs *et al.*, “Particulate Matter, Ozone, and Nitrogen Species in Aged Wildfire Plumes Observed at the Mount Bachelor Observatory,” *Aerosol Air Qual. Res.*, vol. 16, no. 12, pp. 3075–3087, 2016, doi: 10.4209/aaqr.2016.03.0120.

[78]

K. Sumitomo *et al.*, “Conifer-Derived Monoterpenes and Forest Walking,” *Mass Spectrometry*, vol. 4, no. 1, pp. A0042–A0042, 2015, doi: 10.5702/massspectrometry.A0042.

APPENDIX A: CHAPTER 2 SUPPLEMENTAL FIGURES

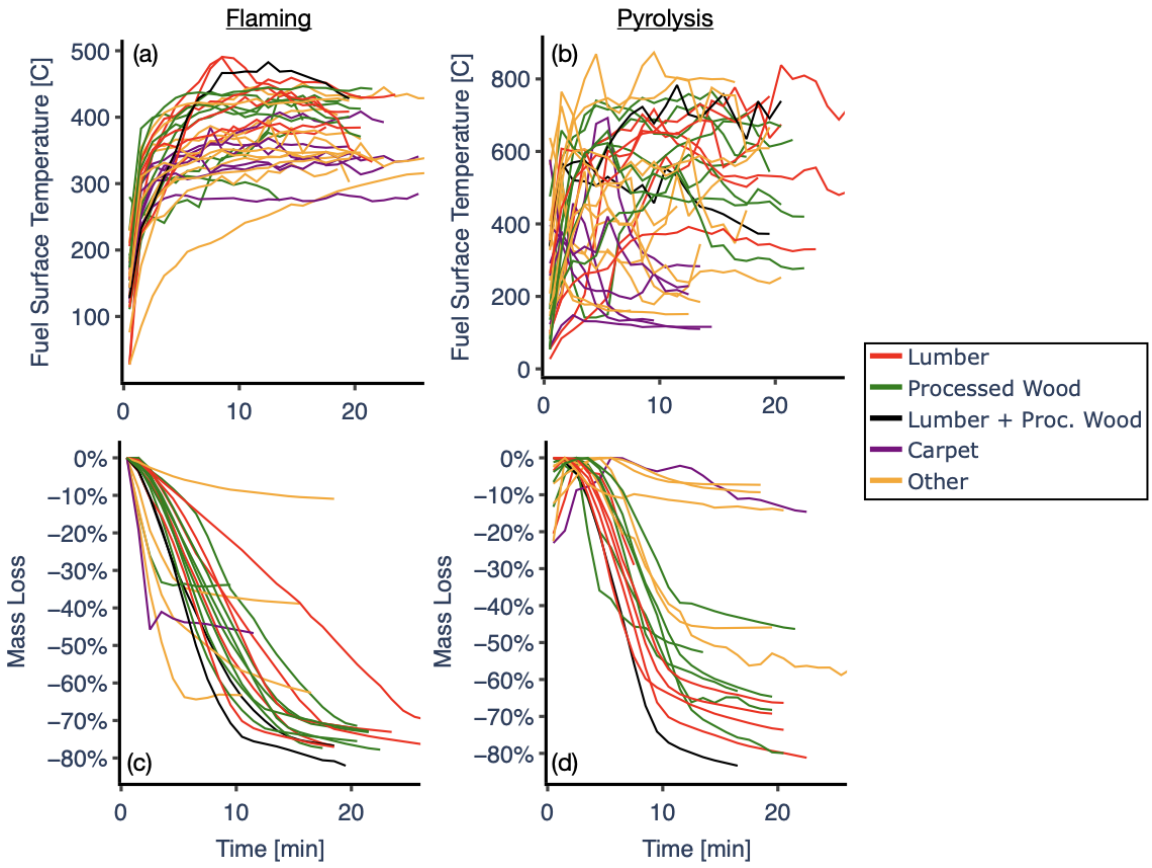

Figure A1: (a-b) Fuel surface temperature, and (c-d) fuel mass loss for small-scale experiments under (a, c) flaming and (b, d) pyrolysis conditions; data missing for experiments where temperature or fuel mass loss were not measured.

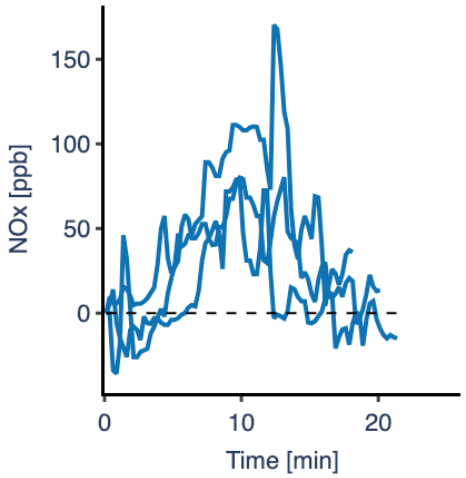

Figure A2: Background- and blank-corrected mixing ratios of NO_X for small-scale experiments performed with southern yellow pine (SYP) under pyrolysis (n=3) conditions.

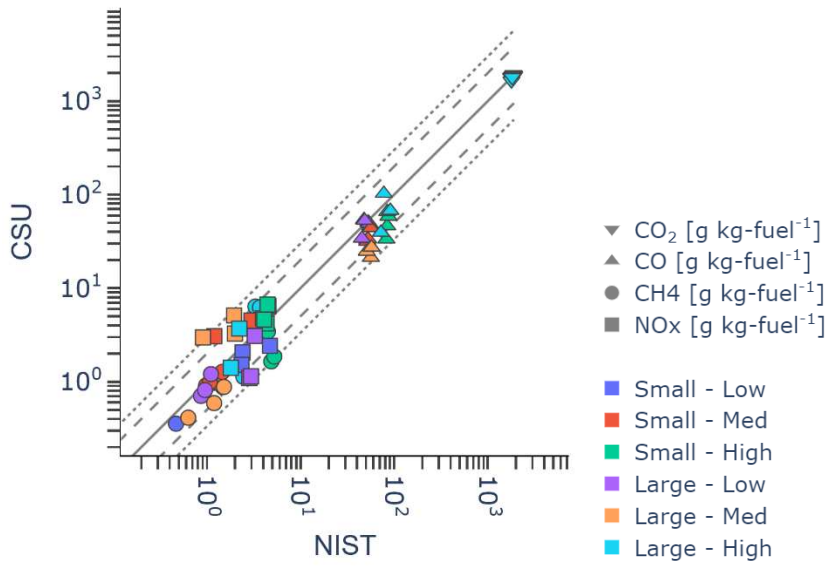

Figure A3: Emission factors for NIST cribs for the CSU sub-sampling duration compared to the entire NIST experimental duration. “Small” and “Large” refers to crib size, and “Low”, “Med”, “High” refer to the packing density. Dashed and dotted lines represent 1:1, 1:2, and 1:3 lines.

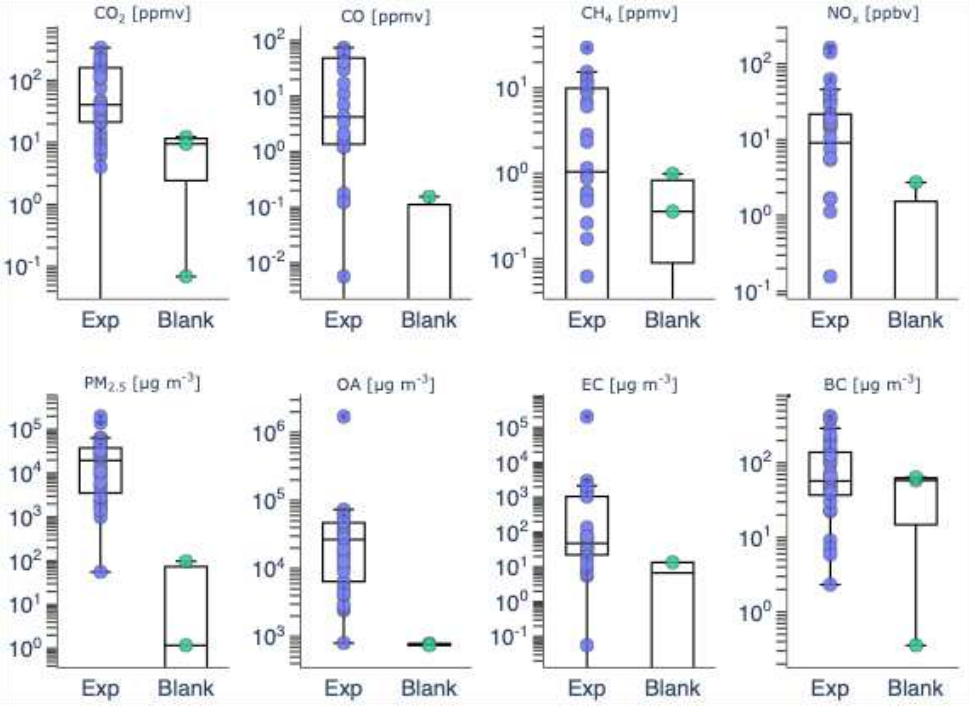

Figure A4: Uncorrected mixing ratios and mass concentrations compared against blank values for the small-scale fires performed under pyrolysis conditions.

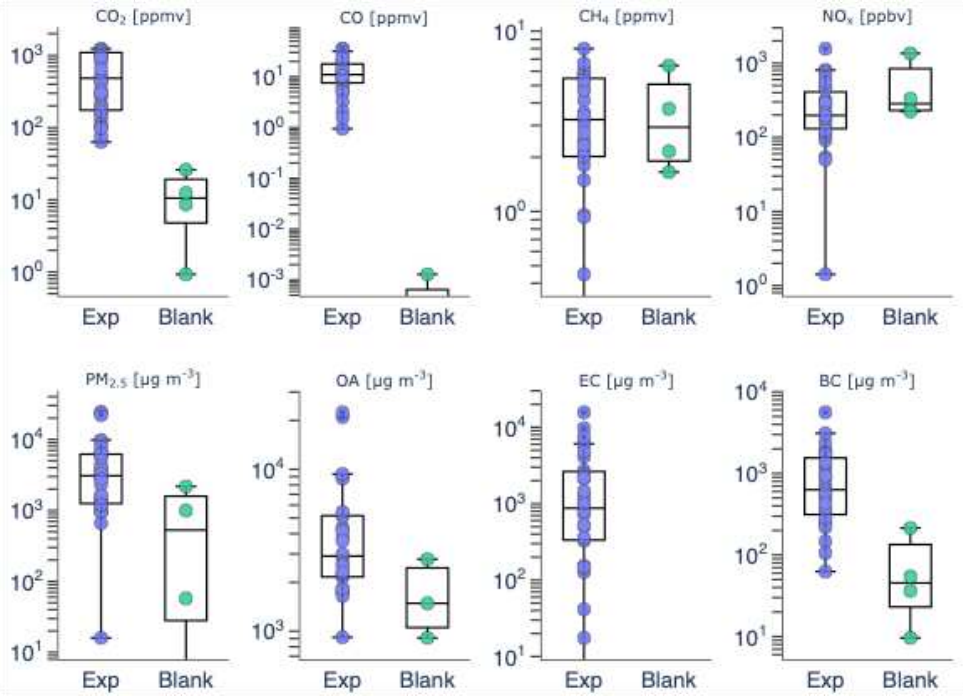

Figure A5: Uncorrected mixing ratios and mass concentrations compared against blank values for the small-scale fires performed under flaming conditions

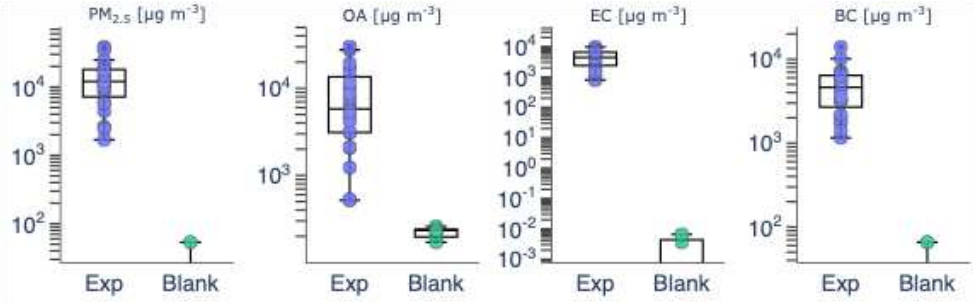

Figure A6: Uncorrected mixing ratios and mass concentrations compared against blank values for the large-scale fires.

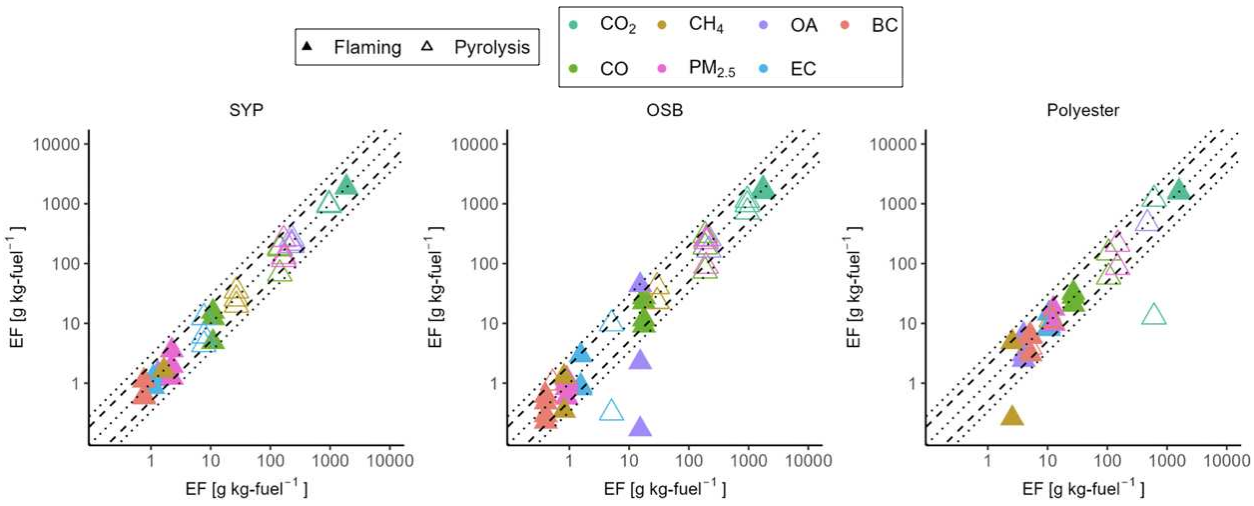

Figure A7: Emission factors from left to right, SYP, OSB, and Polyester from three different experiments compared against the average from those three experiments. Emission factors are shown for both pyrolysis and flaming conditions. Dashed and dotted lines represent 1:1, 1:2, and 1:3 lines.

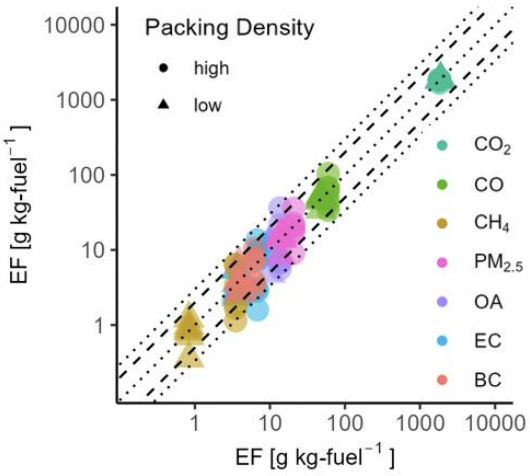

Figure A8: Emission factors for NIST cribs from individual experiments (n=6) compared against the average from those experiments. Data are resolved by 'high' and 'low' packing densities. Dashed and dotted lines represent 1:1, 1:2, and 1:3 lines.

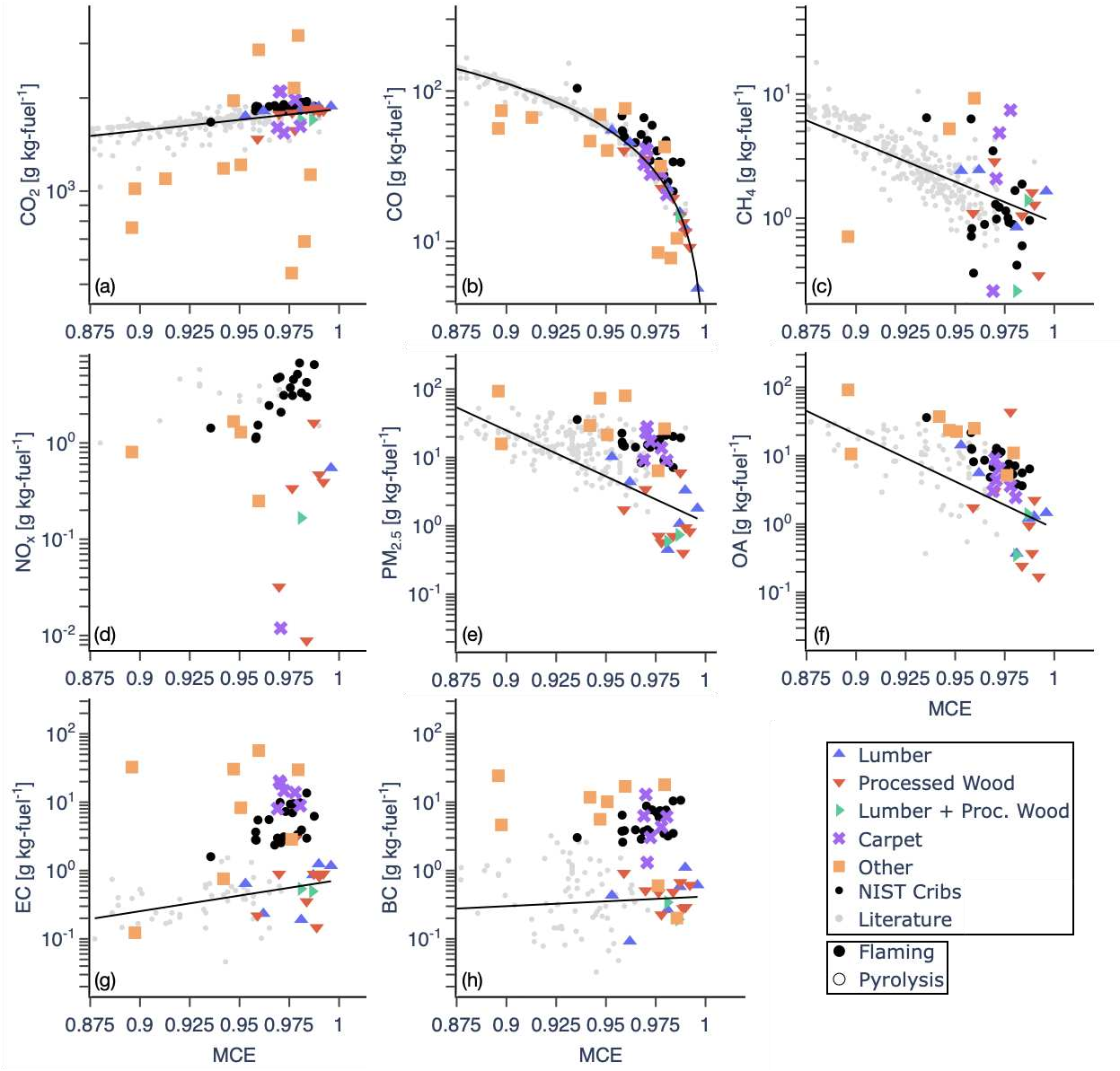

Figure A9: Same as Figure 6 but plotted against MCE and MCE>0.875. Solid lines represent the best fits to wood-based fuel data from this work and SERA data. No fits were developed for NO_X.

APPENDIX B: CHAPTER 3 SUPPLEMENTAL FIGURES

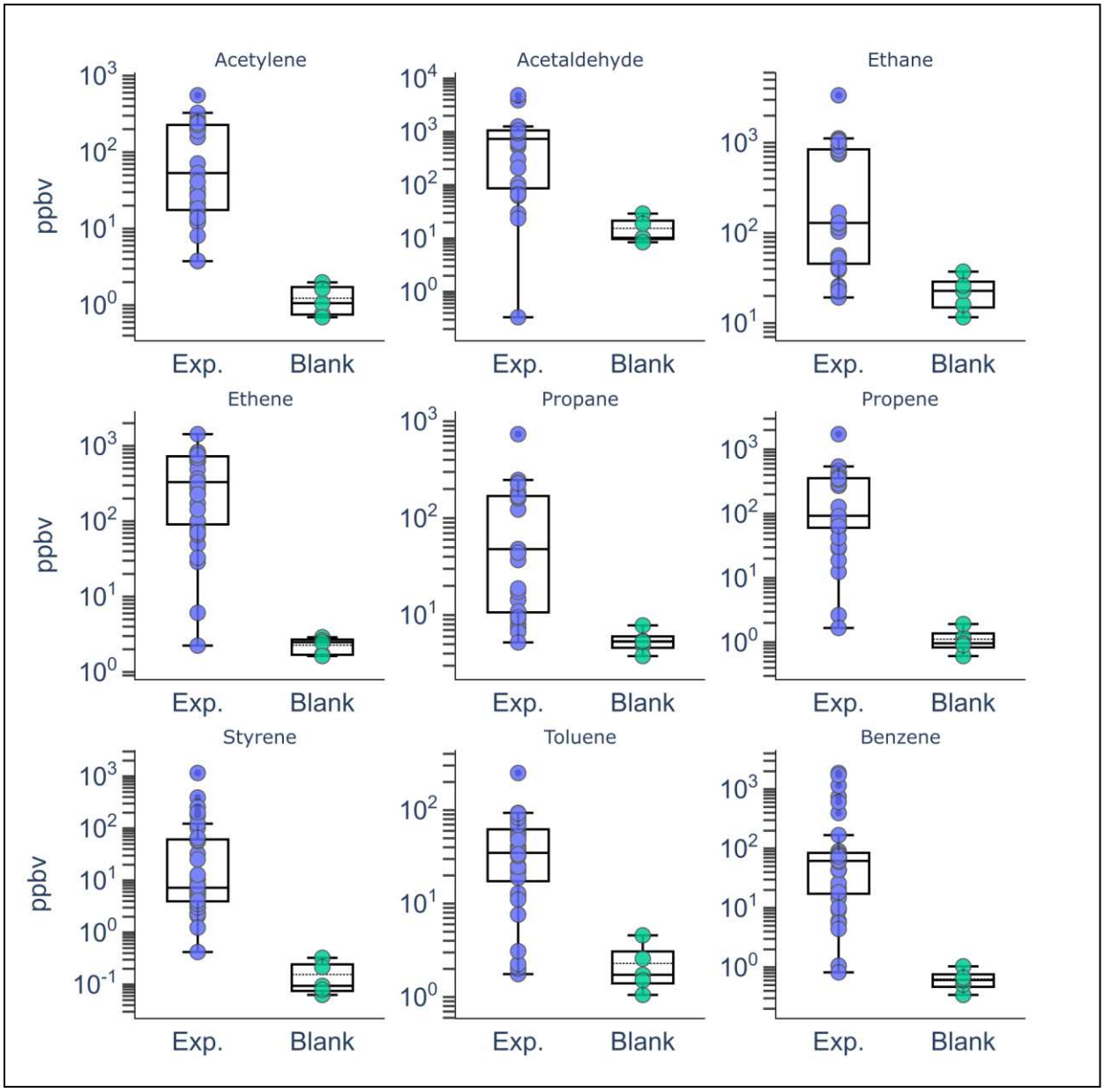

Figure B1: Blank versus experimental mixing ratios for select VOC species under pyrolysis combustion conditions for the small-scale campaign. Experimental results in left column and colored blue, note that concentration values are plotted prior to background correction. Blank

experiment in right column and colored green. Over both columns are statistical boxplots where solid black line within boxplot is the median and dashed line is the mean.

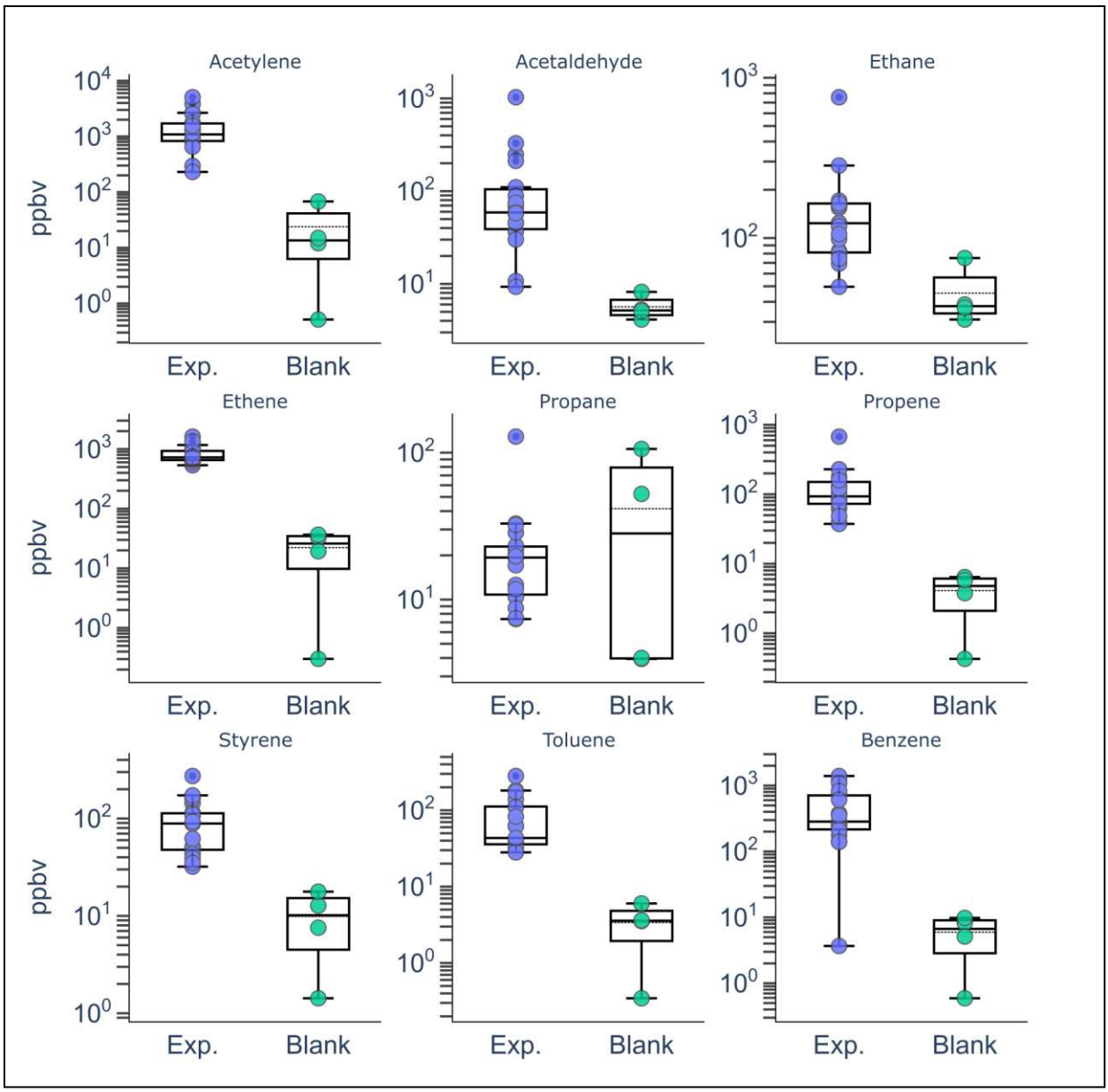

Figure B2: Blank versus experimental mixing ratios for select VOC species for the large-scale mixed fuels campaign. Experimental results in left column and colored blue, note that concentration values are plotted prior to background correction. Blank experiment in right column and colored green. Over both columns are statistical boxplots where solid black line within boxplot is the median and dashed line is the mean.

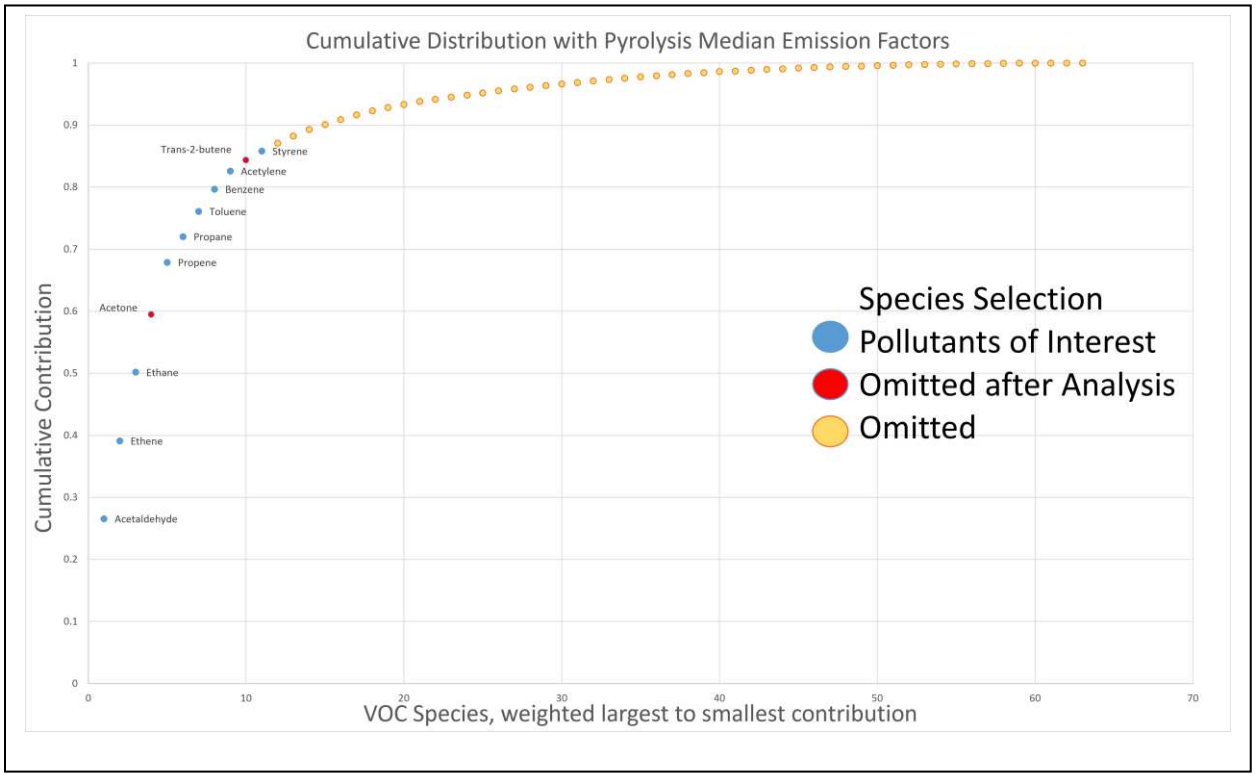

Figure B3: Cumulative distribution for pyrolysis combustion mode. Species selected for primary analysis color in blue, with post-analysis removal done for species in red. All species in yellow have considerably lower cumulative contribution and were removed from the detailed primary analysis.

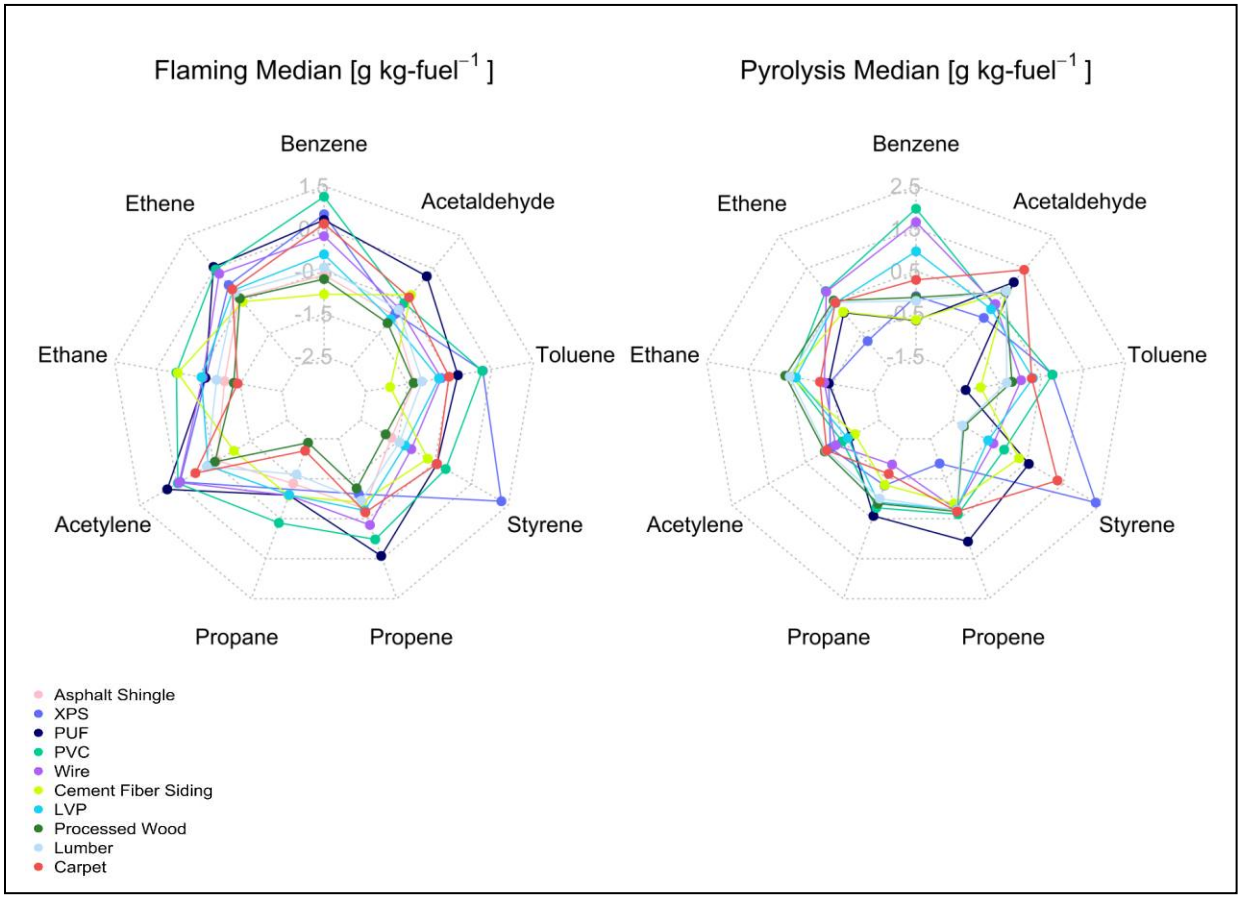

Figure B4: Relative contribution of 'Other' fuel group species with processed wood, lumber and carpet provided as reference. Alternative version of Figure 14, with axes on log scale. Incremental values represent 10 to the "X" value. Colors delineate VOC species.

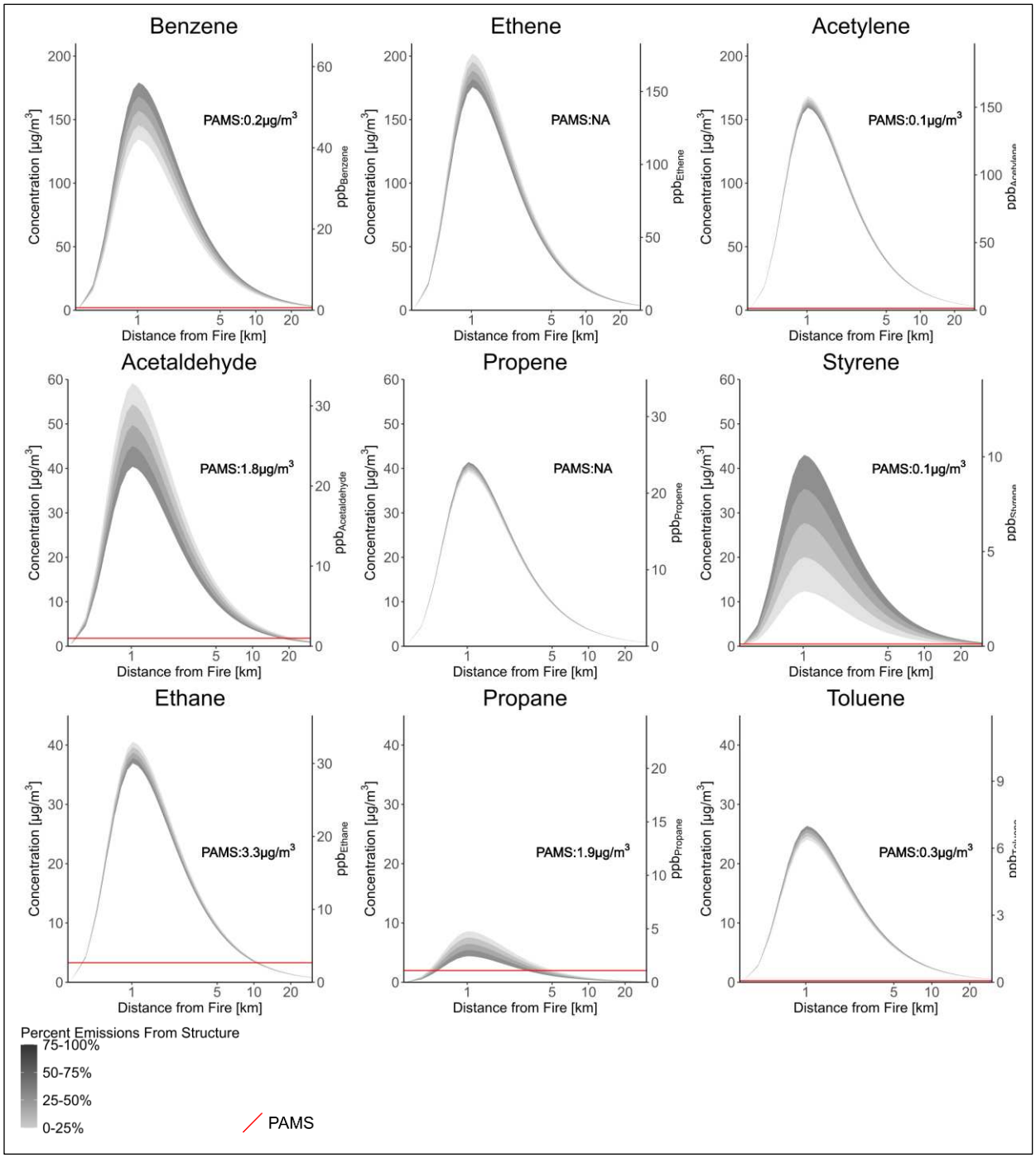

Figure B5: Plume model for nine primary VOCs under same conditions as Figure 15. Additional left y-axes provided in units of mixing ratio (ppb_voc).